

6. BERMUDA RISE AND SOHM ABYSSAL PLAIN, SITES 1063 AND 1064¹

Shipboard Scientific Party²

HOLE 1063A

Position: 33°41.204'N, 57°36.898'W (Bermuda Rise)
Start hole: 0119 hr, 25 March 1997
End hole: 2230 hr, 28 March 1997
Time on hole: 94.18 hr (3.92 days)
Seafloor (drill-pipe measurement from rig floor, mbrf): 4595.2
Distance between rig floor and sea level (m): 11.7
Water depth (drill pipe measurement from sea level, m): 4583.5
Total depth (from rig floor, mbrf): 5013.6
Penetration (mbsf): 418.4
Coring totals:
Type: APC; Number: 22; Cored: 201.4 m; Recovered: 217.00 m (107.75%)
Type: XCB; Number: 23; Cored: 217.0 m; Recovered: 203.65 m (93.85%)
Total: Number: 45; Cored: 418.4 m; Recovered: 400.34 m (95.68%)
Oldest formation cored: middle Pliocene clay with silt and nannofossils

HOLE 1063B

Position: 33°41.189'N, 57°36.898'W (Bermuda Rise)
Start hole: 2230 hr, 28 March 1997
End hole: 0210 hr, 31 March 1997
Time on hole: 50.67 hr (2.11 days)
Seafloor (drill pipe measurement from rig floor, mbrf): 4594.7
Distance between rig floor and sea level (m): 11.7
Water depth (drill pipe measurement from sea level, m): 4583.0
Total depth (from rig floor, mbrf): 4946.3
Penetration (mbsf): 351.60
Coring totals:
Type: APC; Number: 23; Cored: 213.8 m; Recovered: 215.33 m (100.72%)
Type: XCB; Number: 15; Cored: 137.8 m; Recovered: 126.62 m (91.89%)
Total Number: 38; Cored: 351.6 m; Recovered: 341.95 m (97.26%)
Oldest formation cored: middle Pliocene nannofossil clay

HOLE 1063C

Position: 33°41.181'N, 57°36.903'W (Bermuda Rise)
Start hole: 0210 hr, 31 March 1997

End hole: 0620 hr, 1 April 1997
Time on hole: 28.17 hr (1.17 days)
Seafloor (drill pipe measurement from rig floor, mbrf): 4596.0
Distance between rig floor and sea level (m): 11.9
Water depth (drill pipe measurement from sea level, m): 4584.1
Total depth (from rig floor, mbrf): 4808.7
Penetration (mbsf): 212.70
Coring totals:
Type: APC; Number: 24; Cored: 212.7 m; Recovered: 204.39 m (96.09%)
Oldest formation cored: lower Pleistocene clay with nannofossils

HOLE 1063D

Position: 33°41.172'N, 57°36.907'W (Bermuda Rise)
Start hole: 0620 hr, 1 April 1997
End hole: 1730 hr, 3 April 1997
Time on hole: 59.17 hr (2.47 days)
Seafloor (drill pipe measurement from rig floor, mbrf): 4596.2
Distance between rig floor and sea level (m): 11.9
Water depth (drill pipe measurement from sea level, m): 4584.3
Total depth (from rig floor, mbrf): 4769.3
Penetration (mbsf): 173.10
Coring totals:
Type: APC; Number: 19; Cored: 173.10 m; Recovered: 176.54 m (101.99%)
Oldest formation cored: lower Pleistocene clay with nannofossils

HOLE 1064A

Position: 32°32.720'N, 57°4.588'W (Sohm Abyssal Plain)
Start hole: 0114 hr, 4 April 1997
End hole: 2215 hr, 5 April 1997
Time on hole: 45.02 hr (1.88 days)
Seafloor (drill pipe measurement from rig floor, mbrf): 5580.0
Distance between rig floor and sea level (m): 11.7
Water depth (drill pipe measurement from sea level, m): 5568.3
Total depth (from rig floor, mbrf): 5608.5
Penetration (mbsf): 28.50
Coring totals:
Type: APC; Number: 3; Cored: 28.5 m; Recovered: 28.83 m (101.16%)
Oldest formation cored: Pleistocene clay

¹Keigwin, L.D., Rio, D., Acton, G.D., et al., 1998. *Proc. ODP, Init. Repts.*, 172: College Station, TX (Ocean Drilling Program).

²Shipboard Scientific Party is given in the list preceding the Table of Contents.

Principal results: Site 1063 is located on the northeast Bermuda Rise, in the northern Sargasso Sea, at a water depth of 4584 m. This location is close to the interface between Antarctic Bottom Water (AABW) and North Atlantic Deep Water (NADW), marked by bottom-water temperatures of about 2°C. Four holes were cored, with total recovery in excess of 100%. The interval 0–201.4 meters below seafloor (mbsf) was triple cored with the advanced hydraulic piston corer (APC) and appears to provide a complete composite sequence back to the early Pleistocene, and a fourth APC penetrated to 173 mbsf. Double extended core barrel (XCB) coring extended the site to the lower Pliocene with penetration to 418.4 mbsf at Hole 1063A and 342 mbsf at Hole 1063B.

The base of acoustically stratified sediments appears to be latest Pliocene to early Pleistocene in age, but the most reflective sediment was deposited beginning about 1 Ma. These reflectors seem to correlate with a late Pleistocene climate change from 40-k.y. to 100-k.y. variability. Despite the “biscuiting” in the cores drilled with the XCB, good sedimentary structures could still be observed. Overall, an excellent and continuous sedimentary succession highly suitable for paleoceanographic studies was recovered at Site 1063.

The sediments recovered at Site 1063 reflect the rapid deposition of clays and silts by deep recirculating gyres in the western North Atlantic. Only one lithostratigraphic unit is recognized at Site 1063, characterized by 70%–100% clays alternating with nannofossil-bearing intervals (commonly 15%–30%, but occasionally exceeding 60%). The persistence of one sedimentary unit for more than 3 m.y. suggests that sediment focusing by deep currents has been the dominant depositional process during the late Neogene at this site. In addition to the clays and nannofossils, two other accessory components are silt and biogenic silica. The presence of 15%–30% biogenic silica (mostly diatoms) within clays and silty clays marks Subunit IA (0–135 mbsf). Within the last glacial maximum, at 4–11 mbsf, a region of black diagenetic mottles containing troilite and hydrotroilite is correlatable with Sites 1061 and 1062 on the Blake-Bahama Outer Ridge (BBOR). As in the upper sections of other Leg 172 sites, Bermuda Rise sediments contain distinct red lutite beds, which are thought to reflect increased advection of fine-grained sediment from the Nova Scotia region during cold climates. Subunit IB also contains these red lutites, and their lowermost occurrence at 270 mbsf defines its lower boundary. Between 270 and 420 mbsf, Subunit IC consists of dark greenish gray homogeneous clays interbedded with light greenish gray carbonate-rich intervals. Erosional events, common at several of the BBOR sites, are virtually absent here, with the exception of a thin (10 cm), laminated deposit at 101 mbsf.

Calcareous nannofossils are the dominant microfossils and are generally well preserved, except for some intervals where they are dissolved. Eleven nannofossil biohorizons have been constrained for the past 3.3 m.y. Foraminifer assemblages are generally dissolved, but eight foraminifer biohorizons have been identified despite poor preservation. Where diatoms are most common, the sediment has the unusual association of high sonic velocity with low bulk density. It is thought that this stems in part from a structural framework provided by the diatoms and other siliceous microfossils. The diatoms seem to be most prevalent in cold climatic episodes, probably reflecting some combination of higher surface-water productivity and better preservation.

Paleomagnetic results from Site 1063 are exceptional, providing an excellent record of geomagnetic secular variation, geomagnetic excursions, transitional field directions during reversals, and a detailed magnetostratigraphy down to the Gauss Chron. In Hole 1063A, the Brunhes/Matuyama reversal boundary (0.78 Ma) is located at 138.5 mbsf, the top and bottom of the Jaramillo Subchron (0.99 and 1.07 Ma, respectively) are located at 175.0 and 187.3 mbsf, respectively, and the top of the Gauss Chron (2.581 Ma) is at 347.7 mbsf. Also, clearly identified are the Cobb Mountain Subchron, Olduvai Chron, and the Reunion I and II Subchrons.

There is excellent agreement between the 19 calcareous plankton biohorizons recognized and the magnetic polarity reversal stratigraphy. The integrated biomagnetostratigraphy suggests a sedimentation rate of 200 m/m.y. from 0 to 0.5 Ma, 140–170 m/m.y. between 0.5 and 1.1 Ma, 100–110 m/m.y. between 1.1 and 2.5 Ma, and 75 m/m.y. in the underlying interval.

The sulfate/methane boundary occurs at 38 mbsf. Methane concentrations below the interface were sufficient to cause significant sediment expansion in the recovered cores. Downhole profiles of interstitial water Ca, Mg, and Sr suggest dissolution of biogenic carbonates and probable dolomitization in the zone of methanogenesis. Mn concentrations (up to 37 mM) in the top of the sulfate reduction zone are higher than at the other sites, which is probably because of the relative proximity of Site 1063 to volcanic sources. Interstitial water profiles indicate decreasing amounts of biogenic silica in the sediment column below 250 mbsf. Chloride concentrations decrease downhole, showing an overall freshening of 3% relative to seawater.

Site 1064 is one sedimentary unit consisting of alternating brown and red clays with exceptionally sharp contacts. The brown clays are probably distal turbidites because of the occurrence of thin basal laminae and scoured contacts. Reddish clays may be turbiditic as well, although there is no evidence of basal scour. The relationship between clays at this site and those on the Bermuda Rise is unclear, because the three APC cores at Site 1064 were too few to establish a reliable biostratigraphy.

BACKGROUND AND OBJECTIVES

The sediment drift that comprises the northeast Bermuda Rise is one of the highest resolution archives of paleoclimate and paleocean information known from the open sea. Sedimentation rates as high as 200 cm/k.y. result from advection of clay and silt by deep recirculating gyres, the strength of which is linked to surface ocean and atmospheric conditions. Because much of the clay and silt is derived from eastern Canada, studies of the Bermuda Rise have the potential to link the marine, terrestrial, and atmospheric components of the climate system. Before Site 1063, the longest continuous core obtained from the Bermuda Rise was 53 m, terminating in sediments of glacial marine isotopic Stage (MIS) 6. Accordingly, one of the most important Leg 172 objectives was to recover a complete sequence of sediments back through the origin of Northern Hemisphere glaciation. Such sediments should document any changes in lithology associated with the first glaciation of eastern Canada, which might also account for the base of the acoustically stratified sediments (at 0.3 s two-way traveltime [TWT]). In addition, they should document any important changes in deep-ocean circulation patterns associated with that event. Finally, Bermuda Rise sediments should be useful for high-resolution study of changes in Earth's magnetic field.

A coring location on the Sohm Abyssal Plain near the northeast Bermuda Rise became an objective during Leg 172 when it was clear that we had the extra time. Site 1064 was identified because it was near some conventional piston cores taken by *CSS Hudson*. One objective of this site was to develop the distal turbidites on the abyssal plain as a link between their Canadian source and the fine-grained sink on the Bermuda Rise. A second objective of Site 1064 was to provide a pore-water record of oxygen isotope ($\delta^{18}\text{O}$) composition from a deep-water location that had not been affected by climatically controlled changes in the flux of NADW. It was assumed that an abyssal plain site at this latitude would have been continuously bathed by AABW during the past 20 k.y. If this proved to be correct, then the change in $\delta^{18}\text{O}$ from modern bottom water to glacial-aged pore water at Site 1064 would reflect mostly the secular change in oxygen isotope composition of the ocean.

OPERATIONS

Site 1063

After leaving Site 1062, the *JOIDES Resolution* made a 943-nmi transit at an average speed of 11.6 kt to the Sohm Abyssal Plain, where we conducted a short seismic survey over a potential supplemental site (SAP-1). At 1130 hr, the *JOIDES Resolution* slowed to deploy seismic equipment. The ensuing seismic survey consisted of

a west-to-east line that passed about 1 km south of the SAP-1 site, a broad turn to the south, and then a crossing line which traversed from south-southeast to north-northwest across the original line and over SAP-1 (see "Site Geophysics" section, this chapter). This survey covered 28 nmi and was conducted at an average speed of 6.4 kt.

We then proceeded to the Site 1063 survey area, and before coring, conducted a 13-nmi seismic survey. This survey began with a south-southeast to north-northwest profile over Site 1063 (scientific prospectus site BR-1), followed by a crossing west-to-east line. The survey was conducted at an average speed of 4.5 kt.

Coring began in Hole 1063A at 1035 hr on 25 March. Following the first core, a near-bottom water sample was obtained with the water sampler and temperature probe (WSTP) for isotope studies. With the APC, coring advanced to 201.4 mbsf, which was considered APC refusal (Table 1). Cores 172-1063A-3H through 9H, 11H through 17H, and 20H through 22H were oriented, with the gaps in the orientation occurring during the interval in which data were being down-loaded from the only operational Tensor tool. Hole 1063A was deepened with the XCB to 418.4 mbsf, which was 68 m deeper than originally planned.

Table 1. Coring summary for Sites 1063 and 1064.

Core	Date (1997)	Time (UTC)	Interval (mbsf)	Length cored (m)	Length recovered (m)	Recovery (%)	Core	Date (1997)	Time (UTC)	Interval (mbsf)	Length cored (m)	Length recovered (m)	Recovery (%)
172-1063A-							27X						
1H	25 March	1100	0.0-5.3	5.3	5.34	100.8	30 March	0555	237.0-246.6	9.6	9.90	103.1	
2H	25 March	1345	5.3-14.8	9.5	8.40	88.4	30 March	0705	246.6-255.8	9.2	8.36	90.9	
3H	25 March	1455	14.8-24.3	9.5	9.79	103.1	30 March	0825	255.8-265.5	9.7	9.88	101.9	
4H	25 March	1605	24.3-33.8	9.5	9.94	104.6	30 March	0940	265.5-275.1	9.6	9.88	102.9	
5H	25 March	1705	33.8-43.3	9.5	9.42	99.2	30 March	1105	275.1-284.7	9.6	9.94	103.5	
6H	25 March	1810	43.3-52.8	9.5	9.56	100.6	30 March	1245	284.7-294.4	9.7	8.05	83.0	
7H	25 March	1915	52.8-62.3	9.5	9.62	101.3	30 March	1425	294.4-304	9.6	9.98	104.0	
8H	25 March	2025	62.3-71.8	9.5	9.65	101.6	30 March	1625	304.0-313.6	9.6	9.48	98.8	
9H	25 March	2130	71.8-81.3	9.5	9.59	100.9	30 March	1830	313.6-323.1	9.5	5.82	61.3	
10H	25 March	2235	81.3-90.8	9.5	8.29	87.3	30 March	2050	323.1-332.7	9.6	9.53	99.3	
11H	25 March	2345	90.8-100.3	9.5	9.62	101.3	30 March	2255	332.7-342	9.3	0.29	3.1	
12H	26 March	0050	100.3-109.8	9.5	9.30	97.9	31 March	0050	342.0-351.6	9.6	10.06	104.8	
13H	26 March	0150	109.8-119.3	9.5	8.77	92.3	Coring totals:						
14H	26 March	0250	119.3-128.8	9.5	9.17	96.5					351.6	341.95	97.3
15H	26 March	0350	128.8-138.3	9.5	9.16	96.4	172-1063C-						
16H	26 March	0450	138.3-147.8	9.5	9.46	99.6	1H	31 March	0345	0.0-2.5	2.5	2.54	101.6
17H	26 March	0550	147.8-157.3	9.5	8.18	86.1	2H	31 March	0440	2.5-12.0	9.5	9.69	102.0
18H	26 March	0650	157.3-166.8	9.5	9.20	96.8	3H	31 March	0540	12.0-21.5	9.5	8.29	87.3
19H	26 March	0750	166.8-176.3	9.5	9.36	98.5	4H	31 March	0640	21.5-31.0	9.5	9.90	104.2
20H	26 March	0855	176.3-185.8	9.5	9.26	97.5	5H	31 March	0740	31.0-40.5	9.5	9.11	95.9
21H	26 March	1000	185.8-195.1	9.3	9.34	100.4	6H	31 March	0840	40.5-50.0	9.5	0.00	0.0
22H	26 March	1100	195.1-201.4	6.3	6.27	99.5	7H	31 March	0940	50.0-59.5	9.5	9.69	102.0
23X	26 March	1220	201.4-207.6	6.2	7.91	127.6	8H	31 March	1035	59.5-69.0	9.5	9.06	95.4
24X	26 March	1330	207.6-217.2	9.6	9.95	103.6	9H	31 March	1135	69.0-78.5	9.5	9.57	100.7
25X	26 March	1440	217.2-226.8	9.6	9.61	100.1	10H	31 March	1240	78.5-88.0	9.5	9.31	98.0
26X	26 March	1555	226.8-236.4	9.6	9.79	102.0	11H	31 March	1345	88.0-97.5	9.5	9.44	99.4
27X	26 March	1705	236.4-246.0	9.6	9.50	99.0	12H	31 March	1450	97.5-107.0	9.5	10.06	105.9
28X	26 March	1815	246.0-255.3	9.3	9.75	104.8	13H	31 March	1550	107.0-116.5	9.5	9.33	98.2
29X	26 March	1930	255.3-264.9	9.6	9.80	102.1	14H	31 March	1650	116.5-126.0	9.5	10.16	106.9
30X	26 March	2110	264.9-274.5	9.6	9.76	101.7	15H	31 March	1800	126.0-135.5	9.5	9.92	104.4
31X	26 March	2230	274.5-284.1	9.6	9.88	102.9	16H	31 March	1905	135.5-142.4	6.9	6.88	99.7
32X	26 March	2350	284.1-293.8	9.7	9.57	98.7	17H	31 March	2025	142.4-151.9	9.5	9.82	103.4
33X	27 March	0115	293.8-303.5	9.7	9.72	100.2	18H	31 March	2140	151.9-160.9	9.0	9.11	101.2
34X	27 March	0255	303.5-313.1	9.6	9.76	101.7	19H	31 March	2245	160.9-170.4	9.5	9.83	103.5
35X	27 March	0445	313.1-322.6	9.5	9.69	102.0	20H	31 March	2350	170.4-179.4	9.0	9.28	103.1
36X	27 March	0630	322.6-332.2	9.6	8.92	92.9	21H	1 April	0115	179.4-187.9	8.5	8.46	99.5
37X	27 March	0825	332.2-341.5	9.3	9.30	100.0	22H	1 April	0235	187.9-195.2	7.3	7.34	100.5
38X	27 March	1020	341.5-351.1	9.6	7.78	81.0	23H	1 April	0340	195.2-204.2	9.0	9.10	101.1
39X	27 March	1225	351.1-360.7	9.6	2.73	28.4	24H	1 April	0505	204.2-212.7	8.5	8.50	100.0
40X	27 March	1440	360.7-370.3	9.6	8.77	91.4	Coring totals:						
41X	27 March	1655	370.3-379.9	9.6	5.41	56.4					212.7	204.39	96.1
42X	27 March	1905	379.9-389.5	9.6	7.35	76.6	172-1063D-						
43X	27 March	2110	389.5-399.1	9.6	9.38	97.7	1H	1 April	0755	0.0-2.3	2.3	2.33	101.3
44X	27 March	2320	399.1-408.7	9.6	9.58	99.8	2H	1 April	0845	2.3-11.8	9.5	9.76	102.7
45X	28 March	0120	408.7-418.4	9.7	9.74	100.4	3H	1 April	0940	11.8-21.3	9.5	9.82	103.4
Coring totals:							4H	1 April	1030	21.3-30.8	9.5	9.86	103.8
				418.4	400.34	95.7	5H	1 April	1125	30.8-40.3	9.5	9.95	104.7
172-1063B-							6H	1 April	1220	40.3-49.8	9.5	9.77	102.8
1H	29 March	0125	0.0-7.8	7.8	7.83	100.4	7H	1 April	1320	49.8-59.3	9.5	9.70	102.1
2H	29 March	0215	7.8-17.3	9.5	7.18	75.6	8H	1 April	1415	59.3-68.8	9.5	9.68	101.9
3H	29 March	0315	17.3-26.8	9.5	9.88	104.0	9H	1 April	1515	68.8-78.3	9.5	9.59	100.9
4H	29 March	0420	26.8-36.3	9.5	9.68	101.9	10H	1 April	1620	78.3-87.8	9.5	9.60	101.1
5H	29 March	0520	36.3-45.8	9.5	9.66	101.7	11H	1 April	1720	87.8-97.3	9.5	9.54	100.4
6H	29 March	0640	45.8-55.3	9.5	9.57	100.7	12H	1 April	1820	97.3-106.8	9.5	9.70	102.1
7H	29 March	0740	55.3-64.8	9.5	9.58	100.8	13H	1 April	1920	106.8-116.3	9.5	9.00	94.7
8H	29 March	0845	64.8-74.3	9.5	9.84	103.6	14H	1 April	2020	116.3-125.8	9.5	9.72	102.3
9H	29 March	0945	74.3-83.8	9.5	9.96	104.8	15H	1 April	2130	125.8-135.3	9.5	9.83	103.5
10H	29 March	1050	83.8-93.3	9.5	10.12	106.5	16H	1 April	2235	135.3-144.8	9.5	9.69	102.0
11H	29 March	1200	93.3-102.8	9.5	9.66	101.7	17H	1 April	2340	144.8-154.3	9.5	9.80	103.2
12H	29 March	1310	102.8-112.3	9.5	9.76	102.7	18H	2 April	0045	154.3-163.8	9.5	9.91	104.3
13H	29 March	1410	112.3-121.8	9.5	9.50	100.0	19H	2 April	0845	163.8-173.1	9.3	9.29	99.9
14H	29 March	1520	121.8-131.3	9.5	9.63	101.4	Coring totals:						
15H	29 March	1625	131.3-140.8	9.5	9.85	103.7					173.1	176.54	102.0
16H	29 March	1730	140.8-149.8	9.0	9.04	100.4	172-1064A-						
17H	29 March	1835	149.8-158.5	8.7	8.71	100.1	1H	4 April	2345	0.0-9.5	9.5	9.61	101.2
18H	29 March	1935	158.5-167.8	9.3	9.30	100.0	2H	5 April	0245	9.5-19.0	9.5	9.56	100.6
19H	29 March	2045	167.8-177.3	9.5	9.67	101.8	3H	5 April	0345	19.0-28.5	9.5	9.66	101.7
20H	29 March	2145	177.3-186.8	9.5	9.56	100.6	Coring totals:						
21H	29 March	2255	186.8-196.3	9.5	9.90	104.2					28.5	28.83	101.2
22H	30 March	0005	196.3-205.8	9.5	9.43	99.3							
23H	30 March	0105	205.8-213.8	8.0	8.02	100.3							
24X	30 March	0220	213.8-217.8	4.0	5.91	147.8							
25X	30 March	0325	217.8-227.4	9.6	9.75	101.6							
26X	30 March	0440	227.4-237	9.6	9.79	102.0							

Notes: UTC = Universal Time Coordinated. For each site, an expanded coring summary table for each hole that includes lengths and depths of sections and sampling comments is included on CD-ROM (back pocket, this volume).

Paleontologists noted the occurrence of glass in several of the core-catcher samples from the upper part of Hole 1063A. An ODP technician later traced the origin of this material to the grit that was used in the sandblasting operations on the drill floor. Perhaps the sand contaminated the core liners that were stored near the logging shack before deployment or fouled the work bench where the core-catcher samples were obtained. Future investigators are warned that some core-catcher samples and perhaps the outer parts of some cores may be contaminated in this manner. The sandblasting material was a low-silica coal slag.

In preparation for logging, Hole 1063A was flushed with a 30-bbl sepiolite sweep and the drill string pulled back to 377.5 mbsf. The drill string was pulled up to 99.1 mbsf with a maximum drag of 20 kilopounds (kips) observed and then run to bottom where it contacted 16 m of soft fill. After a go-devil (a tool that free-falls down the drill pipe) was dropped to ensure opening of the lockable float valve, the hole was swept with 50 bbl of sepiolite mud. The hole was then displaced with 190 bbl of 8.9 lb/gal sepiolite mud. Finally, the drill bit was positioned at the logging depth of 105.0 mbsf.

By 0700 hr on 28 March, the Schlumberger equipment was rigged up. Logs were collected in the interval from 416.8 to 105 mbsf using the triple combo (digital dual induction tool [DITE], HLDT, APS, the hostile environment natural gamma-ray sonde [HNGS]) and the FMS (FMS and sonic digital [SDT]) logging tools, as described in the "Downhole Logging" section (this chapter).

Hole 1063B was spudded 29 m south of Hole 1063A, and the bit was positioned ~2 m deeper than at Hole 1063A. The seafloor depth was established at 4594.7 mbsf, based upon 7.83-m recovery in the first core. Cores 172-1063B-16H through 18H and 23H were not fully stroked, but because of the interest in high-quality cores for magnetic studies, piston coring was extended by advancing by recovery to a depth of 213.8 mbsf. Hole 1063B was then deepened with the XCB to a total depth of 351.6 mbsf. Cores 172-1063B-3H through 9H, 11H through 17H, and 19H through 21H were oriented with the Tensor tool. The Adara heat-flow shoe was deployed at 55.3 (Core 172-1063B-6H), 74.3 (8H), 93.3 (10H), 112.3 (12H), and 140.8 mbsf (15H).

Hole 1063C was spudded 14 m south and 7 m west of Hole 1063B, and APC coring reached a total depth of 212.7 mbsf using advance by recovery. Cores 172-1063C-3H through 10H, 15H through 21H, and 23H through 24H were oriented.

Hole 1063D was spudded 17 m south and 6 m west of Hole 1063C with the bit positioned 2 m higher than at Hole 1063A. APC coring advanced to 163.8 mbsf (Core 172-1063D-18H) without incident, although while coring, the seas began to get rough, with 5- to 6-m swells and up to 4-m ship heave. While attempting to recover Core 172-1063D-19H (163.8–173.1 mbsf), the wireline parted, leaving the sinker bar assembly, Tensor tool, pressure case assembly, and the inner core barrel with Core 172-1063D-9H in the hole. This hardware and the core were later retrieved. The wireline failure was attributed to the poor weather conditions, which continued to deteriorate. Winds were gusting to 52 kt as a massive cold front passed over the location in the early morning on 2 April. Coring operations were halted while we waited for conditions to improve. At 1700 hr on 3 April, there was a momentary lull in the storm, which allowed the vessel to retract hydrophones and thrusters and come about. With time running out for Leg 172 and the storm showing little signs of abating, we decided to transit to Site 1064 (SAP-1). By 1730 hr, the vessel was under way to the last site, leaving behind two positioning beacons, which we were unable to recover because of weather and sea conditions.

Site 1064

The 73-nmi transit to the last site of the leg was accomplished at an average speed of 11.0 kt. The vessel's track from Site 1063 took the storm on the starboard quarter, which was responsible for the very good transit speed.

A beacon was deployed at 0032 hr on 4 April. Shortly after deployment, the signal was lost and a backup beacon was prepared and launched at 0114 hr. The backup beacon started to behave erratically, and a third beacon had to be deployed later in the day. As the vessel was positioned over the beacon, the bottom-hole assembly (BHA) received the routine end-of-leg magnetic particle inspection while drill pipe was being run into the hole.

Hole 1064A was spudded with the APC at 2310 hr on 4 April after two water cores (APC cores that were shot into water above the seafloor). The seafloor depth was established at 5580.0 mbsf, but Core 172-1064A-1H had 101% recovery (Table 1), which indicated that the mudline was probably not recovered. The previous water core, however, was shot from a bit position 6 m above where the bit was positioned for Core 172-1064A-1H. The end of the core catcher from the water core had a little mud on it, which indicated that we should have recovered about 6 m of sediment in Core 172-1064A-1H, rather than the 9.6 m recovered. The larger-than-expected recovery might be attributed to variation in the inclination of the drill pipe, ship heave, dynamic stretching of the more than 5.5 km of drill pipe, or some combination. Indeed, the weight on the bit varied by as much as 50,000 lb, and the seas were still rough. The exact amount by which we missed the mudline is uncertain, but seems unlikely to exceed about 10 m because of the two previous attempts at 6 and 13 m above the drilling-estimated mudline. Seismic information indicates a possible 10 m of missing section, whereas extrapolation of pore-water sulfate profiles indicates as much as 19 m are missing. In addition, the WSTP was deployed 10 m above the inferred seafloor following the mudline core in an attempt to obtain a near-bottom water sample for isotope studies. The WSTP sample was heavily contaminated with mud, indicating that it had contacted the seafloor.

APC coring resumed and advanced to 28.5 mbsf. After recovering the third APC core (28.5 mbsf), the driller heard an unusual noise emanating from the drawworks, which upon investigation revealed a major failure of the forward drawworks traction motor. This failure left the drawworks with limited capability and ended coring at Site 1064 and for Leg 172 approximately one day early. The drill string was raised slowly to the surface and the ship was under way toward Lisbon by 2215 hr on 5 April.

LITHOSTRATIGRAPHY

Site 1063 Lithostratigraphy

The sediments recovered at Site 1063 from the northeast Bermuda Rise record the rapid deposition of clays, silts, and nannofossils and document the dynamics of deep ocean advection and redeposition. Holes 1063A through 1063D, at water depths of ~4584 m, have similar lithologies and meet the primary objective of recovering sediments for high-resolution paleoceanographic studies. The extinction of *Dentoglobigerina altispira* (3.12 Ma) is recorded at 395.45 mbsf, indicating an average sedimentation rate of 12.67 cm/ky from the Holocene to the middle Pliocene, although the late Pleistocene sedimentation rate is probably twice as high (see "Biostratigraphy" section, this chapter). The composition of sediments at Site 1063 ranges from clay to nannofossil ooze, and only one lithologic unit is defined. Three correlatable subunits of Site 1063 are determined by the occurrence of biogenic silica and red lutites: (1) Subunit IA contains variable amounts of biogenic silica in a clay with a nannofossil-dominated matrix that commonly includes red lutites; (2) Subunit IB generally consists of clay with varying proportions of nannofossils, silts, and red lutites, but lacks biogenic silica; and (3) Subunit IC contains 50%–100% clay with smaller quantities of nannofossils. Within these subunits are distinct lithotypes containing features associated with early diagenesis and sedimentation dynamics on the Bermuda Rise.

The Holocene to middle Pliocene lithostratigraphy and depths at Site 1063 were based on Hole 1063A, where the maximum length of sediment was cored (418.4 m). Following the discussion of the three

subunits is a generalized description of features common to the entire unit (Fig. 1).

Subunit IA

Intervals: 172-1063A-1H-1, 0 cm, through 19H-4, 10 cm (0.0–170.8 mbsf); 172-1063B-1H-1, 0 cm, through 19H-2, 40 cm (0.0–169.9 mbsf); 172-1063C-1H-1, 0 cm, through 19H-6, 60 cm (0.0–169.5 mbsf); 172-1063D-1H-1, 0 cm, through 19H-7, 150 cm (0.0–171.2 mbsf)

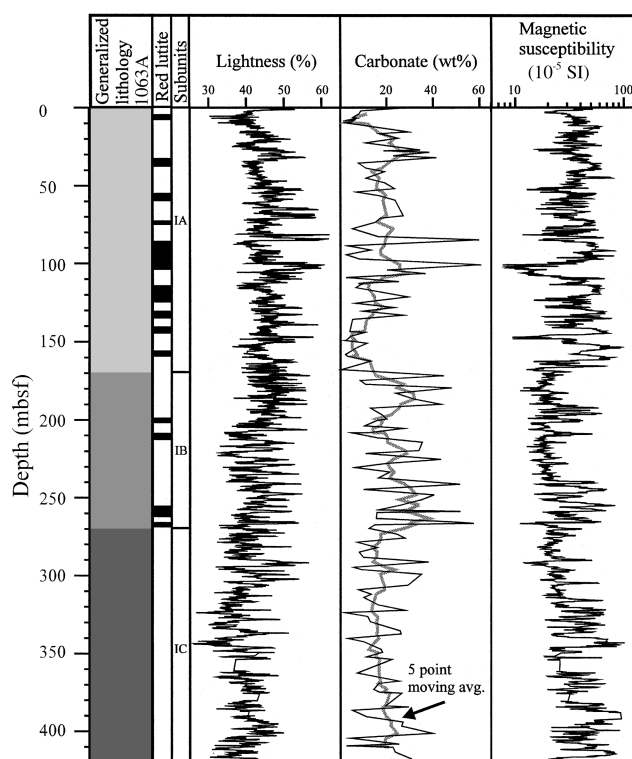
Age: Holocene to early Pleistocene

The dominant lithology of Subunit IA is medium light olive gray (5Y 5/1) to greenish gray (5GY 6/1) clay with varying proportions of silt and carbonate- and siliceous-bearing nannofossils. This subunit is defined by the variable presence of a dark grayish brown (10YR 3/2) to greenish gray (10GY 5/1) clay with biogenic silica. Within these intervals, worm burrows filled with tests of silicoflagellates, radiolarians, and diatoms are quite common. Although the barrel sheets of Site 1063 indicate lithological changes throughout this subunit, these are subtle changes; the sedimentological composition is fairly constant with minor shifts in the abundances of accessory lithologies. The only prominent exception is the relative abundance of biogenic carbonate and nannofossil-rich beds (>50%), which occur at the following depth intervals: 64–68 mbsf, 82–85 mbsf, and 98–112 mbsf. The first and second depth intervals contain two and the third interval one nannofossil-clay mixed sediment to nannofossil ooze bed, ranging in thickness from 0.75 to 1.5 m; the deepest interval is more extensive and contains a nannofossil clay matrix. The other nannofossil-rich intervals within this subunit are generally thinner (<45–50 cm) and less prominent. A common feature of these intervals is a basal contact frequently defined by a sequence of sharp diagenetic color changes and a gradational upper contact. This basal transition usually consists of a moderate to dark greenish gray band (0.5–2 cm thick) and an overlying, thinner, faint purplish band. Occasionally the green-purple color couplet was also observed within the nannofossil-rich interval, and in the low carbonate lithologies it is common to pervasive, sometimes present every 5 cm or less.

Red to reddish brown lutite beds are also common in Subunit IA (Fig. 1). These intervals consist of massive and structureless reddish brown (5YR 5/4) clay and clay with silt and usually contain sharp to very sharp upper and basal contacts. Scouring is absent in the basal contact, and there are no clear features (e.g., silt laminae or cross-bedding) suggesting downslope depositional processes except for a sharp basal contact. Although single lutite intervals range from 20 to 75 cm in thickness, they are generally grouped together over several meters and alternate with beds containing similar lithologies but without reddish brown coloration. On the basis of available color reflectance, biostratigraphic, and magnetic susceptibility data, the occurrence of the red lutites generally coincides with the termination of glacial periods. However, one small (11 cm) bed is known to correspond to the termination of MIS 5e (Adkins et al., 1997). Greenish gray (5GY 6/1) bioturbation mottles with black iron sulfide centers are also common in the red lutite beds, and their greenish gray (5GY 6/1) color is attributed to chemical reduction of the sediment surrounding the organic-rich burrows.

Distinctive zones of black mottling due to iron monosulfide precipitation during early diagenesis are present in all holes. X-ray diffraction (XRD) analyses have shown that hydrotroilite is an important component of these diagenetic features. Although they are most noticeable in the near-sediment surface cores, fainter iron monosulfide laminae are also present throughout other parts of the hole, as indicated by L*-parameter minima in the color reflectance data (Fig. 1).

Another notable feature of Subunit IA is an interval containing interbedded silt and clay laminae (Fig. 2). Like similar features observed on the Blake-Bahama Outer Ridge (BBOR), these four yellowish gray, very well sorted silt laminae are generally less than 2 mm thick and are interbedded with greenish gray clay. This interval



Legend

- Cyclic alternation between biogenic silica-rich and clay-rich sediments
- Clay, nannofossil, and silt mixed sediments
- Clayey sediments
- Red lutites

Figure 1. Generalized lithology, color reflectance, carbonate content, and magnetic susceptibility for Hole 1063A.

has only been observed in Holes 1063B and 1063C at 101.47 m and 100.20 m, respectively (172-1063B-11H-6, 67 cm, and 172-1063C-12H-2, 120 cm) and is interbedded in a light greenish gray (5GY 8/1) clayey nannofossil ooze. Based on linear interpolation between the last appearance of *Pseudoemiliania lacunosa* at 94.48 mbsf and the reentrance of *Truncorotalia crassaformis hessiot* at 133.52 mbsf, the age of this event at Holes 1063B and 1063C corresponds to 0.50 and 0.51 Ma, respectively (see “Biostratigraphy” section, this chapter).

Subunit IB

Intervals: 172-1063A-19H-4, 10 cm, through 30X-4, 128 cm (170.8–269.6 mbsf); 172-1063B-19H-2, 40 cm, through 30X-6, 120 cm (169.9–274.3 mbsf); 172-1063C-19H-6, 60 cm, through 24H-CC (169.5–212.7 mbsf); 172-1063D-19H-7, 150 cm, through 19H-CC (171.2–173.1 mbsf)

Age: early Pleistocene to latest Pliocene

The major distinguishing features of Subunit IB are the disappearance of biogenic silica as a lithologic accessory and a sharp reduction in the number and extent of red lutite beds (Fig. 1). This subunit is dominated by a medium light olive gray (5Y 5/1) to greenish gray (5GY 6/1) clay with variable proportions of silt and nannofossils. Occasionally, the nannofossil content increases to a light greenish gray (10GY 8/1) or medium-light greenish gray (10GY 6.5/1) nannofossil clay mixed sediment. It can be difficult to define the upper boundary for Subunit IB by lithologic analysis because the base of the deepest biogenic silica-bearing bed defines this boundary. To remedy this, an

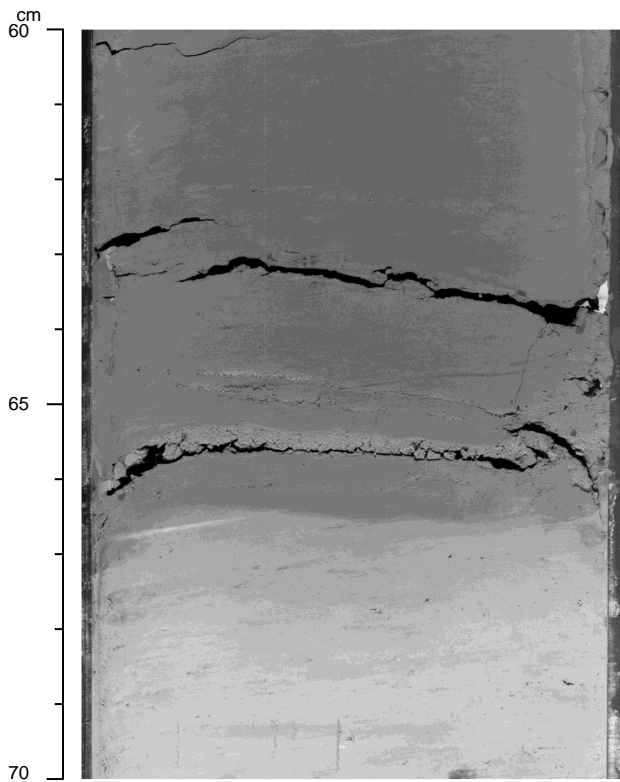


Figure 2. Close-up photograph of silt laminae interbedded with clay (interval 172-1063B-11H-6, 60–70 cm). The contact with the next lower bed (clayey nannofossil ooze) is scoured and marked by an abrupt color change from grayish brown (10Y 5/2) to yellowish gray (5Y 8/1).

abrupt drop in natural gamma radiation in Hole 1063A was used to mark the top of Subunit IB (see “Physical Properties” section, this chapter).

Subunit IC

Intervals: 172-1063A-30X-4, 128 cm, through 45X-CC (269.6–418.8 mbsf), and 172-1063B-30X-6, 120 cm, through 38X-CC (274.3–351.6 mbsf)
 Age: latest Pliocene to middle Pliocene

Subunit IC at Site 1063 contains medium-dark greenish gray (5GY 5/1) clay with silt, medium-light greenish gray (5GY 7/1) clay with nannofossils, and light greenish gray (10GY 7/1) nannofossil clay. The first two lithologies constitute the background sediment, and the more carbonate-rich nannofossil clay appears sporadically in beds less than 100 cm thick. The most obvious lithological change is the disappearance of reddish brown intervals, which are quantified by the color reflectance a*-parameter (Fig. 3). The abundant diagenetic purple to greenish gray color laminae and bioturbation mottling described in Subunit IA are present in Subunit IC, and burrow fills were commonly stretched into thin laminae from XCB drilling. From the “Inorganic Geochemistry” section (this chapter), it appears this subunit is also distinguished by the decrease in the mean calcium carbonate content from 25 to 17 wt%. Discrete sampling, however, may introduce a systematic bias into the carbonate data.

One feature within this subunit, encountered only in Hole 1063B, is the presence of a waxy, yellowish brown (10YR 5/4) amorphous material occupying vertical fractures inside drilling biscuits. These occur in two distinct intervals: interval 172-1063B-30X-1 through 30X-3 (265.5–270.0 mbsf) and interval 1063B-38X-5, 35 cm, through 38X-6, 50 cm (347.44–349.09 mbsf). In the shallower occur-

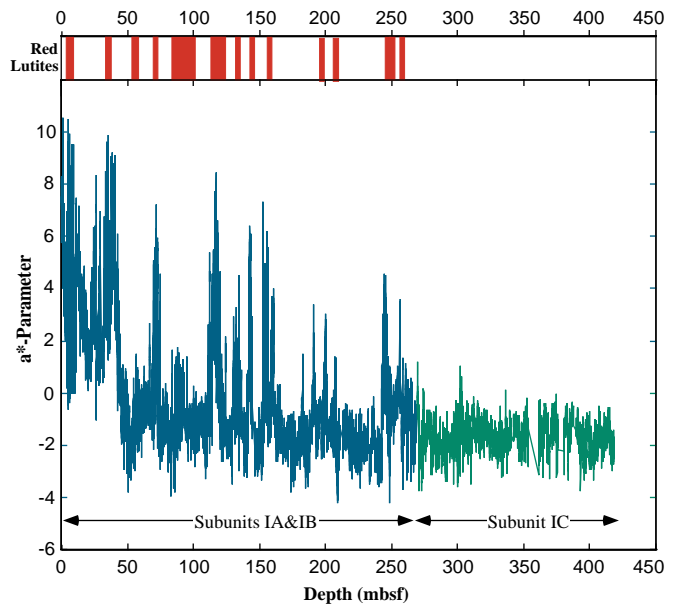


Figure 3. Correspondence of red lutite layers and a*-parameter maxima. Notice the lack of a*-parameter maxima in Subunit IC relative to Subunits IA and IB.

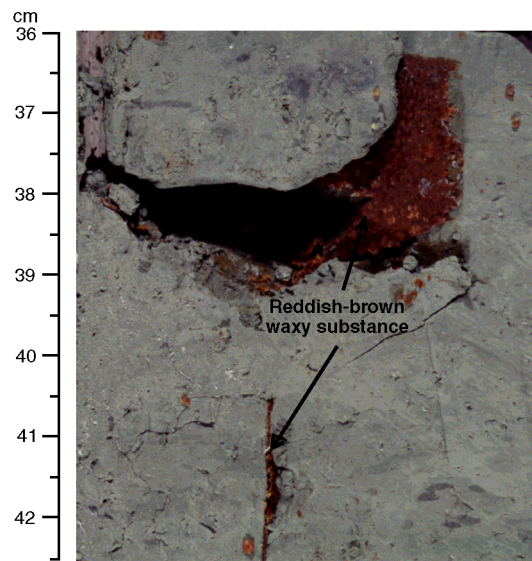


Figure 4. Close-up photograph (interval 172-1063B-38X-5, 36–43 cm) showing a waxy and reddish brown-colored amorphous material concentrated in vertical cracks. A piece of sediment in the upper right corner has been moved to show the face of such a crack. Another crack containing the same material is viewed from the end in the lower part of the figure. Chemical analyses suggest this material contains about 40% organic carbon. For additional information, see “Organic Geochemistry” section, this chapter. A color version is on CD-ROM (back pocket, this volume).

rence the material is softer, stickier, and dusky yellow (5Y 6/4), whereas the deeper specimens are more solid, waxy, and yellowish brown (10YR 5/4) (Fig. 4; color version on CD-ROM, back pocket, this volume). Chemical analysis of a single sample (see “Organic Geochemistry” section, this chapter) from Core 172-1063A-38X has shown it contains about 39% organic carbon, implying the material is a type of thermally degraded kerogen.

Unit I: General Features

Within Subunits IA–IC of Site 1063, several common features were observed in all four holes. In general, Unit I contains between 0.4 and 60.6 wt% carbonate (see “Inorganic Geochemistry” section, this chapter), reflecting variable proportions of clay, biogenic carbonate, and detrital carbonate.

X-ray diffraction data for Hole 1063A are presented in Table 2. Dolomite is present in all of the samples, whereas aragonite is absent. Calcite abundance follows carbonate content (see “Inorganic Geochemistry” section, this chapter), although yielding higher values, and a double peak in the calcite range (~3.03 Å) of the diffractograms suggests the presence of both high and low magnesian calcite. Table 2 also shows that quartz and feldspars are predominant and clay minerals relatively less abundant, suggesting quartz and feldspar comprise much of the clay-size fraction. There are no consistent downcore mineralogical trends among the samples examined. Smear-slide observations show that nanofossils constitute the large part of the calcite, together with accessory amounts of carbonate grains and dolomite rhombs. These accessory components are present in sediments with no biogenic form of calcium carbonate,

suggesting they might be of diagenetic origin, but were also found in the silt laminae (interval 172-1063B-11H-6, 67 cm), supporting a detrital origin.

Throughout Unit I, bioturbation is most apparent at sharp lithologic and/or color transitions. The apparent lack of mottling within the homogeneous intervals may not accurately reflect the bioturbation intensity. Moderate to intense bioturbation is common throughout the entire sediment record. As the most abundant ichnofossils, *Chondrites*, *Planolites*, and *Zoophycos* were noted on the barrel sheets and the Visual Core Descriptions where present.

Interpretation and Discussion

The predominance of clay at Site 1063 is in accordance with the Bermuda Rise being shaped by the advection of abyssal, fine-grained sediments onto the plateau by deep bottom currents (Laine and Hollister, 1981; Laine et al, 1994). However, sediment deposition by mean deep-current circulation patterns will also be subject to episodic modification by benthic storms (Hollister and McCave, 1984) and downslope transportation processes. In contrast to the Blake Outer Ridge, the presence of only one interval on the Bermuda Rise

Table 2. XRD data for Sites 1063 and 1064.

Core, section, interval (cm)	Quartz	K-spar	Plagioclase	Clay	Calcite	Dolomite	Aragonite	Pyrite	Mica group	Hematite	Unit
172-1063A-											
1H-2, 92	51.7	3.2	13.1	9.6	9.2	4.7	0.0	4.4	4.0	0.0	
2H-2, 28	55.9	3.1	12.3	9.3	10.3	4.1	0.0	0.0	5.0	0.0	
2H-2, 81	58.8	2.8	13.9	11.2	6.5	2.1	0.0	0.0	4.8	0.0	
2H-3, 95	53.6	2.9	15.0	7.1	10.3	4.7	0.0	0.9	5.6	0.0	
2H-3, 96	57.3	2.8	12.5	8.9	8.6	2.4	0.0	2.5	4.9	0.0	
2H-4, 136	55.6	3.9	14.5	10.5	4.5	2.6	0.0	3.0	5.5	0.0	
2H-5, 63	55.2	3.2	13.6	10.0	6.7	2.8	0.0	2.2	6.2	0.3	
3H-4, 109	34.5	3.7	13.0	6.5	34.9	4.2	0.0	0.0	3.2	0.0	
4H-3, 86	22.8	1.9	8.1	4.8	53.3	6.2	0.0	0.0	2.8	0.0	
5H-4, 36	44.2	2.6	14.6	10.2	18.1	5.1	0.0	0.0	5.2	0.0	
6H-4, 45	33.0	2.7	14.6	9.6	32.3	4.6	0.0	0.0	3.2	0.0	
7H-4, 83	35.9	1.7	10.9	7.7	34.8	5.6	0.0	0.0	3.4	0.0	
8H-4, 135	11.5	1.6	7.1	3.2	66.1	2.5	0.0	5.8	2.2	0.0	
9H-1, 90	40.7	2.4	11.2	11.0	22.2	7.4	0.0	0.0	5.2	0.0	
10H-3, 99	44.7	2.9	10.2	9.6	23.8	4.6	0.0	0.0	4.1	0.0	
12H-1, 63	10.5	1.3	6.5	4.1	71.5	2.9	0.0	0.0	3.3	0.0	
12H-3, 02	40.7	3.3	17.1	11.5	15.1	7.0	0.0	0.0	5.3	0.0	
13H-6, 59	46.0	2.2	10.9	9.6	18.1	4.7	0.0	0.0	6.4	2.1	
14H-4, 53	48.5	3.3	18.5	8.0	13.8	3.9	0.0	0.0	4.0	0.0	
15H-4, 43	35.1	3.0	11.2	8.0	34.0	4.2	0.0	0.0	4.5	0.0	
16H-5, 86	53.1	3.3	16.4	11.1	6.8	4.7	0.0	0.0	4.5	0.0	
17H-2, 109	24.3	2.1	8.1	9.1	51.0	2.1	0.0	0.0	3.3	0.0	
18H-2, 47	59.0	3.7	15.8	13.2	0.5	2.8	0.0	0.0	5.1	0.0	
19H-1, 50	52.5	4.1	16.3	12.4	1.2	7.0	0.0	1.3	5.1	0.0	
20H-7, 66	46.3	4.6	16.4	8.8	11.9	7.9	0.0	0.0	4.1	0.0	I
21H-4, 45	43.5	3.3	11.2	13.1	17.2	4.7	0.0	0.0	6.9	0.0	
22H-4, 86	34.6	2.9	9.8	7.8	37.9	2.8	0.0	0.0	3.9	0.3	
23X-5, 55	35.5	2.7	5.4	11.3	24.9	2.2	0.0	12.3	5.8	0.0	
24X-1, 50	52.6	4.7	11.8	12.5	5.1	3.0	0.0	3.9	6.4	0.0	
25X-4, 60	48.9	4.3	18.8	8.8	4.1	7.3	0.0	4.4	3.3	0.0	
26X-6, 77	36.8	3.1	15.3	10.0	25.1	3.8	0.0	1.2	4.8	0.0	
27X-5, 110	40.9	3.5	11.8	10.5	22.8	5.6	0.0	0.0	4.8	0.0	
28X-4, 56	26.1	2.4	7.2	6.8	48.3	6.5	0.0	0.0	2.8	0.0	
29X-4, 52	43.1	3.7	8.9	8.2	26.2	6.3	0.0	0.0	3.6	0.0	
30X-3, 54	44.7	3.2	9.7	9.7	21.6	7.2	0.0	0.0	3.8	0.0	
30X-6, 52	19.2	2.0	6.2	6.3	59.4	4.2	0.0	0.0	2.8	0.0	
31X-2, 122	38.5	3.0	11.3	9.3	26.4	7.3	0.0	0.0	4.1	0.1	
32X-4, 56	43.1	5.3	19.4	10.6	10.4	4.8	0.0	2.5	4.0	0.0	
33X-2, 60	51.1	4.5	10.8	8.6	10.2	9.7	0.0	0.0	5.2	0.0	
34X-1, 59	45.2	3.6	11.9	11.1	15.4	8.7	0.0	0.0	4.1	0.0	
35X-6, 96	34.2	2.4	10.4	9.8	33.6	3.4	0.0	0.0	5.9	0.2	
36X-4, 78	15.4	1.9	6.3	6.9	63.1	1.3	0.0	0.0	3.9	1.0	
37X-7, 66	47.8	5.9	16.4	11.7	9.4	3.4	0.0	0.0	5.2	0.2	
38X-1, 91	60.2	4.2	9.8	12.6	1.9	3.0	0.0	1.5	6.6	0.2	
40X-3, 48	46.6	3.5	10.3	12.6	19.1	3.2	0.0	0.0	4.8	0.0	
41X-3, 66	33.5	2.8	6.9	10.4	40.1	2.1	0.0	0.0	4.3	0.0	
42X-3, 85	37.5	2.8	12.3	10.0	30.3	2.2	0.0	1.3	3.5	0.2	
43X-1, 68	39.2	3.3	15.5	10.3	25.3	2.7	0.0	0.0	3.7	0.0	
44X-5, 55	43.2	2.7	10.8	11.9	15.0	1.8	0.0	11.2	3.4	0.0	
45X-4, 92	38.3	3.1	9.6	10.5	31.5	1.4	0.0	1.5	0.0	4.1	
172-1064A-											
1H-2, 103	42.6	3.8	15.0	8.9	21.9	7.7	0.0	0.0	0.0	0.0	I
2H-3, 122	32.0	4.8	17.2	8.0	21.7	4.4	0.0	2.1	8.5	1.3	
3H-2, 58	34.6	4.1	13.6	8.1	22.4	6.2	0.0	2.1	7.9	1.0	

Notes: K-spar = potassium feldspar. All data shown are relative percentiles.

containing silt laminae suggests a lower incidence of high-energy events, although documentation of such events in the sediment record will also be subject to sediment source characteristics.

A unique feature of Subunit IA is the recurrence of intervals with moderate percentages (10%–30%) of biogenic silica, including tests of silicoflagellates, radiolarians, and diatoms. Although all modern water masses are undersaturated with respect to silica, abundant biogenic silica tests can be preserved in the sediment column following saturation of $\text{SiO}_2 \cdot n\text{H}_2\text{O}$ in the pore waters. Although silica is not saturated in the pore waters of Site 1063, high levels of dissolved silica could be reached in a worm burrow micro-environment. Five other mechanisms may explain increases in biogenic silica: (1) enhanced biologic productivity in the upper 200 m of the water column; (2) the predominance of larger, more robust silica-bearing organisms caused by such ecological factors as nutrient supply or sea-surface temperature; (3) ecological changes leading to the predominance of silica-bearing organisms relative to carbonate-secreting organisms (foraminifers, coccolithophores); (4) increased dissolved silica in the bottom-water mass; or (5) increased sedimentation rates.

In the MIS 3 interval of a different Bermuda Rise core, Keigwin and Jones (1994) noted significant biogenic opal during carbonate minima, suggesting the opal may have contributed to the carbonate dilution. During those same events, they found oxygen isotope evidence for substantial surface-water cooling and carbon isotope evidence for reduction in the flux of the lower component of North Atlantic Deep Water (NADW). During such harsh environmental conditions, one may envisage increased wind stress in winter leading to deeper vertical mixing in the Sargasso Sea (Jenkins, 1982; Druffel, 1997) and increased nutrient pumping to surface waters. However, it is not clear that nutrient pumping alone and the resulting increased biological productivity would be sufficient to account for the increased siliceous microfossil content in intervals of Site 1063. First, the Bermuda Rise would have been slightly less corrosive to opaline microfossils if it were bathed by nutrient-rich Antarctic Bottom Water (AABW) during stadial events, but the bottom waters would still have been unsaturated with respect to silica. Second, if MIS 3 carbonate cycles on the Bermuda Rise are related to those of the last glacial maximum and the Holocene (Keigwin and Jones, 1989; Keigwin, 1996), then there may have been times of higher deposition rates as well. Thus, it seems that the occasional presence of abundant opaline microfossils on the Bermuda Rise is most likely a combination of higher siliceous productivity and better opal preservation because of bottom-water circulation change and increased burial rates.

The recurrence of black diagenetic laminae at Site 1063 may have important implications for paleoceanographic or early diagenesis studies. Because they occur as exceptionally sharp laminae in the second core in Holes 1063A–1063D during MIS 2 (inferred from color reflectance and magnetic susceptibility data), we suggest that the black laminae may be features common to glacial periods. The exact mineralogy and organic carbon content of these intervals remains questionable, although multiple XRD analyses on analogous intervals at Site 1060 (see “Lithostratigraphy” section, “Deep Blake-Bahama Outer Ridge” chapter, this volume) and fading color contrasts on exposure to air suggest the presence of metastable troilite. The abundant greenish gray diagenetic laminae at the base of the nanofossil-rich intervals may share a similar diagenetic origin to the black troilite laminae. At Site 1061, the basal laminae are regarded as relic redox boundaries originating from changes in sedimentation rates or organic carbon content at the transition from carbonate-poor to nanofossil-rich intervals.

Finally, the presence of red lutites suggests regional sedimentation processes may affect the lithostratigraphy of the Bermuda Rise. Several features of the Nova Scotian margin and deep-water currents facilitate the transport of sediments to the Bermuda Rise: (1) the voluminous discharge from the St. Lawrence River and estuary creating high sediment loads over the Nova Scotian continental rise (Biscaye et al., 1980); (2) the resuspension of sediments on the margin by fre-

quent abyssal storms promoting downslope transport to the Sohm Abyssal Plain (Hollister and McCave, 1984); and (3) the advection and resuspension of the downslope deposits across the Sohm Abyssal Plain to the northern Bermuda Rise by two deep recirculation gyres (Schmitz and McCartney, 1993). Given the sharp basal contacts, the high recurrence frequency of red lutites in the upper sections (Fig. 1), the distinctive reddish brown color commonly observed in Nova Scotian margin sediments (Piper, 1975; Stow, 1979; Barranco et al., 1989; Keigwin and Jones, 1995), and the homogeneous, very well-sorted lithology, we suggest that the red lutites represent transported, reworked portions of turbidites shed from the Nova Scotian Margin. As suggested by the red lutites of Site 1063, deep circulation patterns and a large sediment supply facilitate the deposition of distal, fine-grained sediments from the Nova Scotian margin on the Bermuda Rise.

Site 1064 Lithostratigraphy

Although coring operations at Site 1064 were terminated early, the three advanced piston corer (APC) cores on the Sohm Abyssal Plain reflect the dynamic patterns of distal abyssal plain sedimentation. The one lithostratigraphic unit is composed of fine-grained slope deposits intercalated with clays of either pelagic or downslope origin (Fig. 5). Despite the shallow penetration at the site, several important links can be made between the sediments of the Sohm Abyssal Plain and the nearby Bermuda Rise.

Unit I

Interval: 172-1064A-1H-1, 0 cm, through 3H-CC (0–28.5 mbsf)
Age: Holocene to late Pleistocene

Unit I consists of alternating reddish brown and brownish gray clay. The reddish brown (10R 4/6) clay typically contains very sharp basal contacts, very fine (<1 mm) silty clay laminae, and exceptionally homogeneous, very well sorted clay. One striking lithologic variation in the reddish brown intervals occurs in Section 1064A-3H-6, where the clay is interbedded with a 31-cm-thick reddish brown sandy silt with clay, and the base of this interval is markedly scoured (Fig. 6). The brownish gray (5YR 4/1) clay consists of sharp and scoured basal contacts, fine (1–2 mm) silty clay laminae, and homogeneous, well-sorted sediment (Fig. 7). XRD analyses (Table 2)

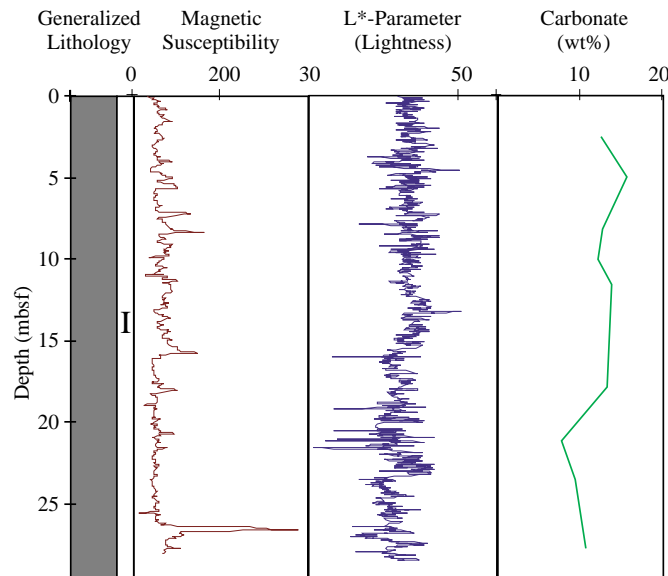


Figure 5. Generalized lithology, magnetic susceptibility, color lightness, and carbonate content for Hole 1064A.

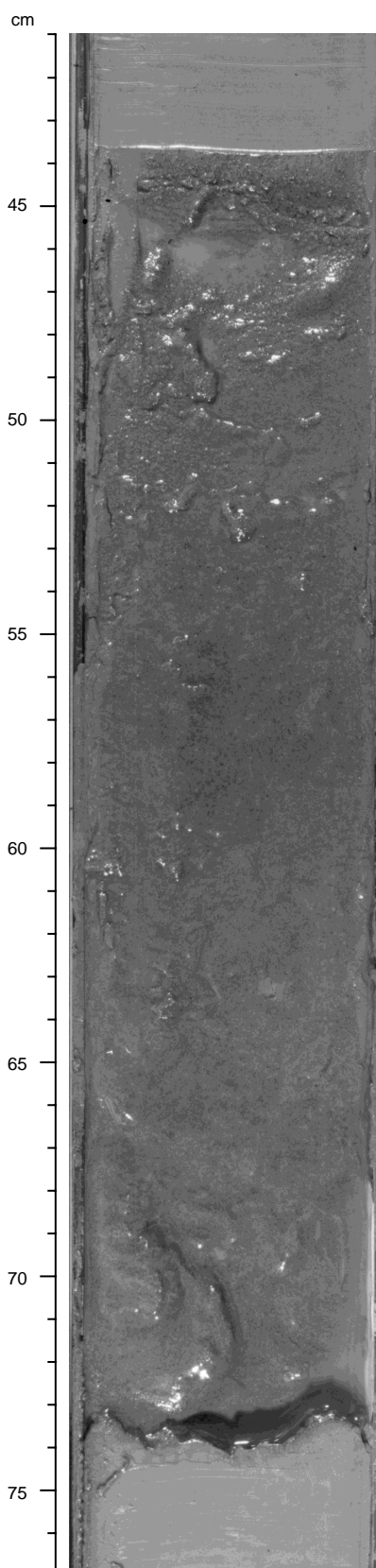


Figure 6. Close-up photograph showing a reddish brown (5YR 5/4) sandy silt with clay with an erosional basal contact and an abrupt upper contact (interval 172-1064A-3H-6, 41–77 cm).

show that Unit I often contains both calcite and dolomite. Biogenic calcite (typically nanofossils) and detrital calcium carbonate grains were observed in the smear slides. Black diagenetic laminae are common to abundant throughout the three cores, and they often occur a few centimeters below the sharp color contacts. Within one hour of core splitting, the black (N3) color of the diagenetic laminae faded to a medium light gray (N7). Iron-stained quartz grains and very fine calcium carbonate grains are present throughout the three cores.

Interpretation and Discussion

The occurrence of thin basal silt laminae, sharp color contacts underlain by black diagenetic bands, and scoured basal contacts suggest that the brown clay intervals represent distal turbidites. These intervals contrast with the high-energy, sandy silt with clay interval originating from either a high-energy event or a source region proximal to the Sohm Abyssal Plain. Whether the reddish brown clay intervals are the result of pelagic sedimentation or a flow deposit remains unclear. Although the reddish brown clays never showed scoured basal contacts, the exceptionally sharp basal contacts and the fine laminations suggest a downslope origin, creating a noteworthy sedimentological link between the red lutites of the Bermuda Rise and the reddish brown clays of the Sohm Abyssal Plain.

BIOSTRATIGRAPHY

Introduction

Biostratigraphic control at Site 1063 was provided by shipboard analyses of calcareous nanofossils and planktonic foraminifers. At Site 1064, no nanofossil or planktonic foraminifer datums were recovered, so there is no age model presented for this hole. Assemblages are dissolved to varying degrees. Carbonate preservation at

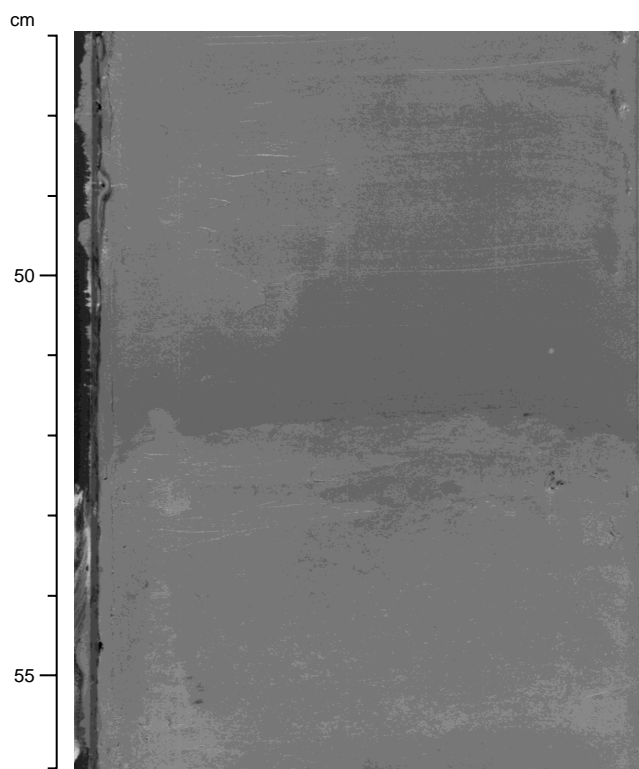


Figure 7. Close-up photograph showing an abrupt upcore color change from pale brown (10YR 6/3) to light olive gray (5Y 6/2) clay with no perceptible grain size variations (interval 172-1064A-2H-5, 47–56 cm).

Site 1064 is occasionally much better than would be expected in 5580 m water depth, possibly because of rapid burial rates associated with sediment transported from the Laurentian Fan. No samples examined at Site 1063 were entirely barren of benthic foraminifers, although some lacked whole planktonic foraminifers. At Site 1064, many samples entirely lacked a >63- μ m fraction. In some intervals at Site 1063, the nannofossil and foraminifer (planktonic and benthic) assemblages are strongly diluted by the terrigenous input. The recovered stratigraphic sequences include the time interval from Holocene to middle Pliocene at Site 1063 (Hole 1063A) and the Holocene to late Pleistocene at Site 1064. The positions of the biohorizons are reported in Tables 3 and 4 and in Figure 8.

Calcareous Nannofossils

The nannofossil biohorizons at Site 1063 were constrained to within a sample spacing of 0.25 to 0.96 m in Hole 1063A, which penetrated to 418 m. The stratigraphic succession recovered represents the interval from the Holocene (interval of *Emiliania huxleyi* acme) to the middle Pliocene (~3.3 Ma, upper range of *Discoaster tamalis*). Calcareous nannofossils were common to abundant in most of the samples analyzed. Their preservation, as well as the input of clay and terrigenous material, varied throughout the section. In some samples, strong dissolution was observed (e.g., within Cores 172-1063A-3H and 11H); other intervals, mainly in the Pleistocene, exhibited mod-

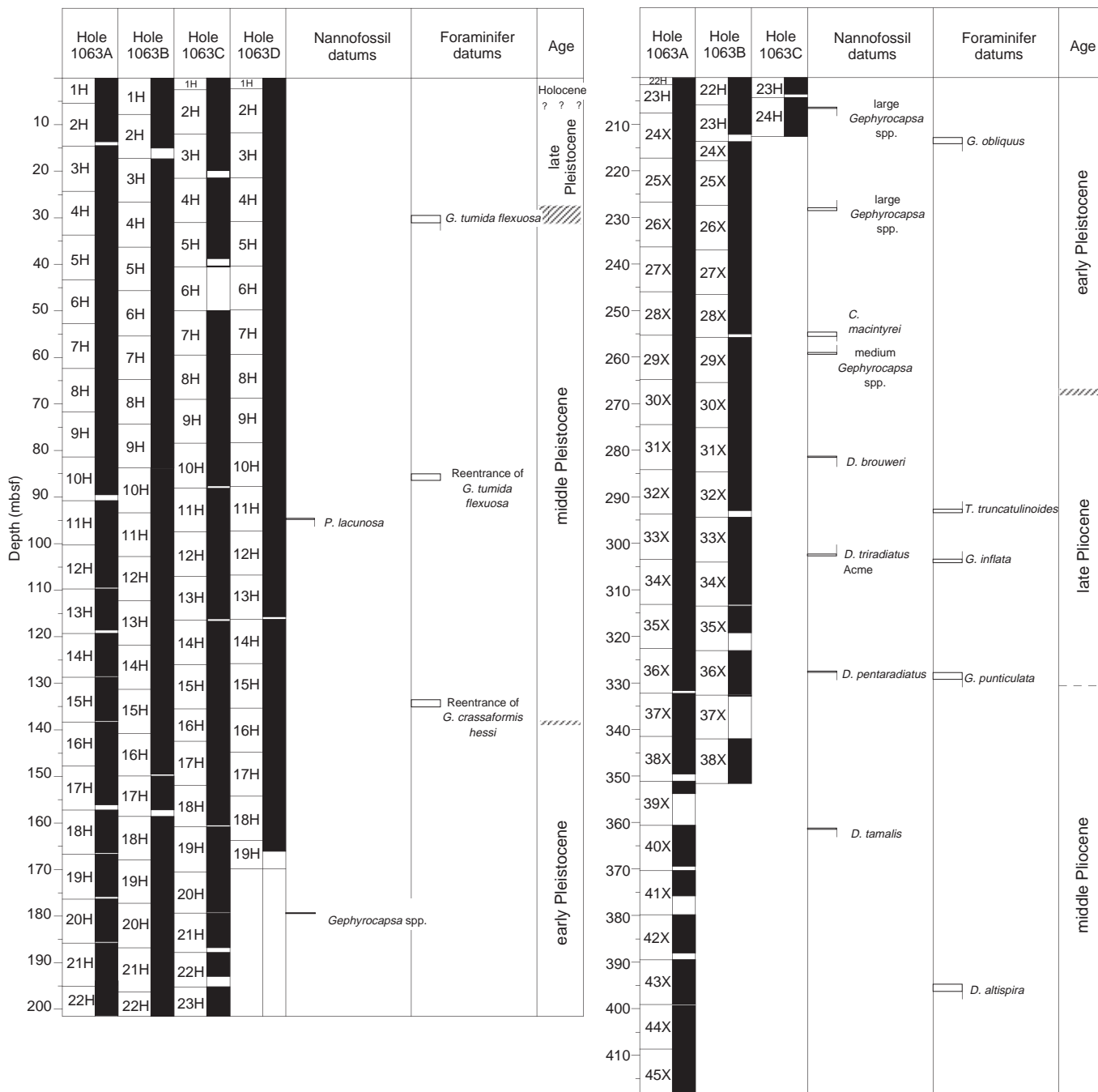


Figure 8. Core recovery and calcareous microfossil datum levels at Site 1063.

erate reworking of Miocene forms. It is impossible to detect and constrain confidently the beginning of the interval of *E. huxleyi* dominance and the first occurrence (FO) of *E. huxleyi* (at 0.085 and 0.26 Ma, respectively) with a light microscope. Consequently, the extinction of *P. lacunosa* within Core 172-1063A-11H was the only nannofossil biohorizon recognized in the middle to upper Pleistocene interval.

The succession of lower Pleistocene and upper Pliocene biohorizons was recognized, and was found to be in good agreement with the age model provided by the detailed paleomagnetic data (Fig. 30). The well-established Pleistocene gephyrocapsid events (see “Carolina Slope” chapter, this volume) were easily constrained in well-preserved and rich assemblages.

The successive extinctions of *Discoaster brouweri*, *Discoaster triradiatus*, *Discoaster pentaradiatus*, and *D. tamalis* identify the upper and middle Pliocene sediments. Note that, in this interval, the abundance of discoasterids was highly variable, and was generally low above the last occurrence (LO) of *D. tamalis*. Despite this fact, it was possible to constrain the interval of abundant *D. triradiatus*; the beginning was observed within the Reunion Subchron, in agreement with its calibration elsewhere (Raffi et al., 1993). The lower part of the sedimentary succession of Hole 1063A, from Core 172-1063A-40X to the bottom of the hole, is within the range of *D. tamalis*. In this interval, discoasterids were abundant and diversified, with the assemblages alternatively dominated by *D. pentaradiatus*, *Discoaster surculus*, *Discoaster asymmetricus*, and *D. tamalis*.

Planktonic Foraminifers

Planktonic foraminifer analyses were confined to Hole 1063A and foraminifer datums were constrained to within 1.5 m, unless dissolution prevented it. One sample per section and the core catchers were examined in Hole 1064A (three cores), but almost no foraminifers were present because of dissolution. In Hole 1063A, preservation of planktonic foraminifers varied from moderate to poor. Numbers of foraminifers in the samples were reduced by both dissolution and dilution and varied from abundant to barren, making it necessary to process at least 20 cm³ of sediment to find a minimum number of foraminifer tests for biostratigraphic studies.

The section recovered at this site spans the interval between the Holocene and the middle Pliocene (Table 3). Preservation of foraminifers is generally moderate to poor at Site 1063 and the datums were subsequently difficult to constrain. Foraminifer numbers were reduced by clay dilution and carbonate dissolution. Several good paleomagnetic reversals were located in Hole 1063A (see “Paleomag-

netism” section, this chapter), and the ages of the biohorizons are assessed largely relative to the age vs. depth relationship established by these events. For a list of the depths of planktonic foraminifer datum levels in Hole 1063A, see Table 3.

The positions of LO and reentrance of *Globorotalia tumida flexuosa* are similar, relative to the magnetic susceptibility record, to those described at previous sites, except that the reentrance of *G. tumida flexuosa* (0.401 Ma) is found at the base of MIS 11 rather than in the transition between MISs 11 and 12. The FO of *Truncorotalia crassaformis hessi* (0.75 Ma) and LO of *Globigerinoides obliquus* (1.3 Ma) were readily constrained in Hole 1063A with 1.5-m resolution. The FO of *Truncorotalia truncatulinoidea* (2.0 Ma) can be defined well enough at this site to use it as a datum, although the event falls below the age vs. depth line determined from the paleomagnetic record. The rare specimens of *Globoconella inflata* that are found below the level that is chosen as its FO (2.15 Ma) extend its range to overlap that of its putative ancestor, *Globoconella puncticulata* (Malmgren and Kennett, 1981; see Table 3). This stratigraphic pattern was also observed at Site 1062. *Menardella exilis* (2.2 Ma), and *M. multicamerata* (3.11 Ma) were not observed at Bermuda Rise, perhaps because of dissolution and dilution. The LO of *Menardella miocenica* could not be constrained to within 1.5 m. The highest specimens were found in Sample 172-1063A-36X-CC, 31–39 cm, but dissolution reduced foraminifer abundance to trace numbers in the lowest two samples in Core 172-1063A-35X. The LO of *G. puncticulata* (2.41 Ma) appears to be useful in this core and was constrained within 1.5 m. The middle Pliocene LO of *Dentoglobigerina altispira* (3.12 Ma) in Core 172-1063A-43X is the deepest datum to be found at this site.

Benthic Foraminifers

Benthic foraminifers were studied in core-catcher samples from Holes 1063A and 1064A. To better constrain the relationship between faunal changes and glacial–interglacial cycles in Hole 1063A, samples from within cores were also examined, with particular attention to the middle to late Pleistocene time interval (top ~160 m). Only a few poorly preserved benthic foraminifers were found in the core catchers of Hole 1064A.

At Site 1063 benthic foraminifers were common to rare and generally well preserved in Pleistocene to Holocene samples, whereas Pliocene samples bore smaller numbers of moderately to poorly preserved specimens.

Species that are common throughout the hole are *Osangularia umbonifera*, *Globocassidulina subglobosa*, *Oridorsalis umbonatus*,

Table 3. Calcareous microfossil datums in Hole 1063A.

Event	ID	Age (Ma)	Core, section, interval (cm)		Depth (mbsf)			Depth (mcd)
			Top	Bottom	Top	Bottom	Mean	Mean
<i>T. G. tumida flexuosa</i>	F1	0.068	4H-4, 70-75	4H-5, 75-80	29.50	31.05	30.28	32.50
Reent. <i>G. tumida flexuosa</i>	F2	0.401	10H-3, 70-75	10H-4, 70-75	85.00	86.50	85.75	93.68
<i>T. P. lacunosa</i>	N1	0.46	11H-3, 68	11H-3 114	94.48	94.84	94.66	103.31
Reent. <i>G. crassaformis hessi</i>	F3	0.75	15H-4, 68-73	15H-5, 68-73	133.52	135.02	134.27	148.17
Reent. m. <i>Gephyrocapsa</i> spp.	N2	1.00	20H-3, 39	20H-3, 70	179.33	179.64	179.49	195.77
T large <i>Gephyrocapsa</i> spp.	N3	1.24	23X-4, 39	23X-4, 70	206.29	206.60	206.45	226.21
<i>T. G. obliquus</i>	F4	1.3	24X-4, 67-76	24X-5, 65-73	212.77	214.25	213.51	234.85
B large <i>Gephyrocapsa</i> spp.	N4	1.58	26X-1, 114	26X-2, 39	227.94	228.69	228.32	250.34
<i>T. C. macintyreii</i>	N5	1.67	28X-6, 114	28X-CC, 60-75	254.64	255.60	255.12	278.30
B m. <i>Gephyrocapsa</i> spp.	N6	1.69	29X-3, 70	29X-3, 114	259.00	259.44	259.22	282.40
<i>T. D. brouweri</i>	N7	1.95	31X-6, 39	31X-6, 64	281.38	281.63	281.51	304.69
<i>B. T. truncatulinoidea</i>	F5	2.0	32X-5, 68-74	32X-CC, 50-65	290.70	293.52	292.11	315.29
Acme <i>D. triradiatus</i>	N8	2.15	33X-6, 114	33X-7, 5	302.44	302.85	302.65	325.83
B (common) <i>G. inflata</i>	F6	2.15	33X-CC, 34-49	34X-1, 69-74	303.37	304.19	303.78	327.10
<i>T. M. miocenica</i>	F7	2.3	36X-4, 67-71	36X-CC, 31-39	327.77	331.44	329.61	356.91
<i>T. G. puncticulata</i>	F8	2.41	36X-4, 67-71	36X-5, 70-75	327.77	329.30	328.54	355.84
<i>T. D. pentaradiatus</i>	N9	2.52	36X-4, 39	36X-4, 67	327.69	327.77	327.73	355.03
<i>T. D. tamalis</i>	N10	2.83	40X-1, 39	40X-1, 69	361.09	361.39	361.24	388.54
<i>T. D. altispira</i>	F9	3.12	43X-4, 70-75	43X-5, 70-75	394.70	396.20	395.45	422.75

Notes: Event abbreviations: T = top, B = base, Reent. = reentrance, m = medium. ID abbreviations: F = planktonic foraminifer datum, N = nannofossil datum. ID numbers correspond to those in Figure 30.

and *Pullenia bulloides*. *Cibicidoides wuellerstorfi* is present in most samples, but there are few specimens.

The recovered succession is characterized by large fluctuations in both benthic foraminiferal abundances and in faunal composition. In the top 160 m, comparison with magnetic susceptibility data indicates that samples with larger numbers of specimens (150 to more than 500 specimens per 20 cm³ of washed sample) were collected in interglacial stages. In these samples the assemblages are dominated by *O. umbonifera*, and *G. subglobosa*; and *Oridorsalis umbonatus* and *Pullenia bulloides* are also common. In some samples *Epistominella exigua*, a “phytodetritus species,” is very abundant, suggesting episodic organic matter input. Glacial intervals are characterized by lower benthic foraminiferal numbers (4 to 50 specimens per 20 cm³) and by the presence of few species, the most common of which are *O. umbonatus*, *C. wuellerstorfi*, and *P. bulloides*.

In the interval between ~160 and 270 mbsf (corresponding to the lower Pleistocene) the most common species are *O. umbonifera*, *G. subglobosa*, *O. umbonatus*, and *Eggerella bradyi*. *Epistominella exigua* is sporadically present with few specimens. The plankton/benthos ratio is lower with respect to the upper part of the hole, and the number of benthic foraminifers per 20 cm³ of sample varies between 4 and 300 through this interval.

The lowermost part of the hole (~270–420 mbsf.) is characterized by the common presence of *O. umbonifera*, *O. umbonatus*, and *E. exigua*. Also, the presence of *Ehrenbergina trigona* is recorded.

In previous North Atlantic studies, high abundances of *O. umbonifera* were consistently correlated with Antarctic Bottom Water. Decreased abundances of this species during middle-late Pleistocene glacial intervals maybe caused by dissolution effects. Corliss and Honjo (1981) showed that *O. umbonatus* and *C. wuellerstorfi* are more dissolution-resistant than *O. umbonifera*.

The large fluctuations in benthic foraminiferal abundances at this site are maybe related, at least for the interval dominated by the 100-k.y. periodicity, either to dissolution cycles or to dilution by increased terrigenous input during glacial stages.

Diatoms

Core-catcher samples from Holes 1063A, 1063B, and 1064A were examined for diatoms (Table 4). The incidence of diatoms in 1063A was confined to the first 12 core catchers. The LO of *Nitzschia reinholdii* is not constrained at Site 1063 because of poor preservation of siliceous material downhole. Thus, the upper 12 cores of 1063A are within the *Pseudoemotia doleolus* Zone (younger than 0.65 Ma; Baldauf, 1984; Barron, 1985).

An interesting aspect of the diatom record at Site 1063 is the correspondence between abundant diatom occurrence and low values in the magnetic susceptibility and bulk density records (see “Physical Properties” section, this chapter). When the bulk density of the sediment is high, diatoms are often absent. This periodic pulsing of diatom occurrence raises some interesting questions about climatic and oceanographic controls on primary productivity and preservation in this area (see “Lithostratigraphy” section, this chapter).

Many of the density “troughs” contain abundant species of *Bacteriastrium* spp. spines, together with whole specimens of other common marine species (*N. marina*, *Coscinodiscus africanus*, *Thalassiothrix* spp, *Thalassionema nitzschioides*, *Thalassionema nitzschioides* var. *parva*, *Asterolampra marylandicus*, and *Thalassiosira oestrupii*). An exception to this general trend of dominance by *Bacteriastrium* spp. spines was noted at 10.04 mbsf (interval 172-1063B-2H-2, 74 cm) and 9.63 mbsf (interval 172-1063A-2H-2, 104 cm), where *Coscinodiscus* cf. *nodulus* is uniquely abundant. The meaning of this change in dominance is unknown at this time.

All three core catchers for the single hole from Site 1064 were barren of diatoms. However, subsampling within Core 172-1064A-2H revealed a few levels with abundant diatoms: 1064A-2H-1, 122 cm, 1064A-2H-3, 39 cm, and 1064A-2H-5, 70 cm.

Table 4. Distribution of diatoms in Holes 1063A and 1064A.

Core, section	Presence of diatoms
172-1063A-	
1H-CC	F - fragments
2H-CC	Barren
3H-CC	A - fragments & whole
4H-CC	Barren
5H-CC	A - fragments & whole
6H-CC	Barren
7H-CC	A - fragments/C - whole
8H-CC	A - fragments/F - whole
9H-CC	F - fragments
10H-CC	F - fragments
11H-CC	Barren
12H-CC	Barren
13H-CC	X - fragments
14H-CC	Barren
15H-CC	X - fragments
16H-CC	Barren
17H-CC	Barren
18H-CC	C - fragments/R - whole
19H-CC	X - fragments
20H-CC	R - fragments
21H-CC	R - fragments
22H-CC	X - fragments
23H-CC	Barren
24X-CC	F - fragments
25X-CC	Barren
26X-CC	Barren
27X-CC	Barren
28X-CC	Barren
29X-CC	Barren
30X-CC	Barren
31X-CC	Barren
32X-CC	Barren
33X-CC	Barren
34X-CC	Barren
35X-CC	Barren
36X-CC	Barren
37X-CC	Barren
38X-CC	Barren
39X-CC	Barren
40X-CC	Barren
41X-CC	Barren
42X-CC	Barren
43X-CC	Barren
44X-CC	Barren
45X-CC	Barren
172-1064A-	
1H-CC	Barren
2H-CC	Barren
3H-CC	Barren

Note: Quantity abbreviations: X = scarce, R = rare, F = few, C = common, and A = abundant.

PALEOMAGNETISM

Introduction

The natural remanent magnetization (NRM) of the archive-half sections from all holes cored at Sites 1063 and 1064 was measured at 5-cm intervals using the pass-through cryogenic magnetometer. After measuring the NRM, most sections were partially demagnetized at 20 mT with the aim of removing overprints to reveal the character of the geomagnetic field changes. A few sections were treated with peak fields up to 60 mT alternating field (AF) to evaluate the demagnetization behavior of the sediments at higher fields. The data for all remanence measurements are given in Tables 5–9 on CD-ROM (back pocket, this volume). Discrete samples were routinely collected from only one hole at Site 1063, with a sampling interval of one per section, or every ~1.5 m. These samples were progressively demagnetized at 5- to 10-mT increments up to 60 mT using the pass-through cryogenic magnetometer.

As mentioned in the previous site chapters, NRM inclinations of the sediments drilled at Site 1063 are also consistently biased toward high positive inclinations (70° to 90°), which is thought to be caused by secondary overprint. This overprint is characterized by steep inclinations and is probably acquired during drilling. At Site 1063, partial demagnetization in peak fields of 20 mT appears to remove most of the overprint for the APC cores at each hole, as evidenced by direc-

tional data downcore (Fig. 9) and demagnetization behavior of discrete samples (Fig. 10). In the XCB-cored intervals, coring disturbance and the overprint complicate the assessment of magnetic polarity from long-core measurements alone. Based on combined discrete and long-core measurements, however, we have been able to reconstruct a reliable polarity stratigraphy through the middle of the Gauss Chronozone at Site 1063. The intensity of magnetization after treatment at 20 mT at both sites covaries proportionally with susceptibility. The intensities vary by up to three orders of magnitude at Site 1063, ranging from 5×10^{-5} to 5×10^{-2} A/m; however, these vary by only one order of magnitude at Site 1064, ranging from 5×10^{-3} to 8×10^{-2} A/m.

Gas Expansion and Coring Disturbance

The cores recovered at Site 1063 suffered low to moderate gas expansion below Core 172-1063A-8H. The routine procedure for reducing core disturbance caused by gas expansion is to drill small holes in the core liner at 20- to 50-cm spacings as soon as the core is brought onto the catwalk. These holes cause the gas to vent so that sediment is not pushed out the ends of the core liner as the gas expands. As a result, the cores often “worm,” meaning that small tubes of sediment extrude through the drill holes as the gas expands. At this and previous sites we were concerned that this extrusion and the resulting gas escape structures might act to degrade the mechanical integrity of the cores and affect the magnetic remanence.

At this site the paleomagnetic marine specialist (M. Hastedt) conducted a blind test in which she recorded the location of each small drill hole and then plotted them for comparison with the remanence measurements for that core. This test was run for Cores 172-1063B-8H through 16H. There appears to be no correlation between either the paleomagnetic directions or intensities and the locations or concentrations of drill holes in the liners. There also does not appear to be a change in the dispersion or scatter of the magnetization directions in the intervals where the core liner was drilled. We conclude from this experiment that, in these sediments, the “worming” sediment (that which is extruded through the small drill holes during the degassing process) involves primarily sediment from the rind of the core, which has already been deformed by the shearing during the piston coring process. The extent of this deformation, however, is likely to be dependent upon lithology, and we recommend that this test be repeated for a range of lithologies exhibiting various magnetization intensities.

Orientation

The Tensor tool was used to orient the APC cores collected from these holes, starting with the third or fourth core at each hole (Table 10 on CD-ROM, back pocket, this volume). The orientation data proved to be successful in aligning the declinations between cores in the majority of cases. As we observed at the previous sites, sharp offsets between some cores suggest that either the Tensor tool did not function properly or that the core twisted or rotated as it entered the core barrel.

Magnetic Polarity Stratigraphy

Only normal polarity directions were recorded at Site 1064 (Fig. 11). A well-defined record of polarity history back to the top of the Gauss Chronozone was obtained from sediments cored at Site 1063 (Fig. 9). Normal and reversed polarity directions are easily identified in the APC cores after partial AF demagnetization at 20 mT. In deeper intervals of the holes, where coring disturbance was greater, and particularly in intervals cored with the XCB, partial demagnetization at peak fields of 30–40 mT was required to define the polarity record. In both cases the characteristic remanent magnetizations (ChRM) of discrete samples exhibit excellent agreement with the

long-core measurements. This sequence of upper Pliocene to Holocene sediments is one of the longest high-sedimentation-rate records of geomagnetic field variability ever obtained in deep-sea sediments.

The depths of the polarity reversals observed in sediments cored at Site 1063 are listed in Table 11. Perhaps one of the most surprising results from this site is the excellent agreement between the long-core measurements of the XCB cores collected from Holes 1063A and 1063B. In spite of the biscuit nature of the cores (see “Lithostratigraphy” section, this chapter), reproducible magnetization directions are observed in the holes.

The Brunhes/Matuyama Polarity Reversal

One of the major difficulties in the study of geomagnetic polarity transitions is assessing the reliability of sediment polarity transition records. There are many processes that may act to bias or produce artifacts in sediment transition records, and for this reason it is important to establish the reproducibility of such records. We made detailed measurements of the magnetizations across the Brunhes/Matuyama reversal as recorded in each of the holes drilled at this site to assess the reproducibility of these records. At each hole we measured this polarity transition zone at 1-cm intervals, and the sections were partially demagnetized using the long-core system at 20, 30, and sometimes 40 mT. The resulting inclination records are shown in Figure 12. The transitional interval spans up to 2 m (138 to 140 mbsf in Hole 1063B), during which the inclinations exhibit remarkably similar behavior in each hole. In particular, the reversal is characterized by a rapid change from negative inclinations to very steep downward (80° – 90°) directions. This change is followed by a return to near-horizontal directions (at 139 mbsf) and then a return again to steep downward directions before settling around full normal polarity values. The reproducible nature of this signal indicates that these sediments contain a high-fidelity recording of transitional field behavior.

Magnetic Field Variability Between Reversals

Paleomagnetic field directional changes that record paleomagnetic secular variation (PSV) are observed in APC cores from Site 1063 within the Brunhes Chronozone on a variety of length scales from 10 cm to more than 10 m. It also appears that reproducible PSV is recorded in the upper Matuyama Chronozone. If composite, reproducible PSV records can be derived from these cores, then this site will provide a unique opportunity to examine geomagnetic field variability during a period of reversed polarity.

Excursions at Site 1063

The paleomagnetic directions recorded at Site 1063 contain 11 of the “plausible” (see “Paleomagnetism” section, “Deep Blake-Bahama Outer Ridge” chapter, this volume, for definition) Brunhes-aged excursions noted at Sites 1060–1063, as well as probably another three to five Matuyama-aged excursions. These records all have anomalous paleomagnetic inclinations (usually negative inclinations) and/or declinations (declination departures more than 90° from the local mean value) and a systematic pattern of directional variability defined by coherent, serially correlated directional changes that fit within the context of the surrounding PSV.

The 11 plausible Brunhes-aged excursions present are 3A, 3B, 5A, 5B, 7A, 8A, 9A, 9B, 11A, 13A, and 14A (notation defined in the previous chapter). Three excursions noted at Sites 1060–1062 (7B, 15A, and 15B) are not present as clear excursions at this site, but distinctive secular variation patterns are present at the times expected from other sites and the excursions may be identified by more complete postcruise paleomagnetic analysis of discrete samples. New plausible excursions noted during occupation of Site 1063 are excursions 3A and 5A. These had been previously noted in one or more

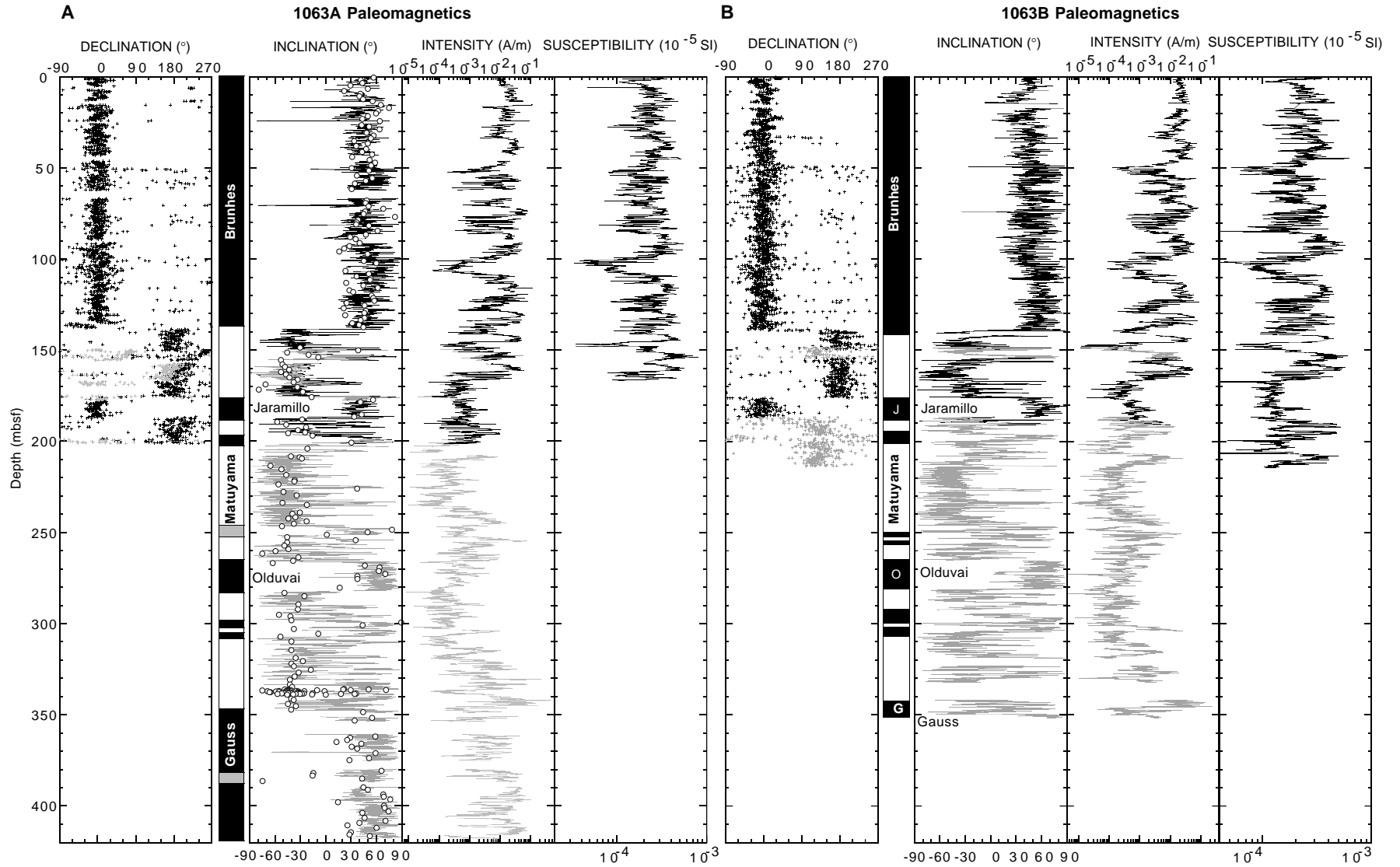
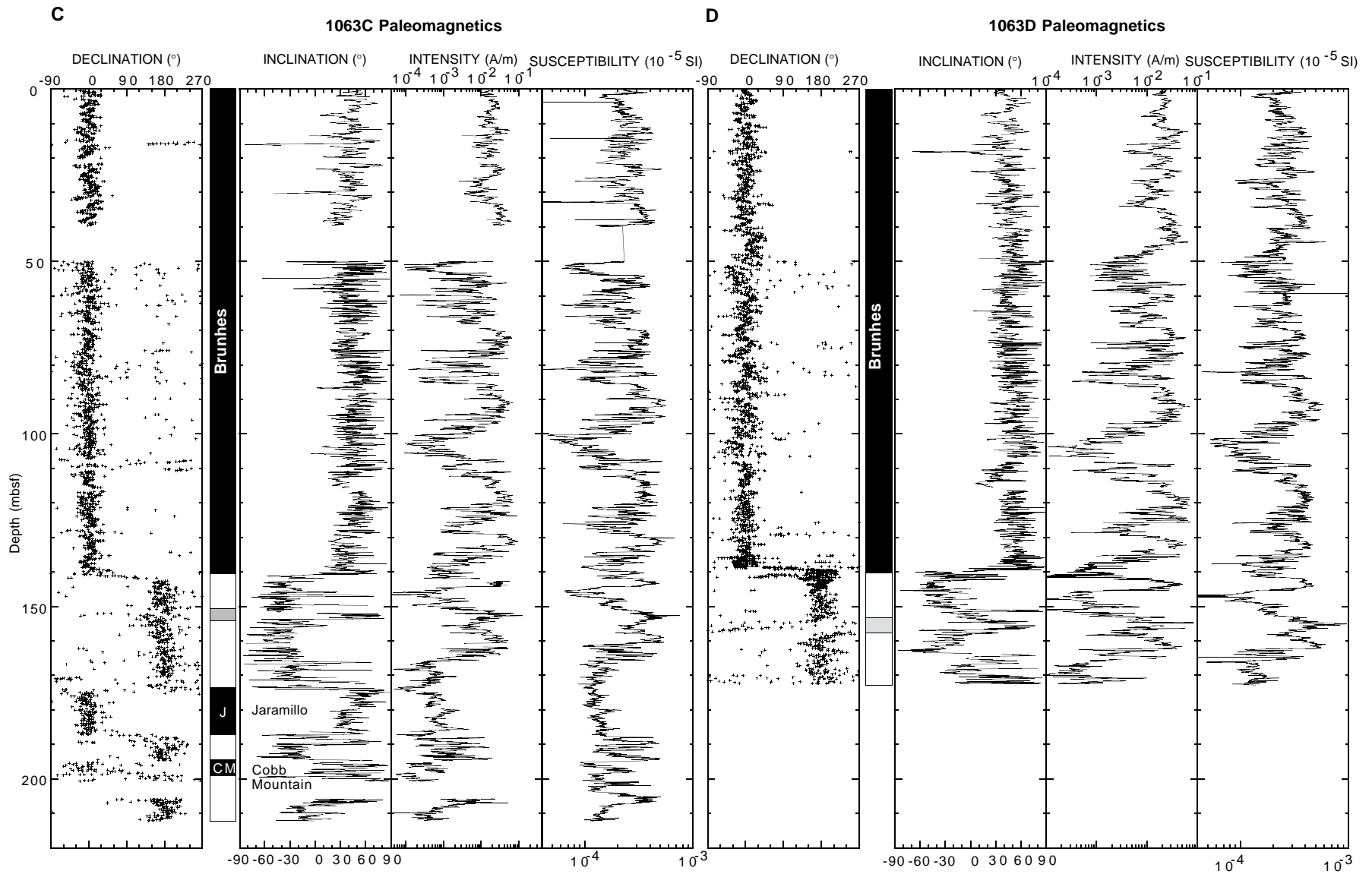


Figure 9. Downhole variation in the remanent magnetization directions after partial AF demagnetization at 20 (black crosses, lines) and 30 (gray crosses, lines) mT from continuous split-core measurements for (A) Hole 1063A, (B) Hole 1063B, (C) Hole 1063C, and (D) Hole 1063D. The open circles in (A) are the ChRM inclinations of discrete samples. J = Jaramillo, O = Olduvai, G = Gauss, and CM = Cobb Mountain.



holes of one or two of Sites 1060–1062, but until they had been seen at Site 1063 as well, we were not certain of their credibility. The importance of these two plausible excursion records is that 3A occurs just after the Laschamp Excursion (3B), at the same time the Mono Lake Excursion (Denham and Cox, 1971; Liddicoat and Coe, 1979) occurs in the western United States. Excursion 3A and the Mono Lake Excursion may be one and the same. Similarly, excursion 5A occurs in the middle of Stage 5 after excursion 5B. One of these (probably 5B) is the Blake Event, but we now consider this interval to have had two probably interrelated excursions.

Excursion records in the Matuyama Chron have not been labeled in any manner because the potential for overprints and other systematic noise make it premature to do so. We see reproducible records of the following excursions/events and subchrons in the Matuyama Chron: (1) at least one excursion/event above the Jaramillo, (2) the Cobb Mountain Event, (3) potentially three excursion/events above the Olduvai Subchron, one of which may be the Gilsa Excursion, and (4) two Reunion Subchrons. If careful analysis and replication with discrete postcruise sampling confirms all of these Brunhes/Matuyama-aged excursions and events, there will have to be a major reassessment of the role of excursions within the context of “normal” secular variation and variability in styles of the core dynamo process.

COMPOSITE DEPTHS AND STRATIGRAPHIC CORRELATION

Multisensor track (MST) and color reflectance data collected for all holes at Sites 1063 and the one hole at Site 1064 (and smoothed over a 31-cm Gaussian window) were used to correlate between individual holes (at Site 1063), to determine depth offsets in the composite section, and to create spliced records. On the composite depth scale (meters composite depth [mcd]), features of the plotted MST and reflectance data present in adjacent holes are aligned so that they occur at approximately the same depth. Working from the top of the sedimentary sequence, a constant was added to the depth (mbsf) for each core in each hole to arrive at a composite depth (mcd) for that core. Spliced records were created by combining intervals of the individual composite depth sections to create an overall stratigraphic section. Intervals having significant disturbance or distortion were avoided if possible. This information, along with the offsets suggested for individual core sections, can be used as a sampling guide to recover a single sedimentary sequence and to identify variability in cored records between sites.

A spliced record was created for Site 1063, but no spliced record could be created for Site 1064. To enable correlation with other sites, data from Site 1064 are plotted on the same scales used at other sites, but with no depth offset. The depth offsets used to construct the composite depth and spliced records at Site 1063 are given in Tables 12 and 13. Affine and splice tables appropriate for use in the Splicer program are on CD-ROM (back pocket, this volume). The integrity of the recovered sedimentary sequence at Site 1063 could be documented to ~232 mcd (~213 mbsf). As at other sites, there are intervals where precise correlations are difficult to make because of nearly constant magnetic susceptibility and sediment color. After detailed correlations were re-established deeper in the core, minor variations in susceptibility and/or color within the previously questionable intervals could be correlated between holes.

Magnetic susceptibility, the color indexes lightness (L^*) and chromaticity (a^* and b^*), and gamma-ray attenuation porosity evaluator (GRAPE) density were the primary parameters used for inter-hole correlation. Gas expansion was noticeably reduced at this site compared to others, and GRAPE provided useful, correlatable signals to ~180 mcd [~167 mbsf]), although it became noisier near the bottom of the interval. Natural gamma-ray measurements were not systematically made in all holes and were not used for correlation. P -wave velocity measurements were of high quality in the uppermost portion of the site (to about 50 mbsf), but they were not used for mak-

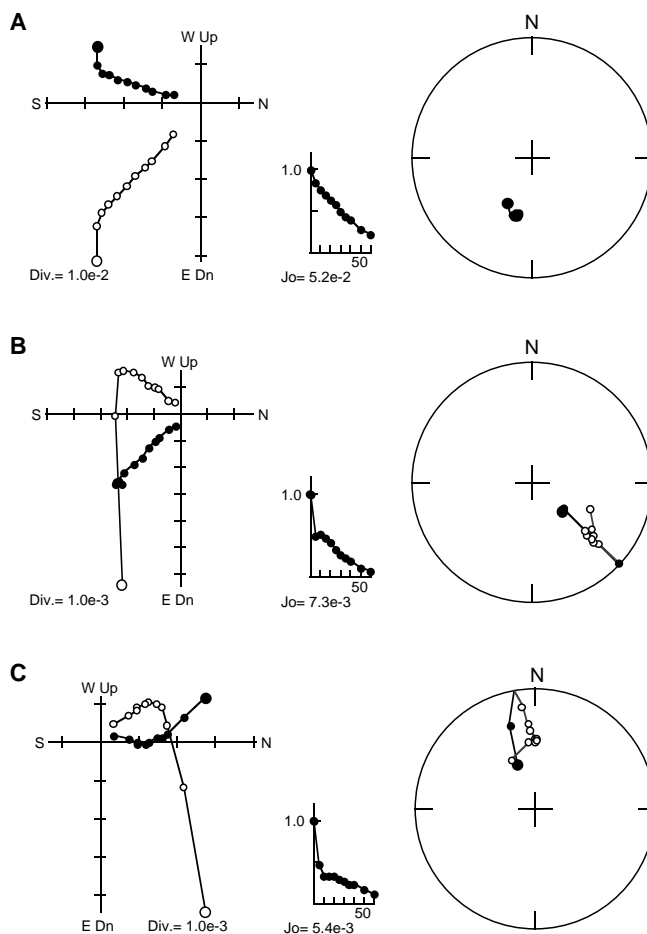


Figure 10. Examples of progressive AF demagnetization of discrete samples taken from Hole 1063A. **A.** 172-1063A-10H-4, 81 cm (86.7 mbsf). **B.** 172-1063A-18H-7, 63 cm (166.5 mbsf). **C.** 172-1063A-33X-2, 80 cm (296.1 mbsf). A steep downward component is removed by treatment of 5 to 20 mT, isolating well-defined characteristic remanence magnetizations.

ing the correlation. The GRAPE records were used to identify voids (values $<1.20 \text{ g/cm}^3$), and GRAPE data from these intervals were not used. No allowance was made, however, for core expansion resulting from large gas voids, decompression, or distributed small gas voids. Within the Splicer computer program, cores can only be shifted as a whole, even where hiatuses are thought to exist within a core. More precise correlation between holes will necessarily be undertaken post cruise based on additional data. Correlation will also be possible between logging and spliced data at Site 1063.

The magnetic susceptibility, GRAPE, and color index (L^* , a^* , and b^*) records used to verify overlap are shown on a composite depth scale in Figures 13–17 for Site 1063. The data used for correlation for each hole (with composite depths) and the spliced data for each site are on CD-ROM (back pocket, this volume). Figures 18–22 show an expanded portion of the spliced record at Site 1063 (from 30 to 80 mcd). Similar data (although unsmoothed) are shown on Figures 23–27 for Site 1064, although, as noted above, insufficient data were available to make a spliced record. A summary of all the splice records at Site 1063 is shown in Figure 28.

Site 1063

The magnetic susceptibility, lightness L^* , chromaticity parameters a^* and b^* , and GRAPE density (in some intervals) appear well correlated among Holes 1063A through 1063D, and a composite section is based on four holes to ~190 mcd and on three holes to ~230

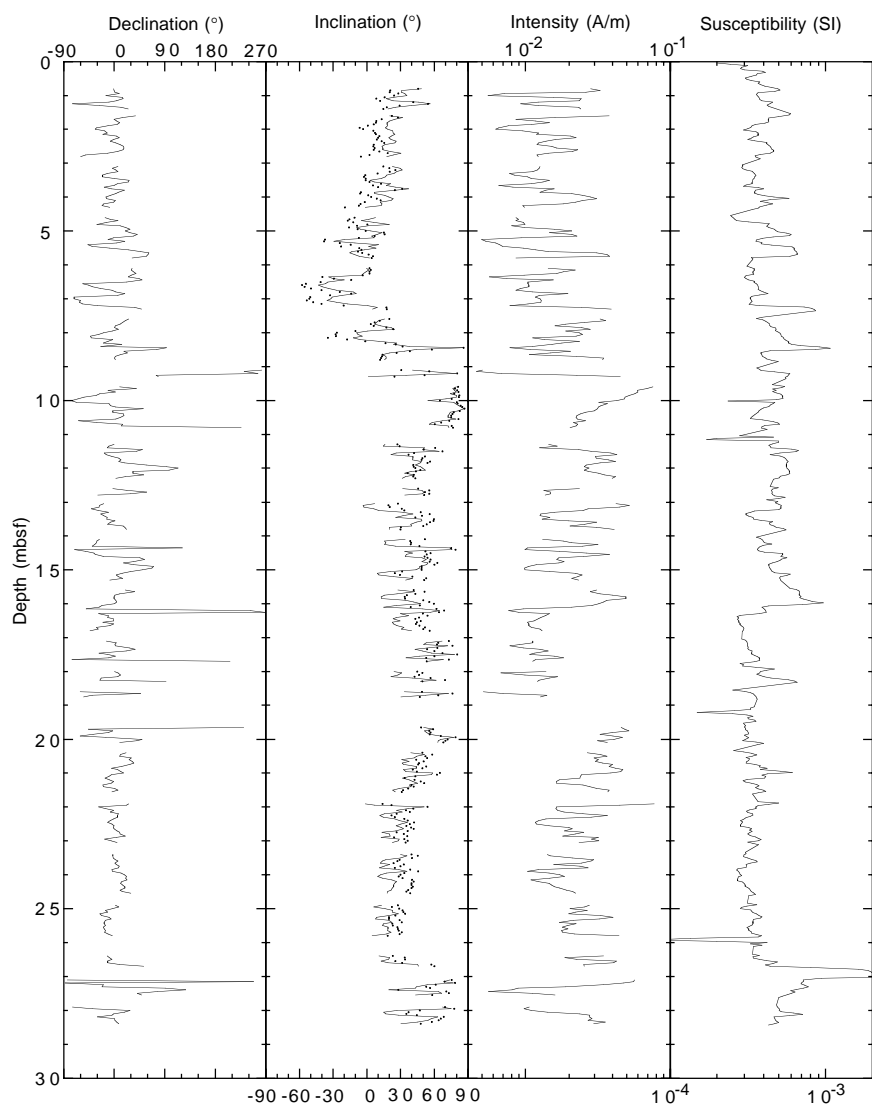


Figure 11. Downhole variation in the remanent magnetization directions measured after partial AF demagnetization at 20 mT using the long-core system for Hole 1064A.

mcd. Correlation can be made for some depths in the interval cored in two holes, but continuous overlap cannot be established.

Correlation between holes in the APC region was more complex at this site than at other Leg 172 sites, in spite of the generally simple lithological variations, for two reasons. First, Hole 1063A was cored when there was considerable wave motion, and some intervals of flow-in were described in the cores. In some cases, flow-in even occurred within a core (e.g., Core 172-1063A-8H). There are also other instances in Hole 1063A and at least one in Hole 1063D where a core appears stretched with respect to core from other holes in the same depth interval, but where no flowed sediment was described. These are interpreted as intervals of mechanically extended sediments, although the degree of extension is less than a few meters. Second, the Minolta calibration (lightness and chromaticity) in the upper seven cores of Hole 1063D appears to be incorrect, as the lightness appears too low and the a^* and b^* appear amplified. This miscalibration occurred in spite of repeated calibration runs within the depth interval. However, the overall patterns in all three parameters appear correlatable between holes even though the actual values are not similar, suggesting that the Hole 1063D data can be recalculated post cruise based on the values measured at correlated levels in other holes. For these reasons, the spliced record is mostly created from the records of Holes 1063B and 1063C in the upper part of the hole. A 46-cm portion of Hole 1063D was used in the splice at about 15 mcd, a level sampled only in the 1063D hole, and the spliced L^* , a^* , and b^*

records show an offset at this depth. Hole 1063A was used in the splice where its pattern was not anomalous, and except for the interval noted above, Hole 1063D was avoided in the upper part of the core. As a result of core expansion, the composite depth scale (mcd) is on average ~8% larger than drilled depths (mbsf) at this site to ~325 mbsf ~355 mcd; Fig. 29). Deeper than ~325 mbsf in Hole 1063A, the offset remains constant at ~2 m. Hole 1063A was logged for its entire depth interval, and postcruise correlations between cored sediment and logs, especially bulk density, natural gamma, and, to a lesser extent, lithology should provide additional information about correlating composite depths to absolute depths.

The high degree of similarity among holes at Site 1063 allowed the recognition of a ~15-m-depth interval (from ~55 to 70 mcd [~50 to 65 mbsf]) where there was an unusual correlation pattern (Figs. 18–22). GRAPE, lightness, and chromaticity b^* showed very good correlation among holes throughout this interval, and high L^* values suggest an interglacial interval at ~54–62 mcd. However, while magnetic susceptibility and chromaticity a^* show some similar patterns between holes, the degree of correlation is not as good as for the other parameters. The poor correlation of magnetic susceptibility and a^* between holes in this depth interval is made more obvious by the much higher degree of correlation both immediately shallower and deeper than this interval.

Although magnetic susceptibility and a^* do not correlate well between holes in this depth range, they do correlate fairly well to one

Table 11. Polarity reversal boundaries observed at Site 1063.

Core, section, interval (cm)	Age (Ma)	Depth* (mbsf)	Reversal
172-1063A-16H-1, 25	0.78	138.50	Brunhes/Matuyama
19H-7, 0	0.99	175.00	Jaramillo top
21H-2, 20	1.07	187.30	Jaramillo base
22H-2, 60	1.201	196.60	Cobb Mountain top
22H-5, 130	1.211	201.30	Cobb Mountain base
30X-2, 10	1.95	265.90	Olduvai top
31X-6, 120	1.77	282.20	Olduvai base
33X-4, 0	2.14	298.30	Reunion top
34X-3, 60	2.15	307.10	Reunion base
38X-5, 20	2.581	347.70	Gauss (top)?
172-1063B-15H-6, 80	0.78	139.60	Brunhes/Matuyama
19H-6, 40	0.99	175.70	Jaramillo top
21H-1, 5	1.07	186.85	Jaramillo base
21H-7, 60	1.201	196.40	Cobb Mountain top
22H-3, 105	1.211	200.35	Cobb Mountain base
29H/30H break	1.95	265.50	Olduvai top
31X-4, 150	1.77	281.10	Olduvai base
33X-1, 120	2.14	295.60	Reunion top
34X-1, 10	2.15	304.10	Reunion base
38X-6, 120	2.581	349.79	Gauss (top)?
172-1063C-16H-4, 85	0.78	140.85	Brunhes/Matuyama
20H-5, 80	0.99	174.05	Jaramillo top
21H-7, 95	1.07	187.21	Jaramillo base
23H-1, 10	1.201	195.30	Cobb Mountain top
23H-2, 140	1.211	198.10	Cobb Mountain base
172-1063D-16H-3, 142	0.78	139.72	Brunhes/Matuyama

Note: * = reversal depths given are the midpoints of the polarity transition intervals.

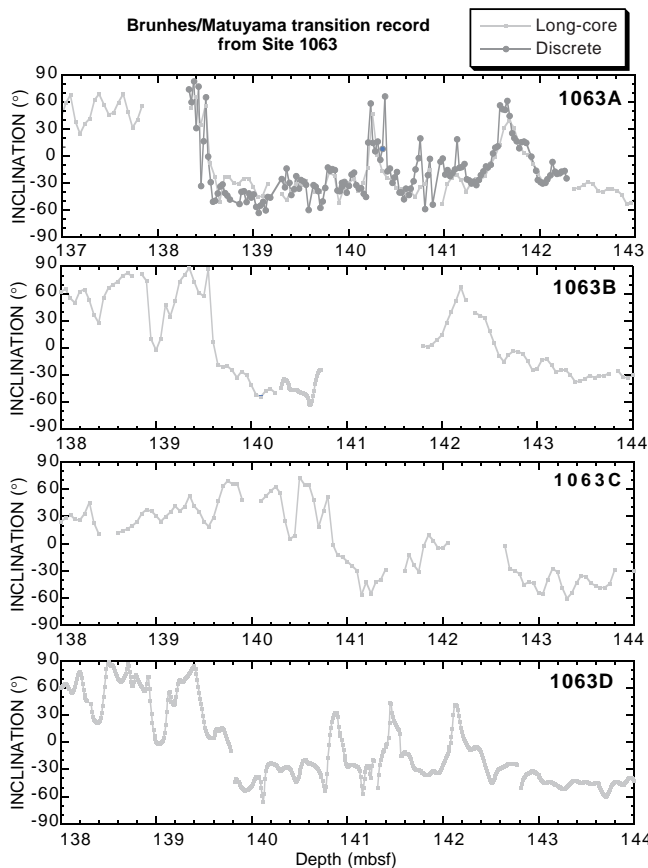


Figure 12. Detailed inclination records of the Brunhes/Matuyama polarity transition recorded in Holes 1063A–1063D.

another, with oscillations in a^* occurring along with oscillations in magnetic susceptibility (increased a^* corresponding to increased magnetic susceptibility). Immediately deeper and shallower than the anomalous interval, there are large variations in a^* that do not correlate closely with large changes in magnetic susceptibility. The parameter a^* generally indicates red sediment color when positive, and red sediment has been described in the anomalous interval. Also, sediment is often red because of the presence of ferric iron oxides. Thus magnetic susceptibility and red probably both vary along with the presence of red ferric iron oxides. The lateral variability of ferric oxide concentration is unusual, and is most likely due to lateral variability in reducing conditions, which have converted the ferric iron oxides into less magnetic ferrous iron oxides. Similar small-scale fluctuations in magnetic mineral abundance and red coloring (a^*) may be present at other levels in the core, but they may be more difficult to identify because of the higher ferric iron oxide concentration.

Site 1064

Although no stratigraphic correlations could be undertaken on the one hole at Site 1064, the unshifted, unsmoothed data are shown in Figures 23–27. The color data confirm the observation of alternating fine-grained sediment units, sometimes graded, with distinctly different colors. These layers appear to represent individual fine-grained turbidites (and one coarser-grained turbidite) on the distal Sohm Abyssal Plain.

Discussion

The cores from three holes at Site 1063 appear highly correlated through the interval cored by the APC and into the interval cored by the XCB, and will provide material suitable for high-resolution climatic and sedimentological studies. However, some core sections, particularly in Hole 1063A, show a record that is expanded with respect to similar depth intervals in the other holes. This lateral change appears to be related to mechanical coring difficulties rather than to lateral variations in sediment thickness. An unusual organic substance was recovered from Cores 172-1063A-30X and 38X (see “Lithostratigraphy” and “Organic Geochemistry” sections, this chapter). Based on stratigraphic correlation, the sediments in Hole 1063A corresponding to these observations are Cores 172-1063B-30X and 38X, but shipboard evaluation of the core photographs does not show whether similar materials were present in those sediments. Also, the high degree of correlation among holes at Site 1063 provides insight into the role of reduction diagenesis on red sediment and magnetic mineral abundance. Spliced records from all sites are plotted on the back-pocket foldout, this volume (Fig. 26, “Carolina Slope” chapter, on the back pocket of this volume; Fig. 27).

SEDIMENTATION AND MASS ACCUMULATION RATES

For Hole 1063A, an average rate of sediment accumulation is calculated through six intervals between the top of the section and the top of the Kaena Subchron. Several paleomagnetic reversals were identified with confidence at Site 1063 (see “Paleomagnetism” section, this chapter) and used as tie points in Figure 30. In addition, one foraminifer and two nannofossil events are used. No dramatic change in sediment accumulation is apparent at the Bermuda Rise after the middle Pliocene onset of large-scale Northern Hemisphere glaciation at ~2.7 Ma (Shackleton et al., 1984), perhaps because the Pliocene ice sheet grew gradually larger over ~500 k.y. before the first major glaciation (Keigwin, 1987; Raymo et al., 1989).

Average sediment accumulation rates in Hole 1063A are comparable in scale and pattern to those calculated at Site 1061 on BBOR, except that the increase to rates above 10 cm/k.y. takes place earlier

Table 12. Site 1063 composite depth section.

Core, section	Depth (mbsf)	Offset (m)	Depth (mcd)	Core, section	Depth (mbsf)	Offset (m)	Depth (mcd)
172-1063A-				19H-1	167.80	13.10	180.90
1H-1	0.00	0.00	0.00	20H-1	177.30	13.02	190.32
2H-1	5.30	0.86	6.16	21H-1	186.80	15.93	202.73
3H-1	14.80	1.68	16.48	22H-1	196.30	18.31	214.61
4H-1	24.30	1.86	26.16	23H-1	205.80	18.03	223.83
5H-1	33.80	3.44	37.24	24X-1	213.80	18.83	232.63
6H-1	43.30	3.52	46.82	25X-1	217.80	21.23	239.03
7H-1	52.80	4.46	57.26	26X-1	227.40	22.39	249.79
8H-1	62.30	4.34	66.64	27X-1	237.00	22.39	259.39
9H-1	71.80	4.56	76.36	28X-1	246.60	22.39	268.99
10H-1	81.30	6.00	87.30	29X-1	255.80	24.21	280.01
11H-1	90.80	6.56	97.36	30X-1	265.50	24.09	289.59
12H-1	100.30	7.00	107.30	31X-1	275.10	24.60	299.70
13H-1	109.80	8.46	118.26	32X-1	284.70	25.56	310.26
14H-1	119.30	10.38	129.68	33X-1	294.40	26.62	321.02
15H-1	128.80	11.25	140.05	34X-1	304.00	30.21	334.21
16H-1	138.30	11.28	149.58	35X-1	313.60	30.21	343.81
17H-1	147.80	11.94	159.74	36X-1	323.10	30.21	353.31
18H-1	157.30	11.96	169.26	37X-1	332.70	26.25	358.95
19H-1	166.80	12.68	179.48	38X-1	342.00	31.74	373.74
20H-1	176.30	13.05	189.35	172-1063C-			
21H-1	185.80	14.44	200.24	1H-1	0.00	0.16	0.16
22H-1	195.10	16.51	211.61	2H-1	2.50	1.14	3.64
23X-1	201.40	17.23	218.63	3H-1	12.00	2.82	14.82
24X-1	207.60	19.23	226.83	4H-1	21.50	2.88	24.38
25X-1	217.20	22.29	239.49	5H-1	31.00	3.96	34.96
26X-1	226.80	22.29	249.09	7H-1	50.00	5.06	55.06
27X-1	236.40	23.45	259.85	8H-1	59.50	6.20	65.70
28X-1	246.00	23.45	269.45	9H-1	69.00	5.91	74.91
29X-1	255.30	23.45	278.75	10H-1	78.50	6.32	84.82
30X-1	264.90	23.45	288.35	11H-1	88.00	6.68	94.68
31X-1	274.50	23.45	297.95	12H-1	97.50	7.54	105.04
32X-1	284.10	24.02	308.12	13H-1	107.00	8.60	115.60
33X-1	293.80	24.02	317.82	14H-1	116.50	9.66	126.16
34X-1	303.50	27.17	330.67	15H-1	126.00	10.59	136.59
35X-1	313.10	30.79	343.89	16H-1	135.50	11.06	146.56
36X-1	322.60	31.89	354.49	17H-1	142.40	12.24	154.64
37X-1	332.20	31.89	364.09	18H-1	151.90	12.80	164.70
38X-1	341.50	31.89	373.39	19H-1	160.90	13.22	174.12
39X-1	351.10	31.89	382.99	20H-1	170.40	14.11	184.51
40X-1	360.70	31.89	392.59	21H-1	179.40	15.20	194.60
41X-1	370.30	31.89	402.19	22H-1	187.90	17.02	204.92
42X-1	379.90	31.89	411.79	23H-1	195.20	19.53	214.73
43X-1	389.50	31.89	421.39	24H-1	204.20	20.97	225.17
44X-1	399.10	31.89	430.99	172-1063D-			
45X-1	408.70	31.89	440.59	1H-1	0.00	0.28	0.28
172-1063B-				2H-1	2.30	1.38	3.68
1H-1	0.00	0.20	0.20	3H-1	11.80	0.32	12.12
2H-1	7.80	0.06	7.86	4H-1	21.30	2.24	23.54
3H-1	17.30	2.22	19.52	5H-1	30.80	2.54	33.34
4H-1	26.80	2.88	29.68	6H-1	40.30	4.00	44.30
5H-1	36.30	3.54	39.84	7H-1	49.80	4.58	54.38
6H-1	45.80	5.08	50.88	8H-1	59.30	5.52	64.82
7H-1	55.30	5.38	60.68	9H-1	68.80	5.62	74.42
8H-1	64.80	5.82	70.62	10H-1	78.30	5.54	83.84
9H-1	74.30	5.30	79.60	11H-1	87.80	5.50	93.30
10H-1	83.80	5.98	89.78	12H-1	97.30	6.36	103.66
11H-1	93.30	6.24	99.54	13H-1	106.80	7.31	114.11
12H-1	102.80	7.44	110.24	14H-1	116.30	7.86	124.16
13H-1	112.30	7.94	120.24	15H-1	125.80	9.28	135.08
14H-1	121.80	9.58	131.38	16H-1	135.30	10.74	146.04
15H-1	131.30	10.66	141.96	17H-1	144.80	10.72	155.52
16H-1	140.80	11.00	151.80	18H-1	154.30	10.42	164.72
17H-1	149.80	11.78	161.58	19H-1	163.80	12.61	176.41
18H-1	158.50	12.34	170.84				

at Bermuda Rise (see Fig. 63, “Deep Blake-Bahama Outer Ridge” chapter, this volume; Fig. 30). Before ~2.5 Ma at Site 1063, the average rate of accumulation was 7.4 cm/k.y. Thereafter, sediment accumulation rates generally increased toward the top of the section.

For the past 900 k.y., the mean sedimentation rate calculated from the magnetic susceptibility record was approximately 19 cm/k.y., and reached, as at the other sites, a maximum of 47 cm/k.y. during the past 70 k.y. (Fig. 31; Table 14). The LO of *P. lacunosa* is calculated to be 469 ka, and the Brunhes/Matuyama boundary to be 782 ka.

Calcium carbonate accumulation rates average 2.8 g/cm²/k.y. (Fig. 32; Table 15). They are comparable to those calculated at Site 1062, and are significantly lower than those calculated for sites located on the Carolina Slope (Site 1055) and on the upper portion of BBOR (Sites 1056, 1057, and 1058). Organic carbon accumulation rates average 0.1 g/cm²/k.y, a value comparable to those calculated in

the previous sites of this leg. Calcium carbonate and organic carbon accumulation rates show a wide range of variation, from ~0.1 to 14.2 g/cm²/k.y. (Table 15), and from 0.01 to 0.36 g/cm²/k.y. (Table 16), respectively.

Above the reentrance of medium-sized *Gephyrocapsa* spp. (~0.9 Ma), carbonate fluxes show cyclic, highly variable values that appear to correlate with magnetic susceptibility cycles (Fig. 32). Except for the high fluxes calculated for MISs 2 to 4, which are mainly the result of apparently high sedimentation rates caused by low sediment compaction, the highest carbonate deposition rates (>7 g/cm²/k.y.) occur during interglacial MISs 11, 13, and 17. This statement contrasts with observations based on Th₂₃₀ studies, which show that the carbonate flux to the Bermuda Rise sediments has been relatively constant through glacial and interglacial intervals over the past 130 ka (Bacon and Rosholt, 1982; Suman and Bacon, 1989; Adkins et al., 1997). Or-

Table 13. Site 1063 splice tie points.

Hole, Core, section, interval (cm)	Depth (mbsf)	Depth (mcd)		Hole, Core, section, interval (cm)	Depth (mbsf)	Depth (mcd)
1063A-1H-2, 48.0	1.98	1.98	Tie	1063B-1H-2, 28.0	1.78	1.98
1063B-1H-5, 4.0	6.04	6.24	Tie	1063C-2H-2, 109.0	5.10	6.24
1063C-2H-6, 80.0	10.80	11.94	Tie	1063B-2H-3, 108.0	11.88	11.94
1063B-2H-5, 64.0	14.44	14.50	Tie	1063D-3H-2, 88.0	14.18	14.50
1063D-3H-2, 144.0	14.74	15.06	Tie	1063C-3H-1, 24.0	12.24	15.06
1063C-3H-5, 64.0	18.64	21.46	Tie	1063B-3H-2, 44.0	19.24	21.46
1063B-3H-7, 24.0	26.54	28.76	Tie	1063C-4H-3, 137.0	25.88	28.76
1063C-4H-6, 144.0	30.44	33.32	Tie	1063B-4H-3, 64.0	30.44	33.32
1063B-4H-6, 92.0	35.22	38.10	Tie	1063C-5H-3, 13.0	34.14	38.10
1063C-5H-4, 144.0	36.94	40.90	Tie	1063B-5H-1, 105.0	37.36	40.90
1063B-5H-6, 36.0	44.16	47.70	Tie	1063A-6H-1, 88.0	44.18	47.70
1063A-6H-5, 24.0	49.54	53.06	Tie	1063B-6H-2, 68.0	47.98	53.06
1063B-6H-7, 16.0	54.94	60.02	Tie	1063C-7H-4, 45.0	54.96	60.02
1063C-7H-6, 112.0	58.62	63.68	Tie	1063B-7H-2, 150.0	58.30	63.68
1063B-7H-6, 120.0	64.00	69.38	Tie	1063C-8H-3, 68.0	63.18	69.38
1063C-8H-5, 92.0	66.42	72.62	Tie	1063B-8H-2, 50.0	66.80	72.62
1063B-8H-5, 80.0	71.60	77.42	Tie	1063C-9H-2, 100.0	71.51	77.42
1063C-9H-4, 132.0	74.83	80.74	Tie	1063A-9H-3, 138.0	76.18	80.74
1063A-9H-6, 104.0	80.34	84.90	Tie	1063B-9H-4, 80.0	79.60	84.90
1063B-9H-6, 68.0	82.48	87.78	Tie	1063C-10H-2, 146.0	81.46	87.78
1063C-10H-6, 52.0	86.52	92.84	Tie	1063B-10H-3, 5.0	86.86	92.84
1063B-10H-6, 116.0	92.46	98.44	Tie	1063C-11H-3, 76.0	91.76	98.44
1063C-11H-6, 128.0	96.78	103.46	Tie	1063B-11H-3, 92.0	97.22	103.46
1063B-11H-6, 112.0	101.92	108.16	Tie	1063C-12H-3, 12.0	100.62	108.16
1063C-12H-5, 60.0	104.10	111.64	Tie	1063B-12H-2, 97.0	104.20	111.64
1063B-12H-7, 52.0	111.24	118.68	Tie	1063C-13H-3, 8.0	110.08	118.68
1063C-13H-6, 44.0	114.14	122.74	Tie	1063B-13H-2, 100.0	114.80	122.74
1063B-13H-5, 56.0	118.86	126.80	Tie	1063C-14H-1, 64.0	117.14	126.80
1063C-14H-7, 4.0	125.54	135.20	Tie	1063B-14H-3, 81.0	125.62	135.20
1063B-14H-6, 104.0	130.34	139.92	Tie	1063C-15H-3, 31.5	129.33	139.92
1063C-15H-5, 124.0	133.29	143.88	Tie	1063B-15H-2, 41.0	133.22	143.88
1063B-15H-7, 38.0	140.68	151.34	Tie	1063A-16H-2, 46.0	140.06	151.34
1063A-16H-6, 72.0	145.94	157.22	Tie	1063C-17H-2, 108.0	144.98	157.22
1063C-17H-6, 14.0	150.04	162.28	Tie	1063A-17H-2, 124.0	150.34	162.28
1063A-17H-6, 48.0	154.88	166.82	Tie	1063C-18H-2, 61.0	154.02	166.82
1063C-18H-6, 52.0	159.92	172.72	Tie	1063B-18H-2, 37.0	160.38	172.72
1063B-18H-6, 108.0	167.08	179.42	Tie	1063C-19H-4, 80.0	166.20	179.42
1063C-19H-6, 124.0	169.64	182.86	Tie	1063B-19H-2, 45.0	169.76	182.86
1063B-19H-6, 104.0	176.34	189.44	Tie	1063C-20H-6, 57.0	175.33	189.44
1063C-20H-8, 76.0	178.51	192.62	Tie	1063B-20H-2, 80.0	179.60	192.62
1063B-20H-6, 32.0	185.12	198.14	Tie	1063C-21H-4, 117.0	182.94	198.14
1063C-21H-7, 68.0	186.94	202.14	Tie	1063A-21H-2, 56.0	187.70	202.14
1063A-21H-7, 104.0	195.35	209.79	Tie	1063B-21H-5, 105.0	193.86	209.79
1063B-21H-7, 28.0	196.08	212.01	Tie	1063A-22H-1, 40.0	195.50	212.01
1063A-22H-5, 76.0	200.68	217.19	Tie	1063B-22H-2, 108.0	198.88	217.19
1063B-22H-6, 56.0	204.36	222.67	Tie	1063A-23X-3, 104.0	205.44	222.67
1063A23X-5, 8.0	207.48	224.71	Tie	1063B-23H-1, 88.0	206.68	224.71
1063B-23H-5, 136.0	213.16	231.19	Tie	1063A-24X-3, 136.0	211.96	231.19
1063A-24X-6, 48.0	215.58	234.81	Tie	1063B-24X-2, 68.0	215.98	234.81
1063B-24X-4, 100.0	219.30	238.13	Append	1063B-25X-1, 0.0-0.0	217.80	239.03
1063B-25X-7, 40.0	227.20	248.43	Append	1063A-26X-1, 0.0	226.80	249.09
1063A-26X-4, 68.0	231.98	254.27	Tie	1063B-26X-3, 148.0	231.88	254.27
1063B-26X-7, 40.0	236.80	259.19	Append	1063B-27X-1, 0.0	237.00	259.39
1063B-27X-7, 44.0	246.44	268.83	Append	1063A-28X-1, 0.0	246.00	269.45
1063A-28X-6, 144.0	254.94	278.39	Append	1063A-29X-1, 0.0	255.30	278.75
1063A-29X-7, 36.0	264.66	288.11	Append	1063A-30X-1, 0.0	264.90	288.35
1063A-30X-7, 84.0	274.16	297.61	Append	1063A-31X-1, 0.0	273.49	296.94
1063A-31X-6, 116.0	282.15	305.60	Tie	1063B-31X-4, 140.0	281.00	305.60
1063B-31X-7, 4.0	284.14	308.74	Tie	1063A-32X-1, 61.0	284.72	308.74
1063A-32X-6, 144.0	292.96	316.98	Append	1063A-33X-1, 0.0	293.80	317.82
1063A-33X-5, 52.0	300.32	324.34	Tie	1063B-33X-3, 32.0	297.72	324.34
1063B-33X-CC, 20.0	304.17	330.79	Tie	1063A-34X-1, 12.0	303.62	330.79
1063A-34X-6, 36.0	311.36	338.53	Tie	1063B-34X-3, 132.0	308.32	338.53
1063B-34X-CC, 44.0	313.31	343.52	Append	1063A-35X-1, 0.0	313.10	343.89
1063A-35X-7, 40.0	322.50	353.29	Append	1063B-36X-1, 0.0	323.10	353.31
1063B-36X-CC, 8.0	332.50	362.71	Append	1063A-37X-1, 0.0	332.20	364.09
1063A-37X-7, 124.0	341.39	373.28	Append	1063A-38X-1, 0.0	341.50	373.39
1063A-38X-CC, 28.0	349.20	381.09	Append	1063A-39X-1, 0.0	351.10	382.99
1063A-39X-CC, 8.0	353.68	385.57	Append	1063A-40X-1, 0.0	360.70	392.59
1063A-40X-CC, 16.0	369.28	401.17	Append	1063A-41X-1, 0.0	370.30	402.19
1063A-41X-CC, 24.0	375.50	407.39	Append	1063A-42X-1, 0.0	379.90	411.79
1063A-42X-CC, 20.0	387.07	418.96	Append	1063A-43X-1, 0.0	389.50	421.39
1063A-43X-7, 24.0	398.74	430.63	Append	1063A-44X-1, 0.0	399.10	430.99
1063A-44X-CC, 8.0	408.50	440.39	Append	1063A-45X-1, 0.0	408.70	440.59
1063A-45X-CC, 24.0	418.22	450.11				

ganic carbon fluxes do not show the same variation patterns as the carbonate flux. The highest values ($>1.5 \text{ g/cm}^2/\text{k.y.}$) occur in glacial MIS 6, as well as at MIS boundaries 11/12 and 15/16. This peculiar pattern, showing no distinction between glacial vs. interglacial periods, may be in part caused by shifts of data points during composite-depth scale conversion. A higher sampling resolution is needed to accurately define the cyclicity of organic carbon supply through the gla-

cial-interglacial stages and to compare it with calcium carbonate accumulation rates.

No clear change in biogenic deposition patterns is observed ~900 ka at Bermuda Rise, as was suggested by accumulation rate data collected at previous sites. Below this boundary, calcium carbonate and organic carbon fluxes at Bermuda Rise show fluctuations comparable to those observed in the younger time interval. In particular, carbon-

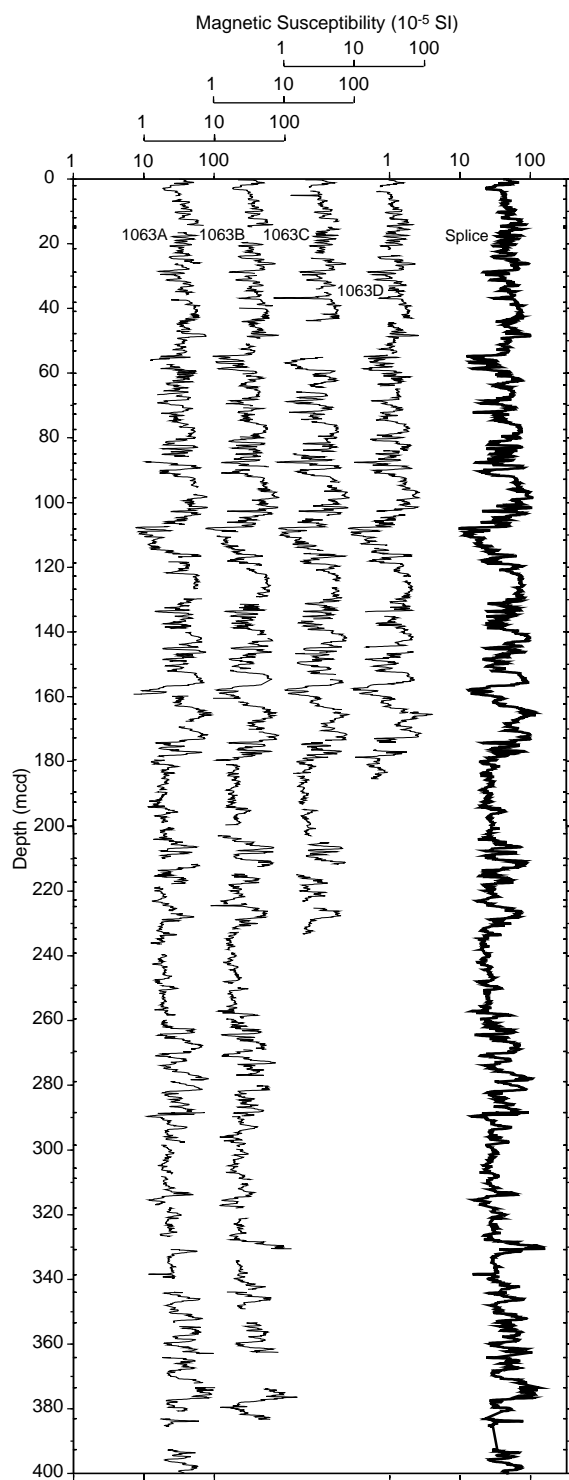


Figure 13. Smoothed magnetic susceptibility data (31-cm Gaussian window; logarithmic scale) from Site 1063 on the mcd scale for Holes 1063A through 1063D and the spliced record.

ate fluxes reach 8–10 $\text{g}/\text{cm}^2/\text{k.y.}$ between 1 and 1.2 Ma and between 1.5 and 2 Ma. Organic carbon fluxes as high as 1.5 $\text{g}/\text{cm}^2/\text{k.y.}$ occur around 1.3 Ma. Once again, variations in calcium carbonate and organic carbon fluxes are not correlative. Before 2 Ma, organic carbon and carbonate fluxes are generally lower and less variable, averaging 2.5 and 0.05 $\text{g}/\text{cm}^2/\text{k.y.}$, respectively.

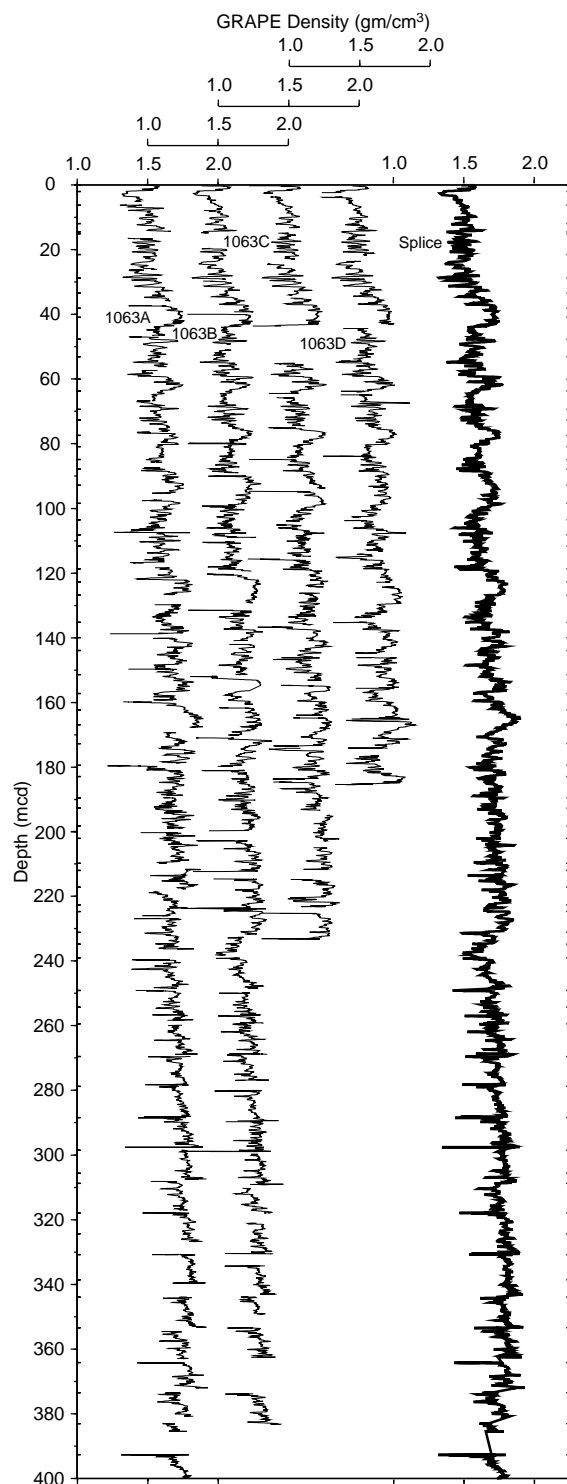


Figure 14. Smoothed GRAPE data (31-cm Gaussian window) from Site 1063 on the mcd scale for Holes 1063A through 1063D and the spliced record.

ORGANIC GEOCHEMISTRY

Routine monitoring of headspace gases was done for drilling safety in at least every core of Holes 1063A and 1064A, located on the northeast Bermuda Rise and the Sohm Abyssal Plain, respectively. Whenever gas expansion voids occurred, the gases were sam-

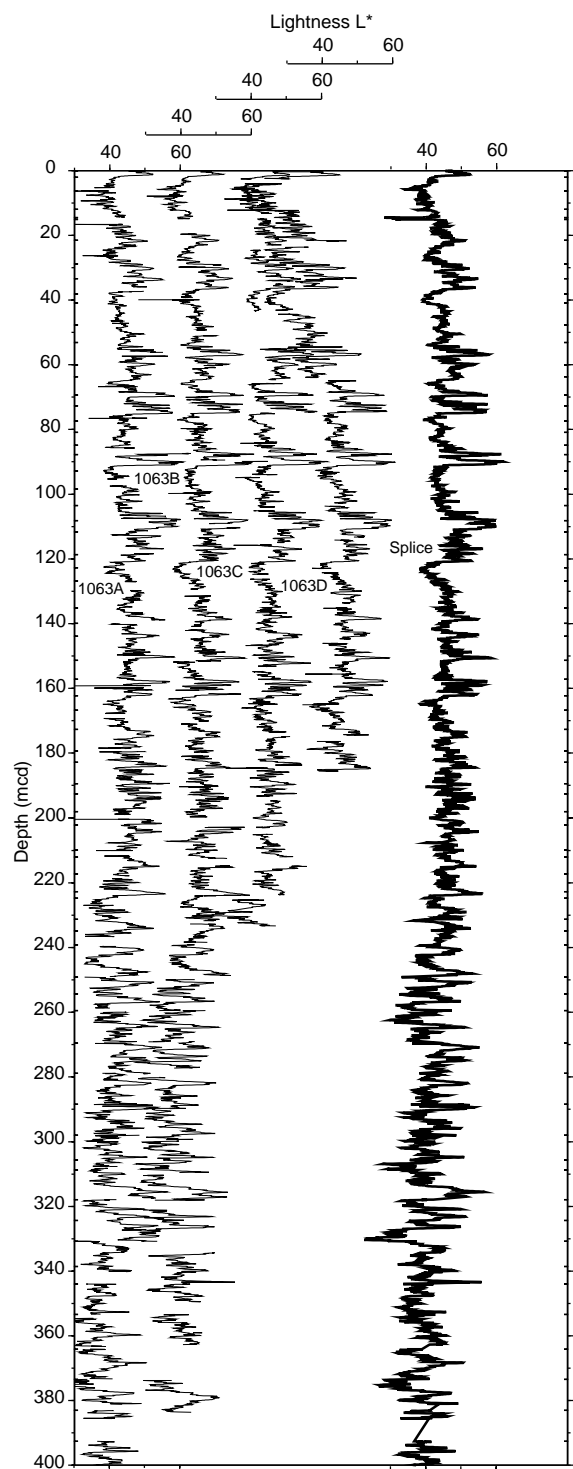


Figure 15. Smoothed lightness (L^*) data (31-cm Gaussian window) from Site 1063 on the mcd scale for Holes 1063A through 1063D and the spliced record.

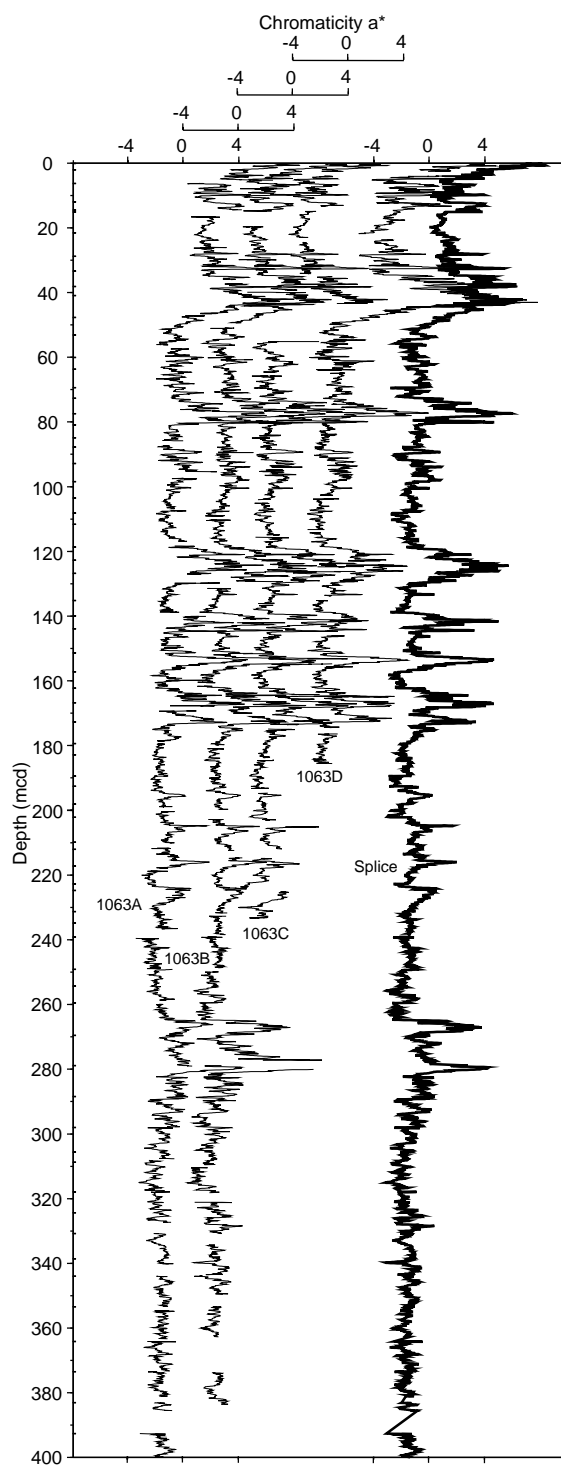


Figure 16. Smoothed chromaticity (a^*) data (31-cm Gaussian window) from Site 1063 on the mcd scale for Holes 1063A through 1063D and the spliced record.

pled using a gas-tight syringe attached to a piercing tool. Calcium carbonate and organic carbon concentrations were also measured on selected samples obtained from all holes. Organic matter atomic C/N values and Rock-Eval analyses were employed to determine the type of sedimentary organic matter. Headspace gas, gas void, carbonate and organic carbon, and C/N values for both sites appear in Tables 17–20, respectively.

Coring operations ended prematurely at Site 1064. Consequently, most data from this site are presented in tables only.

Volatile Gases

Measured concentrations of methane and other low molecular-weight gases generally do not accurately represent in situ concentra-

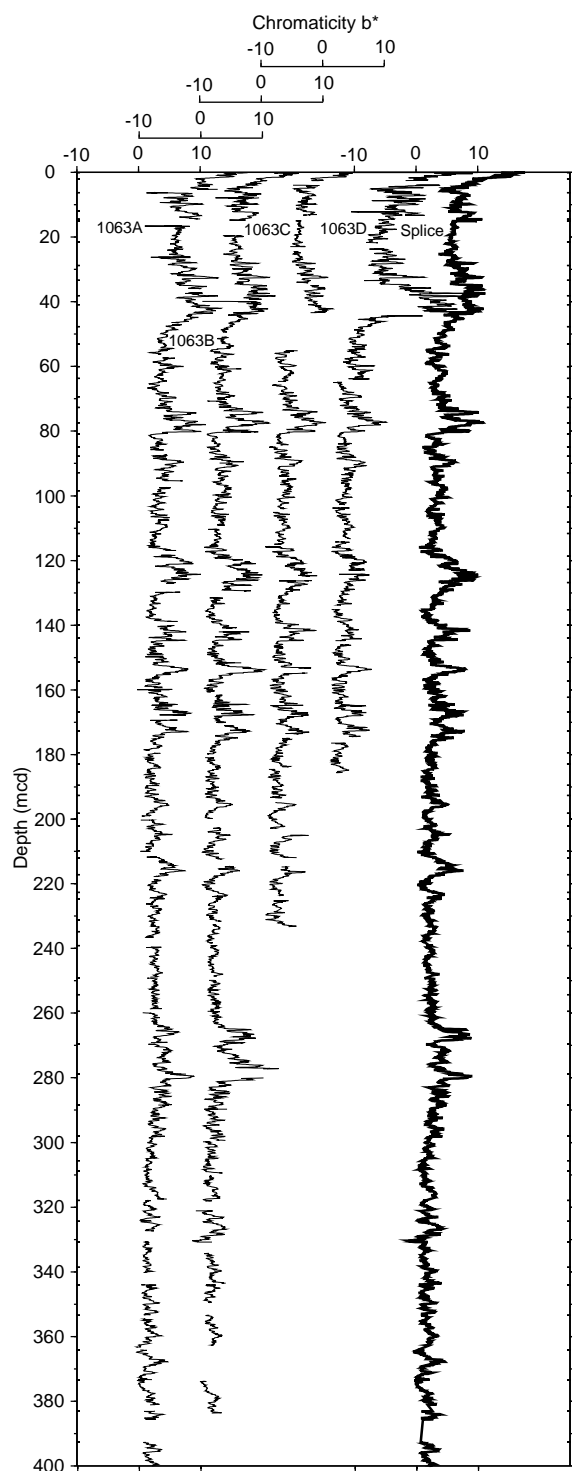


Figure 17. Smoothed chromaticity (b^*) data (31-cm Gaussian window) from Site 1063 on the mcd scale for Holes 1063A through 1063D and the spliced record.

tions (Dickens et al., 1996; see “Organic Geochemistry” section, “Deep Blake-Bahama Outer Ridge” chapter, this volume). However, these measurements are useful for determining relative amounts of the gases, particularly methane-to-ethane ratios (C_1/C_2).

Methane concentrations show the same general profile as those previously observed at the Carolina Slope and Blake Outer Ridge sites. Low concentrations occur above 38 mbsf within the sulfate re-

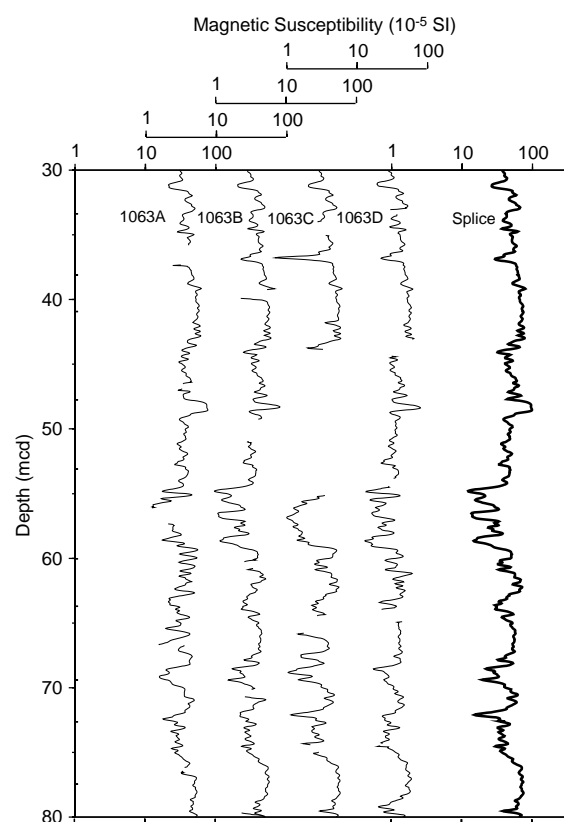


Figure 18. Blow-up of smoothed magnetic susceptibility data (31-cm Gaussian window, logarithmic scale) from Site 1063 for Holes 1063A through 1063D and the spliced record. The magnetic susceptibility data from different holes are highly correlated from ~30 to 55 mcd and from ~70 to 80 mcd, but poorly correlated from ~55 to 70 mcd.

duction zone (see “Inorganic Geochemistry” section, this chapter), and methane begins to increase sharply below the sulfate/methane interface. The highest values occur between ~40 and 195 mbsf, with the maximum value of 62,187 ppm occurring at 126.2 mbsf (Table 18; Fig. 33). Below this methane-enriched interval, methane concentrations generally vary between 10,000 and 22,000 ppm. Ethane generally increases downhole from trace levels at 47.8 mbsf to its highest value of 23 ppm at 384.4 mbsf. Consequently, C_1/C_2 values show a steady decrease downhole from over 10,000 to ~2,000, reflecting rising amounts of ethane. Propane (C_3) is generally found in concentrations of 1–4 ppm.

Gas voids were only observed and sampled at Site 1063. In addition to methane, ethane, and propane seen in headspace samples, *iso*-butane ($i-C_4$) and *iso*-pentane ($i-C_5$) were detected in trace amounts in gas void samples (Table 18). C_1/C_2 values range between 2242 and 5633 and show no trend with depth.

The sedimentary section sampled at Site 1064 lies entirely within the sulfate reduction zone (see “Inorganic Geochemistry” section, this chapter), and thus shows extremely low concentrations of headspace methane. Ethane and propane were not detected, and no gas pockets were observed.

Discussion

The shallow sulfate/methane interface, the gassy, expanding sediments, and the occurrence of higher molecular-weight hydrocarbon gases (C_2 – C_5) at Site 1063 were unexpected. DSDP sites on the southern (Site 386) and western (Site 387) Bermuda Rise did not experience complete sulfate depletion even though they were drilled to

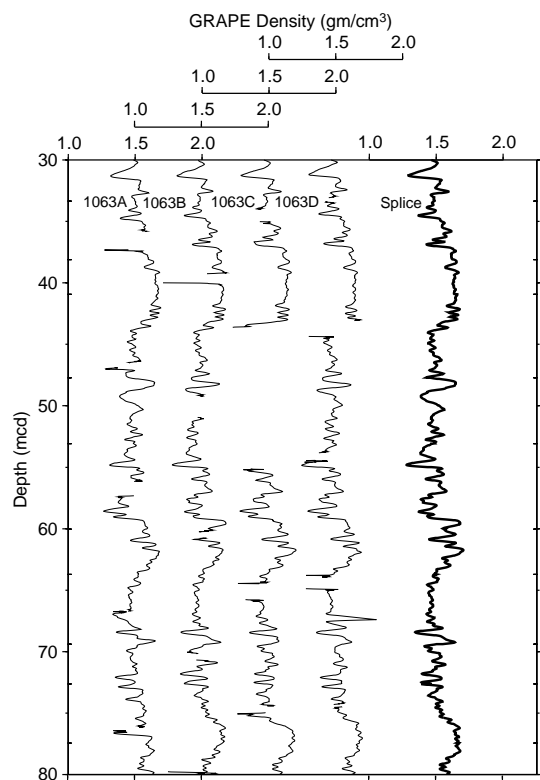


Figure 19. Smoothed GRAPE data (31-cm Gaussian window) for Site 1063 for Holes 1063A through 1063D and the spliced record. The GRAPE data from different holes are highly correlated throughout this entire interval.

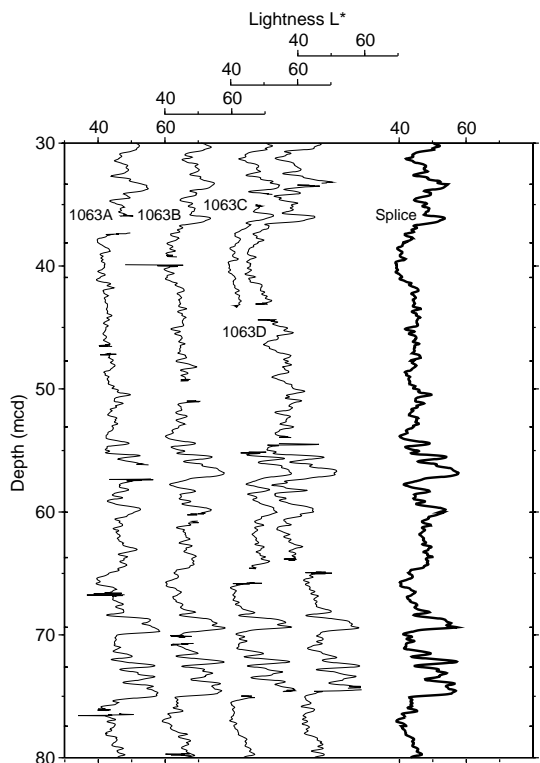


Figure 20. Blow-up of smoothed lightness (L^*) data (31-cm Gaussian window) from Site 1063 for Holes 1063A through 1063D and the spliced record. The lightness data from different holes are highly correlated throughout this entire interval (offset in Hole 1063D was caused by a calibration problem).

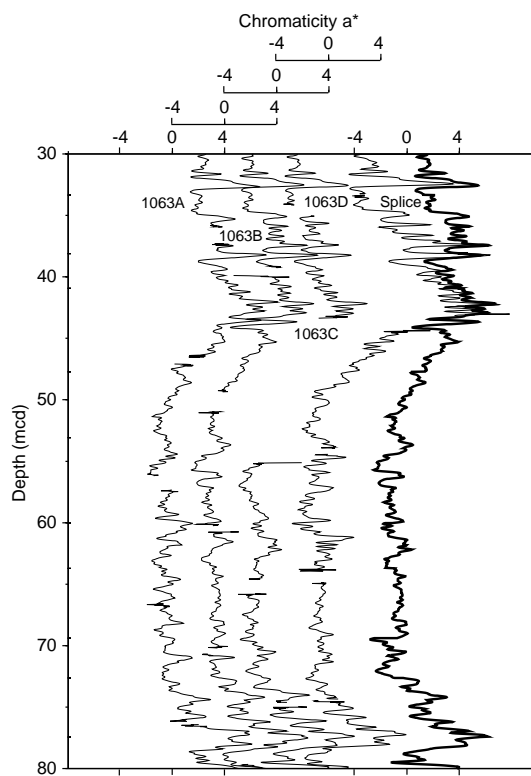


Figure 21. Blow-up of smoothed chromaticity (a^*) data (31-cm Gaussian window) from Site 1063 for Holes 1063A through 1063D and the spliced record. The chromaticity a^* data from different holes are highly correlated from ~30 to 55 mcd and from ~70 to 80 mcd, but poorly correlated from ~55 to 70 mcd.

973 and 794 mbsf, respectively (Tucholke, Vogt, et al., 1979). Apparently, sufficient amounts of organic carbon have been deposited at Site 1063, driving sulfate reduction to completion and allowing the microbial generation of significant amounts of methane.

The high C_1/C_2 values, the reciprocal concentration profiles of sulfate and methane, as well as the type and low level of higher molecular-weight hydrocarbons (C_3-C_5), indicate that the methane is predominantly of microbial origin at Site 1063 (Schoell, 1980). Methane is probably largely formed through microbial CO_2 reduction (see “Organic Geochemistry” section, “Deep Blake-Bahama Outer Ridge” chapter, this volume; Claypool and Kaplan, 1974). Lower molecular-weight gases frequently accompany microbially produced methane in other marine sediments (e.g., Whelan and Sato, 1980). Moreover, the predominance of *iso*-alkanes over straight-chain *n*-alkanes indicates a probable microbial origin for the C_2-C_5 hydrocarbons (Schaefer and Leythaeuser, 1984; Paull, Matsumoto, Wallace, et al., 1996). This conclusion is also supported by Rock-Eval data (see below), which indicate that the recovered sediments at Site 1063 did not reach thermal maturity.

However, the occurrence of an organic, yellow-brown waxy residue (see “Lithostratigraphy” section, this chapter) suggests that thermogenesis may occur at depth, assuming that the material is naturally occurring. The material was found along fracture planes within drilling biscuits at 265 and 347 mbsf, suggesting that it formed elsewhere and migrated. A single sample was analyzed (Sample 172-1063B-38X-5, 40–50 cm, 347.49–347.59 mbsf) and is composed of 39 wt% total organic carbon (TOC) and 6 wt% hydrogen (Table 18). A possible source for this carbonaceous material is the Cretaceous (Cenomanian, Albian, and Aptian) “black clays” of the region, which were recovered from DSDP Sites 386 (725–965 mbsf) and 387 (485–584 mbsf), respectively, on the southern and western Bermuda Rise,

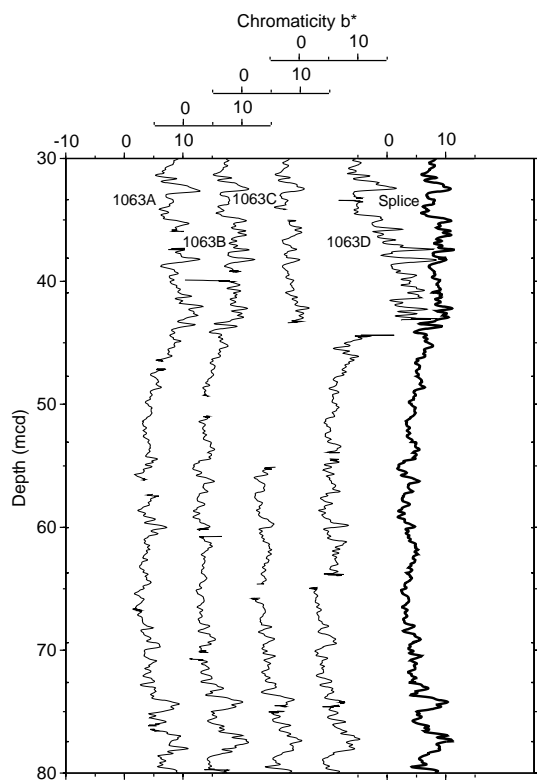


Figure 22. Blow-up of smoothed chromaticity (b^*) data (31-cm Gaussian window) from Site 1063 for Holes 1063A through 1063D and the spliced record. The chromaticity b^* data from different holes are highly correlated throughout this entire interval.

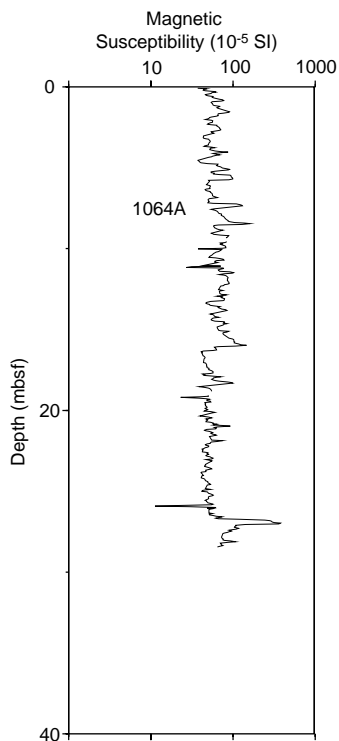


Figure 23. Raw magnetic susceptibility data from Site 1064 on the mbsf scale.

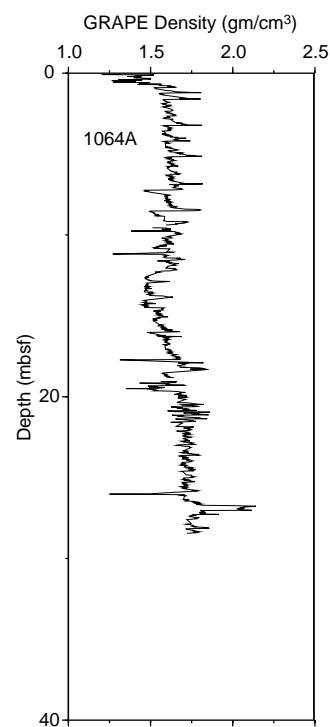


Figure 24. Raw GRAPE data from Site 1064 on the mbsf scale.

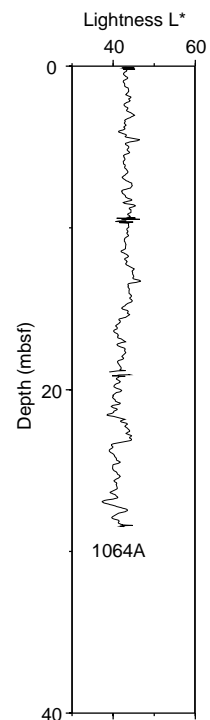


Figure 25. Raw lightness (L^*) data from Site 1064 on the mbsf scale.

(Tucholke, Vogt, et al., 1979). This lithology at these sites is composed of mudstone or claystone with various amounts of organic carbon, pyrite, clay minerals, and radiolarians; the amount of pyrite seems to control the darkness of the sediment (McCave, 1979; Kendrick, 1979). Single-sediment samples at both Sites 386 and 387 have TOC as high as 11 wt% (Tucholke, Vogt, et al., 1979) and are potential source rocks for oil (Kendrick et al., 1979). Pyrolysis of the Site

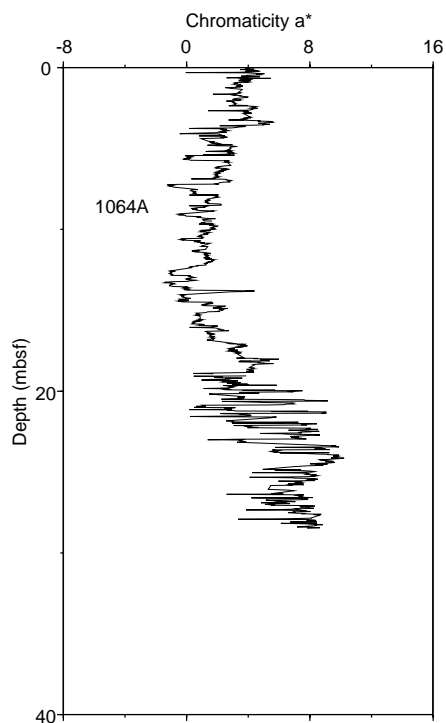


Figure 26. Raw chromaticity (a*) data from Site 1064 on the mbsf scale.

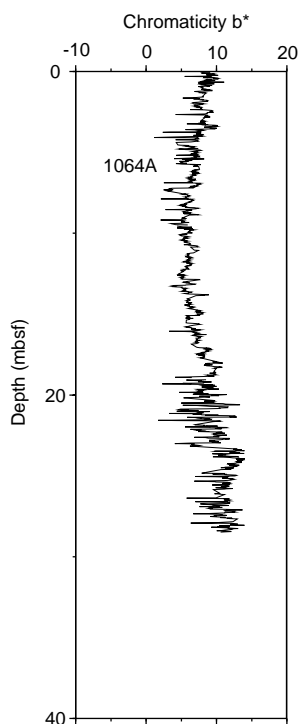


Figure 27. Raw chromaticity (b*) data from Site 1064 on the mbsf scale.

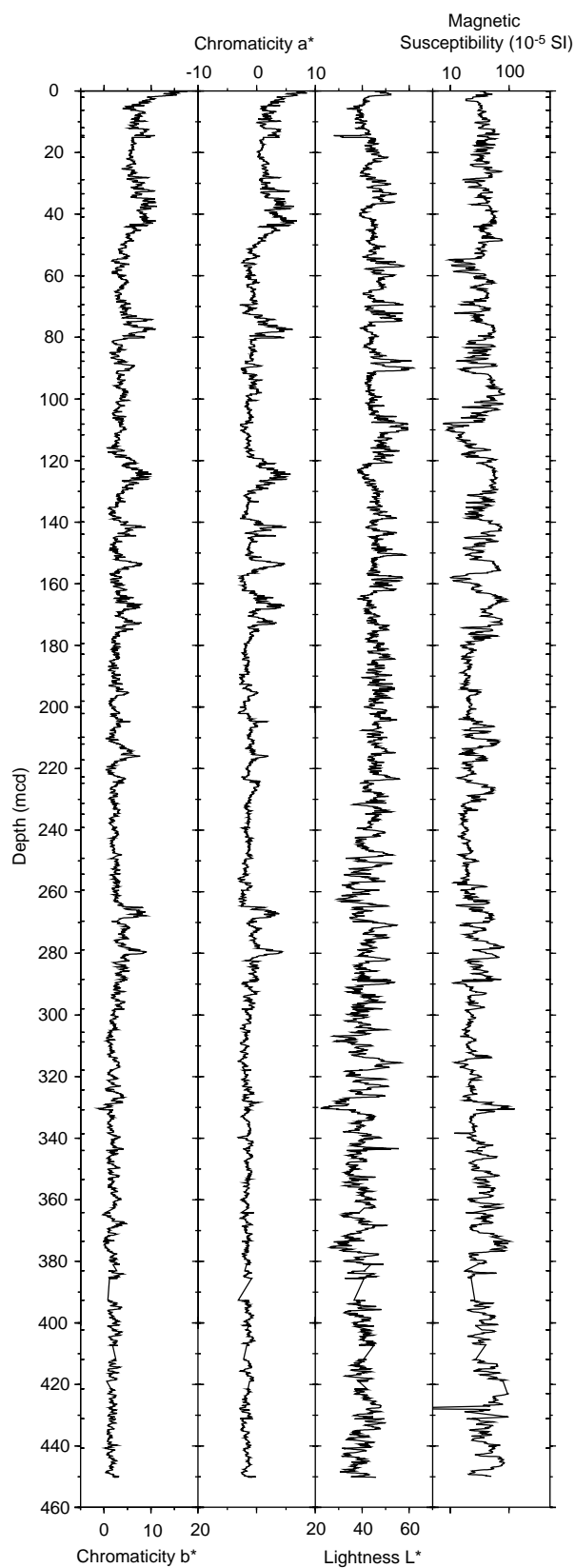


Figure 28. Summary of spliced records for Site 1063.

1063 sample shows that this material is intermediate in composition between type I, lipid-rich, oil prone and type II marine, oil/gas-prone kerogens (see text below; Table 20; Fig. 34).

The possibility for thermogenic generation of hydrocarbons is inconsistent with all other independent evidence gathered at Site 1063. The very low geothermal gradient ($20^{\circ}\text{C km}^{-1}$), the insufficient thick-

ness of the sedimentary section (700–1000 m), the predominance of *iso*-alkanes in the higher molecular-weight hydrocarbons (C₃–C₅), and the geologic setting strongly imply that thermogenesis is not occurring at present. Onshore investigations may clarify the origin of this enigmatic organic material.

Inorganic And Organic Carbon

Samples from Holes 1063A and 1064A were analyzed for inorganic carbon at a minimum frequency of three per core (Table 19; Fig. 35). Elemental analysis and TOC measurements were made on

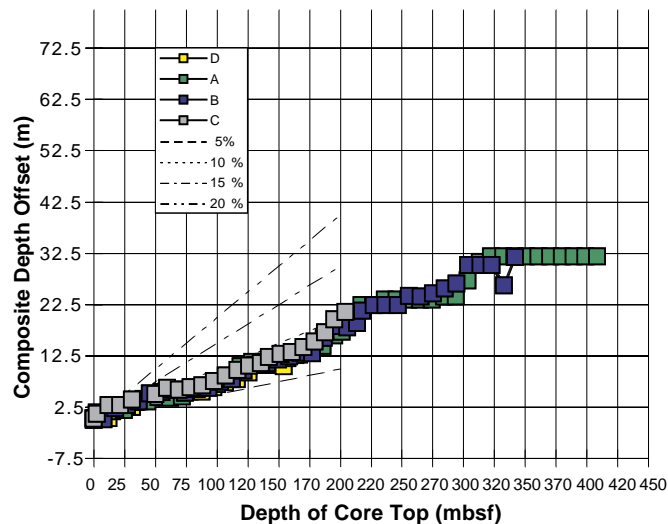


Figure 29. Composite depth offset vs. core-top depth for Site 1063.

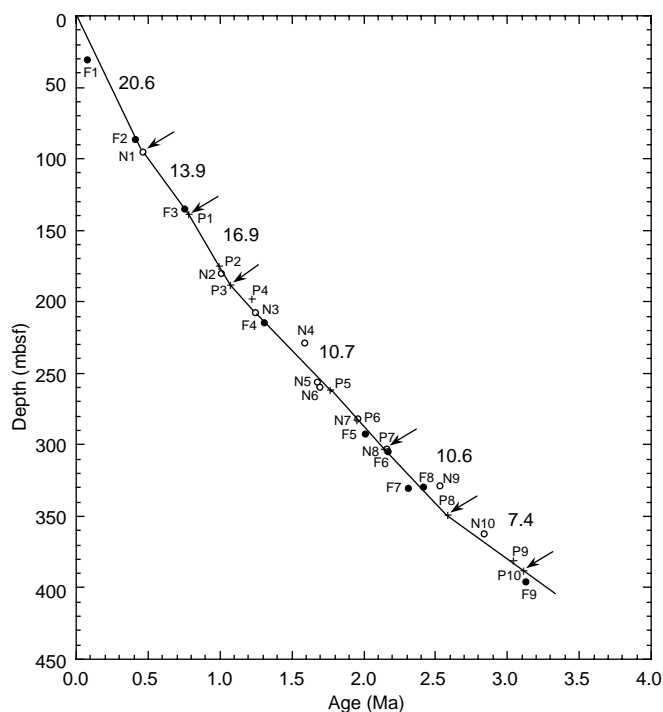


Figure 30. Age/depth plots for Hole 1063A based on biostratigraphic tie points (arrows). Solid circles = planktonic foraminifer markers, open circles = nannoplankton markers, and crosses = magnetostratigraphic markers. See Table 3 in the “Biostratigraphy” section (this chapter) to associate species names with the labels used in this figure. Sedimentation rates are expressed in centimeters per thousand years.

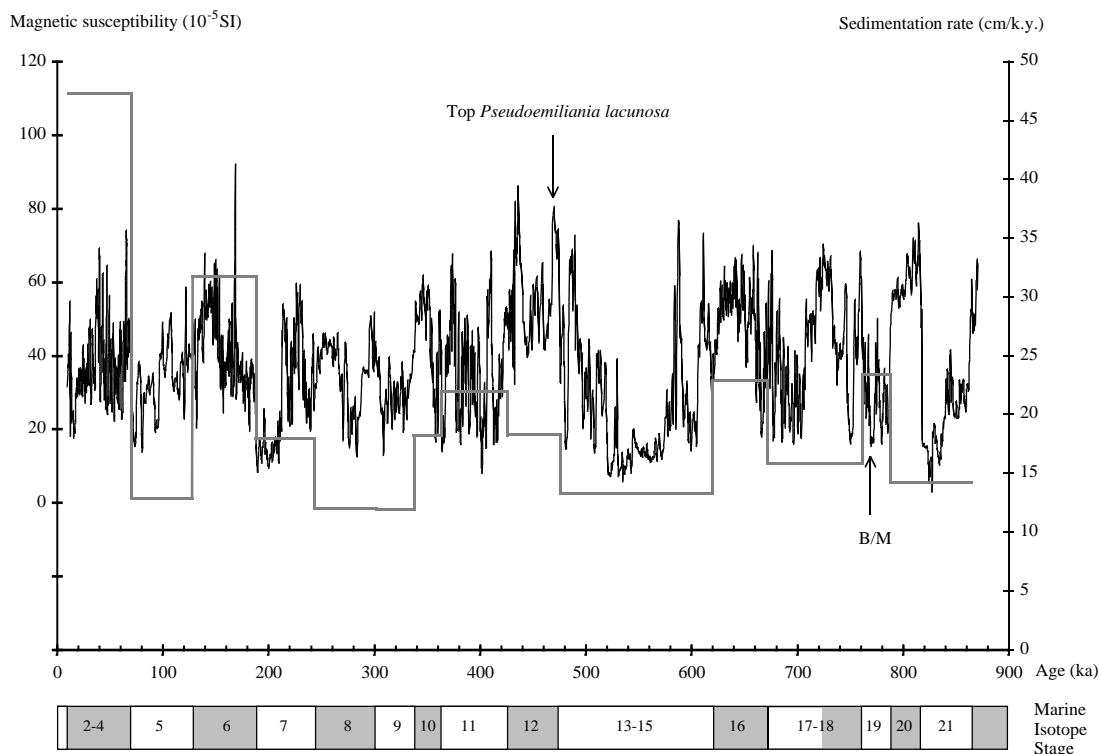


Figure 31. Magnetic susceptibility record (left scale, thin curve) and sedimentation rate (right scale, thick stepwise curve; composite record) of Site 1063 (33°14′N, 56°24′W, 4775 m). B/M = Brunhes/Matuyama boundary. The MISs are indicated, with the glacial ones shaded.

Table 14. Age-depth relation of Site 1063.

Depth (mcd)	Age (ka)	Average sedimentation rate (cm/k.y.)
0.12	10	47.27
28.48	70	47.27
35.96	128	12.90
55.04	188	31.80
65.14	244	18.04
72.1	302	12.00
76.39	338	11.92
81.13	364	18.23
94.75	426	21.97
103.89	476	18.28
123.1	620	13.34
135.02	672	22.92
149.32	762	15.89
155.4	788	23.38
166.21	864	14.22
170.49	900	11.89

selected samples, depending on the inorganic carbon content of the sediments. Results for both sites are presented in Table 19; Figure 35 illustrates the downhole profile of CaCO₃ and TOC at Site 1063.

Calcium carbonate values at Site 1063 range from 1 to 60 wt%, and average 17 wt% (Table 19; Fig. 35). The CaCO₃ concentrations show cyclic variation with depth (Fig. 35) and appear to be correlative with magnetic susceptibility cycles (see "Sedimentation and Mass Accumulation Rates" section, this chapter and other "Organic Geochemistry" sections, this volume). As at the Blake Outer Ridge sites, high carbonate deposition tends to occur during interglacial periods, whereas the lowest carbonate values (<5 wt%) are generally seen during glacial intervals.

Neither the intensity of the peaks showing increased carbonate nor the average amount of sedimentary CaCO₃ are constant with depth or time. The interval from 130 to 150 mbsf shows unusually low carbonate values. On average, and except for the two peaks near 100 mbsf, sediments tend to be richer in CaCO₃ at and below the re-entrance of medium *Gephyrocapsa* spp. (1.0 Ma at ~180 mbsf). Within the sedimentary interval below this biohorizon, the intensity of carbonate peaks seems to generally diminish with depth.

TOC concentrations range from less than 0.05 to 1.17 wt%, and average about 0.6 wt%. TOC is generally higher in the section above the reentrance of medium *Gephyrocapsa* spp., and thus tends to show a reciprocal relationship with CaCO₃. Higher TOC amounts do generally correlate with higher C/N values, which suggest a larger contribution of terrestrial organic matter (see below).

Discussion

The production rate of calcium carbonate, the ratio of calcium carbonate to organic matter, input rates of noncarbonate material, and the saturation state of deep-water masses combine to form a complex interplay that controls the amount of calcium carbonate preserved within sediments. Temporal and stratigraphic variations in carbonate are certainly influenced by fluctuations between glacial and interglacial conditions (see "Biostratigraphy" section, this chapter, and other "Organic Geochemistry" sections, this volume), but these cycles are overprinted with other sedimentological phenomena. The overall stratigraphic record at Site 1063 is dominated by marine sedimentary inputs, with episodes of larger terrigenous sediment contributions. These are clearly seen near 16 mbsf and between 100 and 300 mbsf, where C/N values of organic carbon are significantly higher than 10 (see below). Most likely, these terrestrial contributions are linked to climatic changes in the Canadian Maritime provinces and terrigenous input to the Gulf of St. Lawrence (see "Introduction" section, this chapter).

At Site 1063, dissolution effects are generally not evident in nanofossils, but foraminifer dissolution is pronounced in Pliocene sediments (see "Biostratigraphy" section, this chapter). This suggests

that dissolution may be largely responsible for the generally low carbonate content below 300 mbsf. Lower TOC with C/N values below 10 suggests a marine source for the organic matter (see below).

Organic Matter Source Characterization

Elemental Analysis

Higher terrestrial plants contain significantly more carbon relative to nitrogen than do marine organisms, so that C/N values can be used as an indicator of organic matter provenance (e.g., see "Organic Chemistry" section, "Deep Blake-Bahama Outer Ridge" chapter, this volume). Average C/N values of marine zooplankton and phytoplankton tend to lie between 5 and 8, whereas land plants typically have ratios between 20 and 200 (Emerson and Hedges, 1988).

C/N values are highly variable at Site 1063 (Table 19). Most of the samples range between 5 and 10, but values less than 1 and approaching 17 also occur. The lowest values tend to be grouped below 330 mbsf, roughly coincident with the incidence of lowest TOC values, where almost every sample has a C/N value of less than 5 (Fig. 35). C/N values above 10 generally occur between 100 and 300 mbsf and within the uppermost 20 m.

C/N values at Site 1063 generally indicate that the bulk of organic matter is derived from marine phytoplankton. Most samples possess C/N values between 5 and 10, with an average value of 6.4. Although C/N values may change during diagenesis, the above values reflect a marine organic matter origin (e.g., Meyers, 1994). Nonetheless, admixtures of land-derived material are also indicated, particularly near 16 mbsf and between 100 and 300 mbsf. The highest C/N values may result from influxes of land-derived organic material associated with the St. Lawrence system of eastern Canada (see "Introduction" section, this chapter).

Rock-Eval Analysis

Rock-Eval pyrolysis results clearly indicate that the bulk of the sedimentary organic matter recovered at Site 1063 is immature. T_{max} values (i.e., the temperature values measured when maximum release of hydrocarbons from cracking of kerogen during pyrolysis occurs) of most samples are below 435°C, indicating immaturity. One shallow sample has a T_{max} value of 548°C (Sample 172-1063A-2H-4, 70–71 cm, 9.32 mbsf), but this anomaly is probably caused by mineral matrix effects. Also, higher T_{max} values are not correlated with the occurrence of higher molecular-weight hydrocarbons (C₃–C₅). Thus, no thermal maturation of hydrocarbons can be inferred from our data.

Van Krevelen-type plots of the Hydrogen Index (HI) and Oxygen Index (OI) values of samples having elevated TOC concentrations (>0.5 wt%) suggest that the sedimentary organic matter of Site 1063 is composed of type III, land-derived organic matter (Fig. 34). Most data plot in a field of low HI (<100 mgHC/gTOC) and high OI (>200 mg CO₂/g TOC). The HI does not vary with depth, nor is there any correlation with TOC concentrations.

Discussion

As at all of the previous sites of the Blake-Bahama Outer Ridge, pyrolysis and C/N data seem to give a conflicting source assignment for organic matter. C/N values indicate an admixture of both terrestrial and marine sources, whereas Rock-Eval data suggest that the organic material (with the exception of the anomalous Hole 1063B material) is exclusively terrestrial in origin. Neither method is an unequivocal indicator of organic matter provenance. For example, unusually low C/N values are generally associated with the lower organic carbon concentrations (<0.5 wt%), an artifact probably caused by the absorption of ammonium-nitrogen by clay minerals (Müller, 1977). Microbial oxidation of organic matter can also skew the results of both pyrolysis and C/N analyses toward terrestrial values (Espitalié et al., 1986). We believe that most organic matter at Site

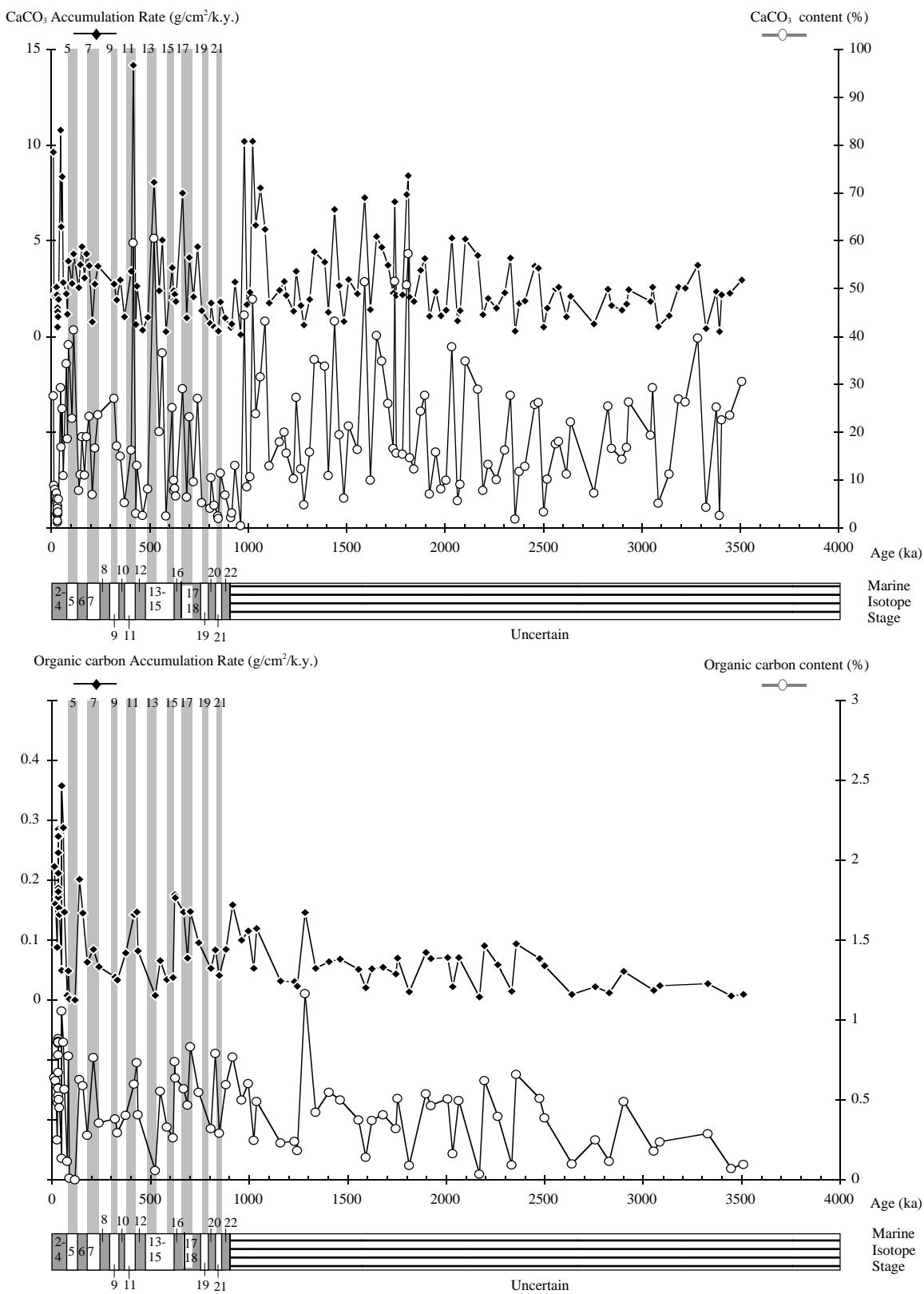


Figure 32. Downhole profiles of organic carbon and calcium carbonate accumulation rates at Site 1063 (composite). Dashed lines = magnetic susceptibility-based boundaries. The MISs are labeled, with glacial ones shaded; striped section of MIS scale = stage assignment uncertain.

Table 15. Estimated ages, concentrations, and accumulation rates of calcium carbonate at Site 1063.

Age (ka)	CaCO ₃ content (wt%)	CaCO ₃ MAR (g/cm ² /k.y.)	Age (ka)	CaCO ₃ content (wt%)	CaCO ₃ MAR (g/cm ² /k.y.)
10.21	27.66	9.62	1107.65	13.04	1.75
14.13	8.93	2.14	1159.92	18.04	2.41
18.15	8.12	2.09	1184.19	20.10	2.88
25.28	5.55	2.01	1193.05	15.74	2.16
26.40	7.37	2.59	1230.00	10.41	1.32
29.08	3.00	1.06	1243.46	27.34	3.40
29.19	6.15	2.18	1268.09	12.40	1.61
31.56	4.55	1.48	1282.97	4.90	0.61
31.60	2.89	0.93	1311.06	15.95	1.94
31.64	3.50	1.13	1335.95	35.30	4.42
31.69	1.33	0.43	1388.48	33.83	3.90
31.77	3.20	1.02	1405.94	10.99	1.28
31.81	2.89	0.92	1439.16	43.32	6.65
31.83	1.55	0.49	1462.81	19.60	2.67
31.88	3.17	1.00	1485.58	6.32	0.79
31.92	4.83	1.52	1510.83	21.33	2.97
31.94	4.13	1.29	1554.41	16.40	2.22
33.23	3.40	1.04	1591.00	51.50	7.25
35.92	6.14	1.93	1621.21	10.09	1.40
46.75	29.33	10.79	1652.57	40.33	5.22
48.99	16.97	5.73	1679.15	34.88	4.67
55.17	24.99	8.36	1709.89	26.06	3.72
61.47	10.97	2.83	1736.38	16.69	2.27
76.75	34.45	2.23	1745.24	51.60	7.03
80.70	18.71	1.17	1751.71	15.73	2.15
87.52	38.34	3.95	1785.19	15.53	2.17
105.05	22.97	2.77	1805.57	50.87	7.42
114.59	41.42	4.31	1812.04	57.37	8.40
139.01	7.92	2.54	1821.69	14.79	2.04
148.85	11.19	3.76	1842.33	12.41	1.82
155.80	19.10	4.70	1875.11	24.42	3.45
169.23	11.14	3.07	1896.64	27.80	4.08
178.28	19.16	4.32	1921.45	7.21	1.07
191.60	23.44	3.72	1951.66	15.95	2.34
208.46	7.05	0.77	1977.88	8.17	1.07
221.82	16.76	2.74	2006.58	10.00	1.39
238.12	23.67	3.68	2033.16	37.95	5.14
319.20	27.17	2.74	2063.19	5.75	0.81
331.71	17.25	1.91	2076.57	9.14	1.35
351.49	15.09	2.95	2102.61	34.90	5.08
372.06	5.33	1.04	2167.01	29.07	4.23
406.61	16.30	3.42	2192.35	7.89	1.14
416.26	59.64	14.17	2217.87	13.35	1.99
428.99	3.15	0.63	2260.37	10.14	1.50
435.15	13.15	2.64	2302.16	16.36	2.29
464.62	2.67	0.33	2331.82	27.79	4.11
489.19	8.20	1.00	2355.57	1.92	0.27
522.25	60.55	8.06	2377.13	11.82	1.71
547.21	20.21	2.39	2405.64	12.88	1.85
563.70	36.69	5.03	2456.94	25.81	3.68
583.27	2.55	0.26	2474.36	26.29	3.56
612.65	25.25	3.59	2500.05	3.37	0.50
620.61	7.92	1.89	2518.97	10.24	1.49
621.70	10.00	2.40	2562.17	17.64	2.51
626.06	8.29	2.22	2578.27	18.19	2.58
632.78	6.72	1.82	2617.08	11.32	1.02
680.00	29.15	7.50	2638.38	22.26	2.10
687.94	6.55	0.97	2756.66	7.37	0.65
702.03	23.26	4.13	2827.05	25.50	2.48
723.19	9.75	2.08	2847.13	16.63	1.61
743.35	27.13	4.70	2899.76	14.42	1.39
763.15	5.33	1.35	2923.36	16.84	1.69
805.80	4.15	0.68	2933.40	26.42	2.45
822.00	10.57	1.76	3043.81	19.48	1.82
827.22	4.79	0.51	3054.12	29.42	2.58
846.67	2.54	0.35	3083.28	5.25	0.53
847.47	1.99	0.28	3138.89	11.33	1.10
858.78	11.49	1.80	3185.69	26.98	2.58
882.00	6.92	0.98	3220.41	26.44	2.53
910.86	2.27	0.46	3283.21	39.70	3.74
917.19	3.17	0.65	3325.94	4.37	0.41
931.80	13.18	2.86	3377.08	25.29	2.35
960.58	0.48	0.10	3392.95	2.66	0.27
979.33	44.54	10.18	3404.48	22.68	2.19
994.42	8.71	1.67	3446.53	23.65	2.27
1010.49	10.76	2.30	3507.16	30.65	2.95
1021.99	47.86	10.18			
1038.44	23.91	5.82			
1061.67	31.59	7.77			
1084.97	43.30	5.59			

Notes: Estimates based on geochemical measurements at Hole 1063A.
MAR = mass accumulation rate.

Table 16. Estimated ages, concentrations, and accumulation rates of organic carbon at Site 1063.

Age (ka)	C _{org} content (wt%)	C _{org} MAR (g/cm ² /k.y.)
10.21	0.64	0.22
18.15	0.62	0.16
26.40	0.25	0.09
29.19	0.48	0.17
31.56	0.58	0.19
31.60	0.53	0.17
31.64	0.88	0.28
31.69	0.86	0.28
31.77	0.85	0.27
31.81	0.87	0.28
31.83	0.86	0.27
31.88	0.57	0.18
31.92	0.67	0.21
31.94	0.78	0.25
33.23	0.50	0.15
35.92	0.45	0.14
46.75	0.13	0.05
48.99	1.06	0.36
55.17	0.86	0.29
61.47	0.57	0.15
76.75	0.11	0.01
80.70	0.77	0.05
87.52	0.01	0.00
114.59	0.00	0.00
139.01	0.63	0.20
155.80	0.59	0.14
178.28	0.28	0.06
208.46	0.77	0.08
238.12	0.35	0.06
319.20	0.38	0.04
331.71	0.29	0.03
372.06	0.40	0.08
416.26	0.60	0.14
428.99	0.73	0.15
435.15	0.41	0.08
522.25	0.06	0.01
547.21	0.55	0.07
583.27	0.33	0.03
612.65	0.26	0.04
620.61	0.74	0.18
626.06	0.64	0.17
667.90	0.57	0.15
687.94	0.47	0.07
702.03	0.71	0.12
743.35	0.55	0.09
805.80	0.32	0.05
815.00	0.79	0.08
847.47	0.29	0.04
882.00	0.60	0.08
917.19	0.77	0.16
960.58	0.50	0.10
994.42	0.60	0.12
1021.99	0.25	0.05
1038.44	0.49	0.12
1159.92	0.23	0.03
1230.00	0.24	0.03
1243.46	0.18	0.02
1282.97	1.17	0.15
1335.95	0.42	0.05
1405.94	0.55	0.06
1462.81	0.50	0.07
1554.41	0.37	0.05
1591.00	0.14	0.02
1621.21	0.37	0.05
1679.15	0.41	0.05
1745.24	0.32	0.04
1751.71	0.51	0.07
1812.04	0.09	0.01
1896.64	0.54	0.08
1921.45	0.46	0.07
2006.58	0.51	0.07
2033.16	0.16	0.02
2063.19	0.50	0.07
2167.01	0.03	0.01
2192.35	0.62	0.09
2260.37	0.40	0.06
2331.82	0.09	0.01
2355.57	0.66	0.09
2474.36	0.51	0.07
2500.05	0.39	0.06
2638.38	0.10	0.01
2756.66	0.25	0.02
2827.05	0.12	0.01
2899.76	0.49	0.05
3054.12	0.18	0.02
3083.28	0.24	0.02
3325.94	0.29	0.03
3446.53	0.07	0.01
3507.16	0.10	0.01

Note: Estimates based on geochemical measurements at Hole 1063A.

Table 17. Results of headspace gas analyses of sediments from Sites 1063 and 1064.

Core, section, interval (cm)	Depth (mbsf)	C ₁ (ppm)	C ₂ (ppm)	C ₃ (ppm)	C ₁ /C ₂
172-1063A-					
1H-2, 0-5	1.5	4	ND	ND	—
2H-4, 0-5	8.6	65	ND	ND	—
3H-4, 0-5	19.3	189	ND	ND	—
4H-4, 0-5	28.8	278	ND	ND	—
5H-4, 0-5	38.3	1,244	ND	ND	—
6H-4, 0-5	47.8	6,246	0.5	ND	12,492
7H-4, 0-5	57.3	11,377	1.1	ND	10,158
8H-4, 0-5	66.8	24,219	2.0	ND	12,110
9H-4, 0-5	76.3	32,445	2.8	0	11,588
10H-3, 0-5	84.3	23,191	2.0	ND	11,596
11H-3, 0-5	93.8	18,684	2.0	ND	9,342
12H-6, 0-5	107.3	47,751	4.4	ND	10,853
13H-3, 0-5	112.3	8,397	1.1	ND	7,634
14H-6, 0-5	126.2	62,187	6.4	1	9,717
15H-5, 0-5	134.3	46,226	5.7	1	8,110
16H-6, 0-5	145.2	50,092	6.1	1	8,212
17H-6, 0-5	154.4	17,984	3.2	1	5,620
18H-6, 0-5	164.3	42,134	6.4	0	6,583
19H-6, 0-5	173.7	29,095	4.3	ND	6,766
20H-6, 0-5	183.4	47,007	7.3	1	6,439
21H-6, 0-5	192.9	47,469	7.8	1	6,086
22H-2, 0-5	196.0	20,083	3.5	ND	5,738
23X-5, 0-5	207.4	21,075	5.1	1	4,116
24X-6, 0-5	215.1	27,176	6.0	1	4,529
25X-5, 0-5	223.2	18,687	4.6	ND	4,062
26X-5, 0-5	232.8	16,421	4.0	1	4,105
27X-2, 0-5	237.9	23,636	6.0	1	3,939
28X-2, 0-5	247.5	23,636	6.0	1	3,939
29X-4, 0-5	259.8	18,465	5.1	1	3,621
30X-4, 0-5	268.8	20,887	6.0	1	3,481
31X-4, 0-5	278.0	25,510	7.0	2	3,644
32X-4, 0-5	288.5	10,390	3.6	1	2,886
33X-6, 0-5	301.3	14,878	4.4	1	3,381
34X-4, 0-5	308.0	20,933	7.3	2	2,868
35X-4, 0-5	317.6	22,513	8.6	2	2,618
36X-4, 0-5	327.1	10,267	5.0	1	2,053
37X-6, 0-5	339.6	6,946	4.0	1	1,737
38X-4, 0-5	346.0	26,039	8.6	1	3,028
39X-2, 0-5	352.6	12,213	5.0	1	2,443
40X-5, 0-5	366.7	24,095	9.3	2	2,605
41X-3, 0-5	373.3	15,487	7.0	2	2,212
42X-4, 0-5	384.4	24,720	23.0	4	1,075
43X-5, 0-5	395.5	7,601	4.0	1	1,900
44X-6, 0-5	406.6	13,051	6.5	2	2,008
45X-6, 0-5	416.2	15,616	7.0	2	2,231
172-1064A-					
1H-5, 0-5	6.0	10	ND	ND	—
2H-3, 0-5	12.5	15	ND	ND	—
3H-3, 0-5	21.8	7	ND	ND	—

Notes: ND = not detected. — = not applicable.

1063 is of marine origin, except where unusually high C/N values indicate terrestrial sources. These inputs are likely provided from eastern Canada (see “Introduction” section, this chapter).

INORGANIC GEOCHEMISTRY

Interstitial waters were collected and analyzed from 74 whole-round section samples from Sites 1063 and 1064. Samples from Hole 1063A were collected at a frequency of two per core to a depth of 100 mbsf, and one sample per core thereafter, and samples from Hole 1064A were collected at a frequency of one per section along its 27.7-m length (Table 21). Interstitial water data for the two sites are presented as depth concentration profiles in Figures 36–40. The main objectives are to document the early diagenetic changes and to sample pore water for stable isotope studies.

Early Diagenesis Associated with Organic Matter Decomposition

Interstitial water sulfate, alkalinity, ammonium, and phosphate profiles reflect microbial decomposition of sedimentary organic mat-

Table 18. Results of vacutainer gas analyses of sediments from Site 1063.

Core, section, interval (cm)	Depth (mbsf)	C ₁ (ppm)	C ₂ (ppm)	C ₃ (ppm)	i-C ₄ (ppm)	i-C ₅ (ppm)	C ₁ /C ₂
172-1063A-							
12H-1, 35-36	100.7	797,128	270	2	ND	ND	4,851
16H-1, 94-95	139.2	930,582	312	13	ND	ND	4,873
20H-1, 117-118	177.5	943,174	388	16	2.4	ND	3,401
21H-7, 73-74	195.0	938,198	285	17	0.1	ND	4,767
24X-2, 58-59	209.7	791,142	230	15	ND	ND	4,812
25X-2, 79-80	219.5	717,856	193	13	ND	ND	5,225
26X-5, 60-61	233.4	786,802	220	15	ND	ND	5,608
27X-2, 26-27	238.2	822,259	248	17	ND	ND	5,608
28X-3, 117-118	250.2	775,372	244	17	ND	ND	5,578
30X-5, 134-135	271.7	601,099	178	14	ND	ND	5,512
31X-6, 134-135	281.5	790,620	246	18	ND	ND	6,231
32X-5, 135-136	291.4	924,418	298	23	ND	ND	5,269
33X-6, 143-144	302.7	878,718	299	23	ND	ND	5,622
34X-6, 110-111	312.1	917,076	409	30	ND	ND	2,242
35X-3, 81-82	316.9	920,832	368	32	0.1	ND	3,281
36X-4, 79-80	327.9	917,046	376	40	0.3	ND	2,928
37X-4, 18-19	336.9	914,049	415	46	0.1	0.7	2,634
38X-1, 41-42	341.9	916,550	434	44	1	ND	3,348
45X-6, 11-12	416.3	910,087	418	65	ND	ND	2,325

Note: ND = not detected.

Table 19. Results of coulometric and elemental analyses from Sites 1063 and 1064.

Core, section, interval (cm)	Depth (mbsf)	IC (wt%)	CaCO ₃ (wt%)	TC (wt%)	TOC (wt%)	TN (wt%)	TS (wt%)	C/N
172-1063A-								
1H-1, 22-23	0.22	3.32	27.66	3.96	0.64	0.05	0.00	13.5
1H-2, 57-58	2.07	1.07	8.93					
1H-3, 97-98	3.97	0.98	8.12	1.60	0.62	0.06	0.09	9.7
2H-2, 28-29	6.22	0.67	5.55					
2H-2, 81-82	6.75	0.89	7.37	1.13	0.25	0.05	0.62	4.6
2H-3, 90-91	8.02	0.36	3.00					
2H-3, 95-96	8.07	0.74	6.15	1.22	0.48	0.07	0.29	7.1
2H-4, 57-58	9.19	0.55	4.55	1.12	0.58	0.36	0.00	1.6
2H-4, 58.5-60	9.21	0.35	2.89	0.88	0.53	0.06	0.06	8.2
2H-4, 60.5-62	9.23	0.42	3.50	1.30	0.88	0.10	0.04	9.0
2H-4, 62.5-63.5	9.25	0.16	1.33	1.02	0.86	0.08	0.26	10.4
2H-4, 66.5-67.5	9.29	0.38	3.20	1.24	0.85	0.09	0.00	9.4
2H-4, 68.5-69.5	9.31	0.35	2.89	1.21	0.87	0.08	0.06	11.2
2H-4, 70-71	9.32	0.19	1.55	1.05	0.86	0.10	0.19	9.0
2H-4, 72-73	9.34	0.38	3.17	0.95	0.57	0.08	0.08	7.4
2H-4, 73.5-74.5	9.36	0.58	4.83	1.25	0.67	0.10	0.05	6.6
2H-4, 75-76	9.37	0.50	4.13	1.28	0.78	0.07	0.06	10.5
2H-4, 136-137	9.98	0.41	3.40	0.91	0.50	0.08	0.14	6.2
2H-5, 33-34	10.45	0.74	6.14	1.19	0.45	0.08	0.10	5.9
3H-1, 77-78	15.57	3.52	29.33	3.65	0.13	1.27	0.14	0.1
3H-2, 33-34	16.63	2.04	16.97	3.09	1.06	0.07	0.07	16.0
3H-4, 25-26	19.55	3.00	24.99	3.86	0.86	0.07	0.00	13.1
3H-6, 23-24	22.53	1.32	10.97	1.88	0.57	0.11	0.15	5.2
4H-2, 133-134	27.13	4.14	34.45	4.25	0.11	0.04	0.00	2.7
4H-3, 34-35	27.64	2.25	18.71	3.02	0.77	0.08	0.05	10.1
4H-3, 122-123	28.52	4.60	38.34	4.61	0.01	0.03	0.00	0.3
4H-5, 48-49	30.78	2.76	22.97					
4H-6, 21-22	32.01	4.97	41.42	4.93	0.00	0.05	0.00	
5H-2, 22-23	35.52	0.95	7.92	1.58	0.63	0.06	0.11	10.2
5H-4, 35-36	38.65	1.34	11.19					
5H-5, 106-107	40.86	2.29	19.10	2.88	0.59	0.07	0.04	7.9
6H-2, 35-36	45.15	1.34	11.14					
6H-4, 23-24	48.03	2.30	19.16	2.58	0.28	0.04	0.16	7.2
6H-6, 97-98	51.77	2.81	23.44					
7H-1, 113-114	53.93	0.85	7.05	1.61	0.77	0.08	0.07	10.1
7H-3, 54-55	56.34	2.01	16.76					
7H-5, 48-49	59.28	2.8						
10H-3, 38-39	84.68	7.16	59.64	7.76	0.60	0.16	0.00	3.7
10H-5, 121-122	88.51	0.38	3.15	1.11	0.73	0.10	0.00	7.0
11H-1, 48-49	91.28	1.58	13.15	1.98	0.41	0.05	0.00	7.5
11H-3, 45-46	94.25	0.32	2.67					
12H-3, 111-112	104.10	2.43	20.21	2.98	0.55	0.05	0.13	12.0
12H-5, 54-55	106.30	4.40	36.69					
13H-2, 60-61	111.44	3.03	25.25	3.29	0.26	0.06	0.00	4.5
13H-3, 22-23	112.56	0.95	7.92	1.69	0.74	0.06	0.00	12.4
13H-3, 47-48	112.81	1.20	10.00					
13H-5, 18-19	113.81	0.99	8.29	1.63	0.64	0.06	0.04	10.5
13H-6, 36-37	115.35	0.81	6.72					
14H-2, 60-61	121.20	3.50	29.15	4.07	0.57	0.04	0.08	16.0
14H-5, 57-58	125.26	0.79	6.55	1.25	0.47	0.09	0.06	5.0
14H-7, 48-49	128.02	2.79	23.26	3.62	0.83	0.05	0.12	16.6
15H-2, 19-20	130.30	1.17	9.75					
15H-4, 12-13	132.96	3.26	27.13	3.81	0.55	0.03	0.00	16.8
15H-6, 32-33	135.69	0.64	5.33					
16H-4, 97-98	143.28	0.50	4.15	0.82	0.32	0.06	0.00	5.1
16H-5, 18-19	143.85	1.27	10.57					
16H-6, 83-84	146.05	0.58	4.79	1.37	0.79	0.07	0.09	12.1
17H-1, 97-98	148.77	0.31	2.54					

Table 19 (continued).

Core, section, interval (cm)	Depth (mbsf)	IC (wt%)	CaCO ₃ (wt%)	TC (wt%)	TOC (wt%)	TN (wt%)	TS (wt%)	C/N
17H-1, 110-111	148.90	0.24	1.99	0.53	0.29	0.08	0.00	3.7
17H-3, 32-33	150.72	1.38	11.49					
17H-5, 80-81	153.70	0.83	6.92	1.43	0.60	0.06	0.00	10.2
18H-1, 53-54	157.83	0.27	2.27					
18H-2, 53-54	159.13	0.38	3.17	1.15	0.77	0.07	0.00	10.5
18H-4, 79-80	162.13	1.58	13.18					
19H-1, 78-79	167.58	0.06	0.48	0.56	0.50	0.08	0.33	6.0
19H-4, 63-64	171.43	5.35	44.54	5.27	0.00	0.04	0.00	0.0
19H-6, 84-85	174.53	1.05	8.71	1.65	0.60	0.10	0.19	6.2
20H-1, 60-61	176.90	1.29	10.76					
20H-3, 32-33	179.26	5.75	47.86	5.99	0.25	0.05	0.00	4.8
20H-5, 80-81	182.64	2.87	23.91	3.36	0.49	0.04	0.00	12.0
21H-1, 49-50	186.29	3.79	31.59					
21H-3, 119-120	189.69	5.20	43.30					
21H-5, 91-92	192.25	1.57	13.04					
22H-2, 53-54	196.53	2.17	18.04	2.40	0.23	0.03	0.00	6.7
22H-4, 65-66	199.27	2.41	20.10					
22H-5, 35-36	200.27	1.89	15.74					
25X-3, 110-111	221.30	1.32	10.99	1.87	0.55	0.11	0.00	5.2
25X-6, 35-36	225.05	5.20	43.32					
26X-1, 92-93	227.72	2.35	19.60	2.85	0.50	0.04	0.00	11.6
26X-3, 49-50	230.29	0.76	6.32					
26X-5, 34-35	233.14	2.56	21.33					
27X-1, 50-51	236.90	1.97	16.40	2.34	0.37	0.06	0.18	6.8
27X-4, 13-14	241.03	6.18	51.50	6.32	0.14	0.05	0.00	3.0
27X-6, 129-130	244.44	1.21	10.09	1.58	0.37	0.10	0.00	3.7
28X-2, 48-49	247.98	4.84	40.33					
28X-4, 48-49	250.98	4.19	34.88	4.59	0.41	0.04	0.00	10.1
28X-6, 95-96	254.45	3.13	26.06					
29X-2, 64-65	257.44	2.00	16.69					
29X-3, 14-15	258.44	6.19	51.60	6.37	0.32	0.03	0.00	10.7
29X-3, 87-88	259.17	1.89	15.73	2.40	0.51	0.07	0.00	7.0
29X-6, 15-16	262.95	1.86	15.53					
30X-1, 35-36	265.25	6.11	50.87					
30X-2, 16-17	265.9							
30X-2, 125-126	267.07	1.78	14.79					
30X-4, 58-59	269.40	1.49	12.41					
30X-6, 128-129	273.10	2.93	24.42					
31X-2, 54-55	275.53	3.34	27.80	3.87	0.54	0.15	0.73	3.7
31X-4, 34-35	278.33	0.87	7.21	1.33	0.46	0.09	0.17	5.4
31X-6, 75-76	281.74	1.92	15.95					
32X-1, 60-61	284.70	0.98	8.17					
32X-3, 84-85	287.94	1.20	10.00	1.71	0.51	0.07	0.23	6.9
32X-5, 92-93	290.94	4.56	37.95	4.72	0.16	0.05	0.04	3.5
33X-1, 53-54	294.33	0.69	5.75	1.19	0.50	0.19	0.00	2.7
33X-2, 54-55	295.84	1.10	9.14					
33X-4, 48-49	298.78	4.19	34.90					
34X-2, 79-80	305.79	3.49	29.07	3.52	0.03	0.06	0.00	0.6
34X-4, 67-68	308.67	0.95	7.89	1.57	0.62	0.08	0.00	8.2
34X-6, 57-56	311.57	1.60	13.35					
35X-1, 56-57	313.66	1.22	10.14	1.62	0.40	0.08	0.00	5.0
35X-4, 81-82	318.41	1.96	16.36					
35X-6, 118-119	321.78	3.34	27.79	3.43	0.09	0.16	0.00	0.6
36X-1, 78-79	323.38	0.23	1.92	0.89	0.66	0.07	0.05	10.1
36X-3, 23-25	325.83	1.42	11.82					
36X-5, 47-48	329.07	1.55	12.88					
37X-2, 120-121334.94								
40X-1, 125-126	361.95	0.88	7.37	1.14	0.25	0.14	0.12	1.8
40X-5, 44-45	367.14	3.06	25.50	3.18	0.12	0.28	0.00	0.4
40X-6, 42-43	368.62	2.00	16.63					
41X-2, 70-71	372.50	1.73	14.42	2.22	0.49	0.07	0.03	6.8
41X-3, 94-95	374.24	2.02	16.84					
41X-4, 18-19	374.98	3.17	26.42					
42X-3, 22-23	383.12	2.34	19.48					
42X-3, 98-99	383.88	3.53	29.42	3.71	0.18	0.06	0.00	2.9
42X-3, 22-25	386.03	0.63	5.25	0.87				
43X-1, 63-64	390.13	1.36	11.33					
43X-3, 108-109	393.58	3.24	26.98	3.23	0.00	0.07	0.00	
43X-5, 64-65	396.14	3.17	26.44					
44X-2, 17-19	400.77	4.77	39.70					
44X-4, 32-33	403.92	0.52	4.37	0.81	0.29	0.08	0.00	3.8
44X-6, 109-110	407.69	3.04	25.29					
45X-1, 16-17	408.86	0.32	2.66					
45X-1, 101-102	409.71	2.72	22.68					
45X-3, 111-112	412.81	2.84	23.65	2.91	0.07	0.08	0.00	0.9
45X-6, 108-109	417.28	3.68	30.65	3.78	0.10	0.15	0.07	0.7
172-1063B-								
38X-5, 14-17	347.18	2.179	18.15	3.10	0.09	0.06	0.11	16.7
38X-5, 40-50	347.44	1.608	13.39	40.96	39.36	0.79	0.35	49.7
172-1064A								
1H-2, 98-99	2.68	1.49	12.40	2.15	0.66	0.04	0.00	2.2
1H-4, 54-55	5.04	1.87	15.60	2.51	0.64	0.05	0.00	2.5
1H-6, 75-76	8.25	1.51	12.60	2.22	0.71	0.04	0.05	2.2
2H-1, 65-66	10.15	1.47	12.20	2.13	0.66	0.06	0.00	2.1
2H-2, 77-78	11.77	1.64	13.70	2.24	0.60	0.06	0.00	2.2
2H-6, 119-120	18.19	1.59	13.30	2.28	0.69	0.05	0.07	2.3
3H-2 120-122	21.50	0.92	7.67	1.62	0.70	0.06	0.11	1.6
3H-4, 64-65	23.94	1.13	9.44	1.73	0.60	0.04	0.00	1.7
3H-7, 43-44	28.23	1.28	10.70	1.92	0.64	0.04	0.00	1.9

Note: IC = inorganic carbon, TC = total carbon, TOC = total organic carbon, TN = total nitrogen, TS = total sulfur.

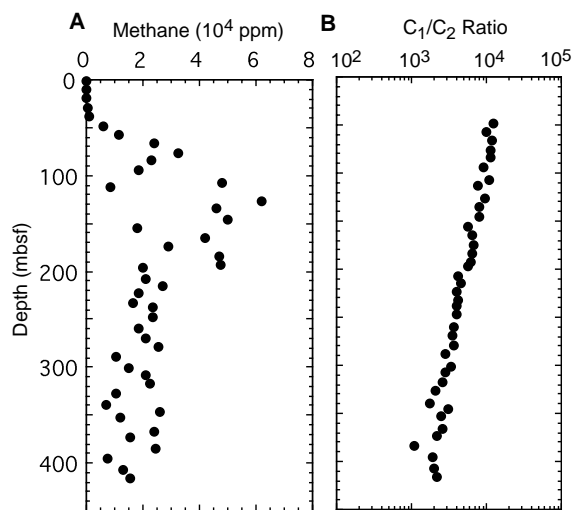


Figure 33. **A.** Downhole profiles of methane concentrations. **B.** Methane-to-ethane (C_1/C_2) ratios from headspace gas samples of Sites 1063 and 1064.

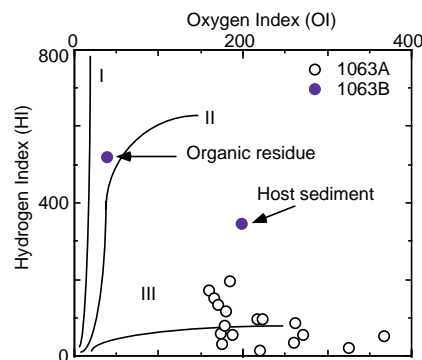


Figure 34. Organic matter properties as shown by Rock-Eval analyses of selected sediment samples from Site 1063 plotted on a van Krevelen-type diagram. Sediment samples from Hole 1063A are distinguished from the occurrence of waxy, organic residue in Hole 1063B by different symbols. This plot relates the chemical characteristics of sedimentary organic matter to the general source of organic matter, its maturity, and type of hydrocarbon produced by thermogenesis. The curves I, II, and III refer to three types of organic matter: type I = algal, oil prone organic matter; type II = marine, oil/gas prone organic matter; and type III = terrestrial, gas-prone organic matter. (HI = mg HC/g TOC, OI = mg CO_2 /g TOC).

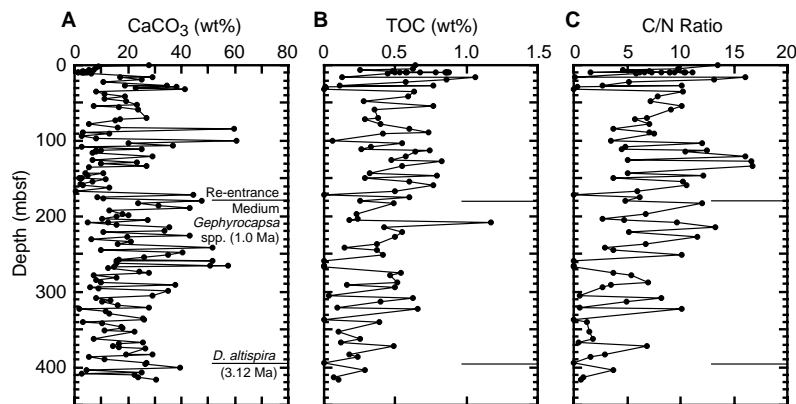


Figure 35. Downhole profiles of (A) calcium carbonate ($CaCO_3$) content, (B) total organic carbon (TOC) content, and (C) C/N ratio of sediment samples from Sites 1063 and 1064.

Table 20. Results of Rock-Eval analyses from Site 1063.

Core, section, interval (cm)	Depth (mbsf)	TOC (wt%)	T_{max} ($^{\circ}C$)	S_1	S_2	S_3	S_2/S_3	PC	HI	OI	PI
172-1063A-											
2H-4, 60.5-62	9.23	0.88		0.10	1.18	1.50	0.79	0.10	134	170	0.08
2H-4, 62.5-63.5	9.25	0.86		0.12	1.48	1.38	1.07	0.13	172	160	0.07
2H-4, 66.5-67.5	9.29	0.85		0.10	1.00	1.53	0.65	0.09	117	180	0.09
2H-4, 68.5-69.5	9.31	0.87		0.11	1.31	1.45	0.90	0.11	150	166	0.08
2H-4, 70-71	9.32	0.86	548	0.10	1.67	1.59	1.05	0.14	194	184	0.06
2H-4, 75-76	9.37	0.78		0.09	0.76	1.74	0.44	0.07	97	223	0.11
3H-2, 33-34	16.63	1.06	383	0.09	0.33	1.86	0.18	0.03	31	175	0.21
3H-4, 25-26	19.55	0.86	377	0.12	0.17	2.81	0.06	0.02	19	326	0.43
4H-3, 34-35	27.64	0.77	370	0.11	0.40	2.83	0.14	0.04	51	367	0.22
7H-1, 113-114	53.93	0.77		0.11	0.65	2.02	0.32	0.06	84	262	0.14
10H-5, 121-122	88.51	0.73		0.08	0.71	1.59	0.45	0.06	97	217	0.10
14H-7, 48-49	128.02	0.83	372	0.03	0.11	1.83	0.06	0.01	13	220	0.21
16H-6, 83-84	146.05	0.79	523	0.08	0.45	1.49	0.30	0.04	56	188	0.15
18H-2, 53-54	159.13	0.77		0.06	0.62	1.38	0.45	0.05	80	179	0.09
24X-1, 50-51	208.10	1.17	413	0.08	0.68	2.04	0.33	0.06	58	174	0.11
34X-4, 67-68	308.67	0.62	395	0.05	0.33	1.69	0.20	0.03	53	272	0.13
35X-1, 56-57	313.66	0.40	380	0.05	0.22	1.72	0.13	0.02	33	260	0.19
172-1063B-											
38X-5, 14-17	347.18	0.09	344	0.70	3.19	1.83	1.74	0.32	346	198	0.18
38X-5, 40-50	347.44	39.36	352	98.59	204.57	15.02	13.62	25.26	519	38	0.33

Note: TOC = total organic carbon, PC = petroleum potential, HI = hydrogen index, OI = oxygen index, PI = production index.

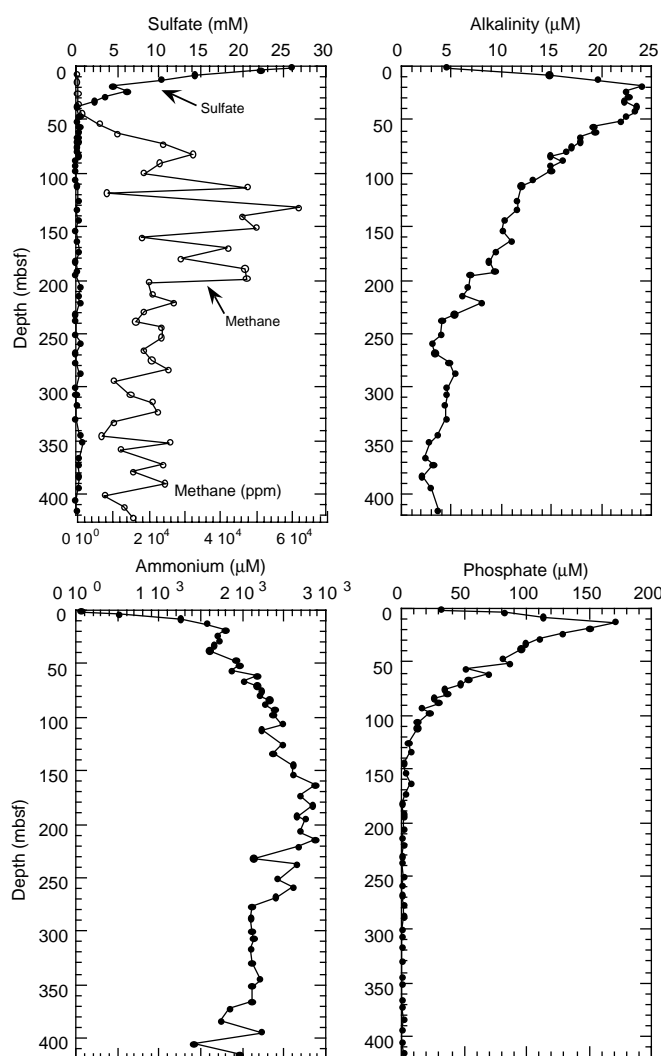


Figure 36. Concentration vs. depth profiles for interstitial waters at Hole 1063A.

ter during early diagenesis. The depth to the sulfate/methane interface is at 38 mbsf at Site 1063 (Fig. 36). The sulfate profile at this site has a concave-down shape and displays the characteristic reciprocal relationship with methane that shows a downhole increase below the sulfate/methane interface. At Site 1064, only part of the sulfate zone is cored. Assuming a linear downhole sulfate profile and a near-sea-floor sulfate concentration of 27.5 mM in the sediments, it seems that Hole 1064A overpenetrated the seafloor by about 19 m, and that the base of the sulfate reduction zone is 58 m below the true seafloor, resulting in a sulfate reduction zone of 75–80 m thickness (Table 21; Fig. 37).

At Site 1063, alkalinity shows a sharp downhole increase to a peak value of 24 mM within the top 20 m of the sulfate reduction zone and sustains the high values between 20 and 52 mbsf. It then decreases to 3–5 mM at about 235 mbsf and varies between 2 and 4 mM below this depth. In part of the sulfate reduction zone cored at Site 1064, the alkalinity ranges between 10.6 and 12.9 mM, increasing in the 3–18-mbsf depth interval (Fig. 37). The alkalinity values at this site are considerably lower than those over the corresponding depth interval at Site 1063.

Ammonium and phosphate show rapid downhole increases in the top part of the sulfate reduction zone at Site 1063 (Fig. 36). Ammonium continues to increase at a reduced rate in the lower part of the

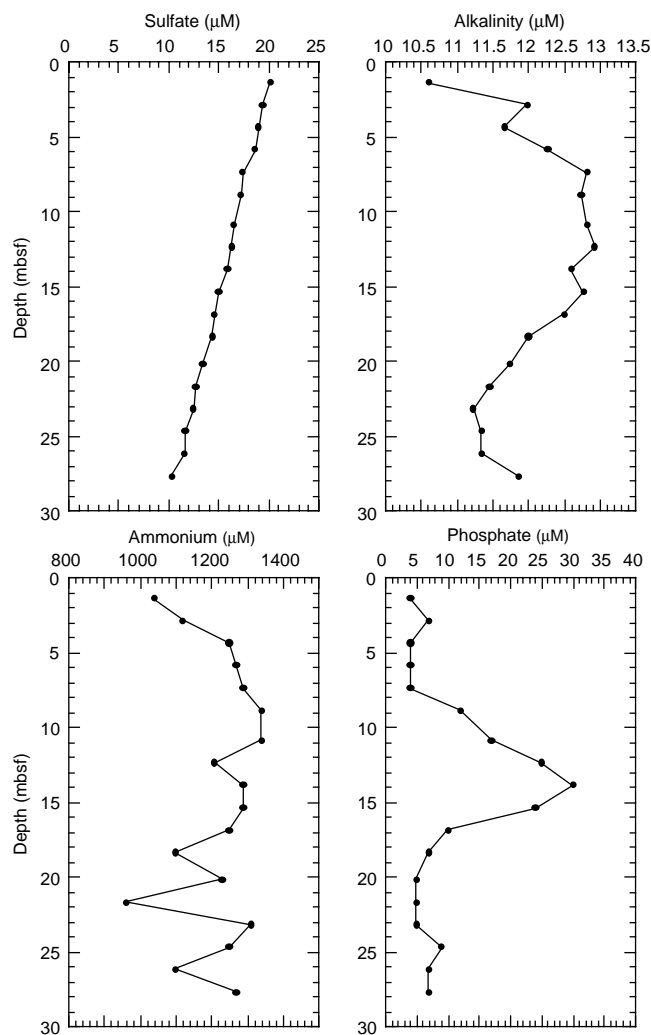


Figure 37. Concentration vs. depth profiles for interstitial waters at Hole 1064A.

sulfate reduction zone and upper part of the methanogenesis zone, but shows a several hundred micromole decrease below 275 mbsf. After peaking at 175 μM at 20 mbsf, phosphate concentrations show a rapid downhole decrease to $<10 \mu\text{M}$ at about 125 mbsf and to 1–2 μM range at depths >180 mbsf. At Site 1064, both ammonium and phosphate are lower than those values in the sulfate reduction zone at Site 1063 (Fig. 37). A phosphate peak (30 μM) is observed at 14 mbsf at Site 1064 that is about six times less than the peak at Site 1063.

Discussion

The rapid downhole decrease in the sulfate and increases in the alkalinity, ammonia, and phosphate concentrations at Site 1063 are caused by the microbial decomposition of organic matter in the sulfate reduction zone. The concave-down shape of the sulfate profile at this site suggests that the sulfate depletion results predominantly from “normal” sulfate reduction caused by microbial activity, $\text{SO}_4^{2-} + 2\text{CH}_2\text{O} \rightarrow \text{H}_2\text{S} + 2\text{HCO}_3^-$ (Berner, 1980; Gieskes, 1981), and that the upward methane flux is low so that sulfate consumption by anaerobic methane oxidation, $\text{CH}_4 + \text{SO}_4^{2-} \rightarrow \text{HCO}_3^- + \text{HS}^- + \text{H}_2\text{O}$, (Reeburgh, 1976) is a minor process. The lower alkalinity, ammonium, and phosphate in the sulfate reduction zone at Site 1064 compared to those in the same zone at Site 1063 are probably the result of the rel-

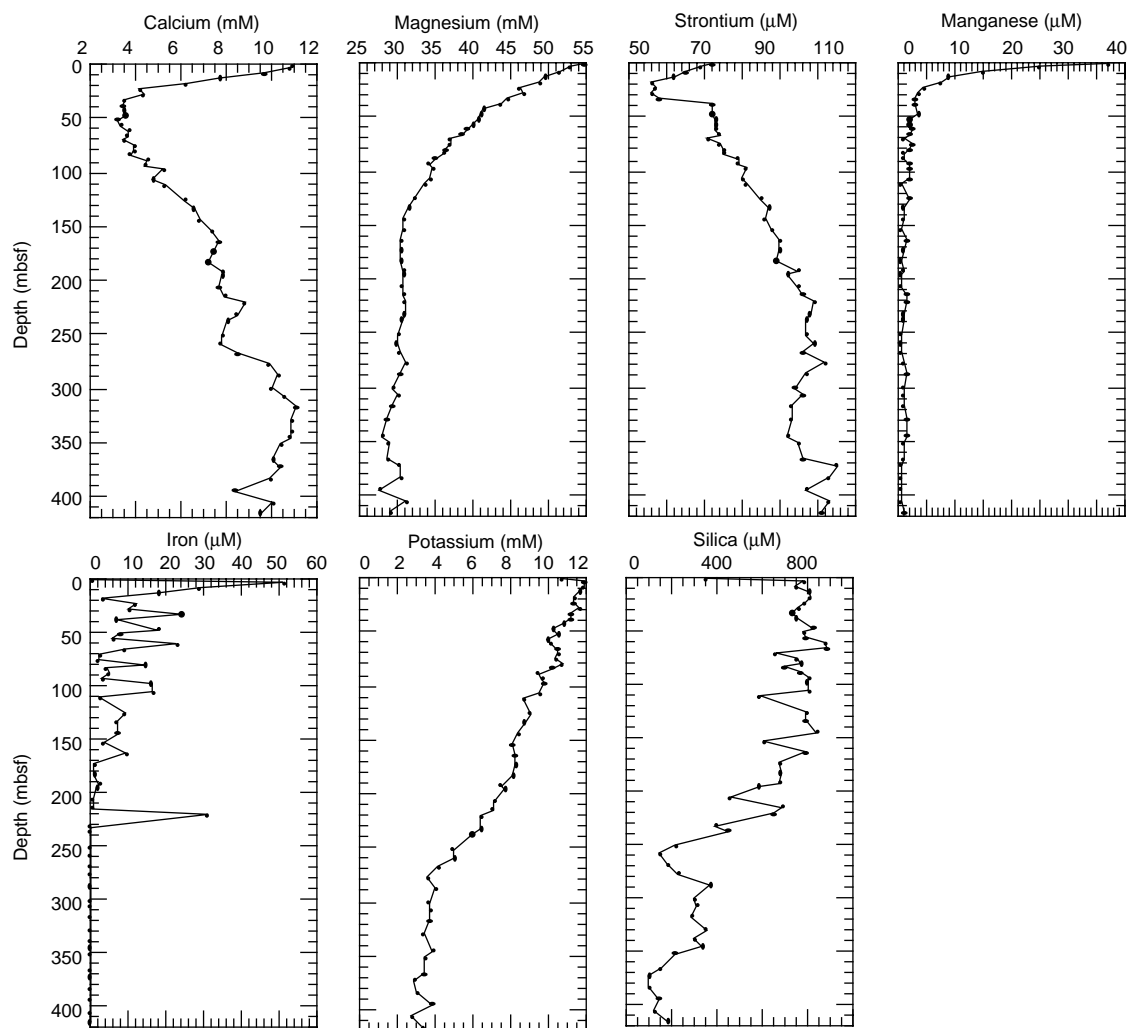


Figure 38. Concentration vs. depth profiles for interstitial waters at Hole 1063A.

atively lower organic carbon content of the sediments at the former site (see “Organic Geochemistry” section, this chapter).

At Site 1063, the downhole decrease in the phosphate concentrations in the lower part of the sulfate reduction zone and upper methanogenesis zone indicates a reduced rate of organic matter degradation and probable adsorption of this anion on the carbonate minerals (e.g., Morse and Mackenzie, 1990). Similarly, the reduced ammonium concentrations in the lower part of the sediment column at Site 1063 can be explained by a low degree of organic matter decomposition and by adsorption of ammonium ions on clay minerals (Rosenfeld, 1979; Mackin and Aller, 1984).

Authigenic Precipitation and Dissolution of Minerals

Interstitial water calcium, magnesium, and strontium concentrations are sensitive indicators of carbonate diagenesis. Rapid downhole decreases in the concentrations of these three elements occur in the sulfate reduction zone at Site 1063 (Fig. 38). In the sulfate reduction zone at Site 1064, the downhole decrease in these species is somewhat gradual (Fig. 39). The lowest values of calcium and strontium and a reversal to a downhole increasing trend all occur at or near the sulfate/methane interface at Site 1063. In the methanogenesis zone at Site 1063, the calcium and strontium concentrations increase, whereas magnesium concentrations decrease downhole. Calcium and strontium concentrations show a reciprocal relationship between 270 and 360 mbsf.

Iron and manganese are redox-sensitive elements. At Site 1063, downhole interstitial water concentrations of these elements show enrichments in the upper sulfate reduction zone and to a lesser extent in the upper methanogenesis zone (Fig. 38). Iron shows a more variable profile than manganese. With increasing depth, iron and manganese concentrations decline to low levels in the lower part of the sediment column in the methanogenesis zone. Interstitial manganese concentrations are very low at Site 1064, further indicating the overpenetration of the hole (Fig. 39).

Interstitial silica and potassium concentrations decrease downhole starting near the top of the sulfate reduction zone at Site 1063, with the decrease being more gradual in the top 200 m of the sediment column than between 200 and 260 mbsf (Fig. 38). At depths >260 mbsf, the concentrations of silica and potassium are relatively uniform within the low ranges of 99–370 μM and 3–5 mM, respectively. The potassium concentrations are uniform along the length of Hole 1064A, ranging between 9.5 and 10.5 mM, while silica concentrations vary between 363 and 777 μM and show an increase to >700 μM between 7 and 18 mbsf (Fig. 39).

Discussion

At Site 1063, calcium, magnesium, and strontium concentrations decrease with depth in the sulfate reduction zone as a result of diffusion of these ions from overlying seawater into the sediment, and their removal by precipitation of carbonate minerals in the lower part

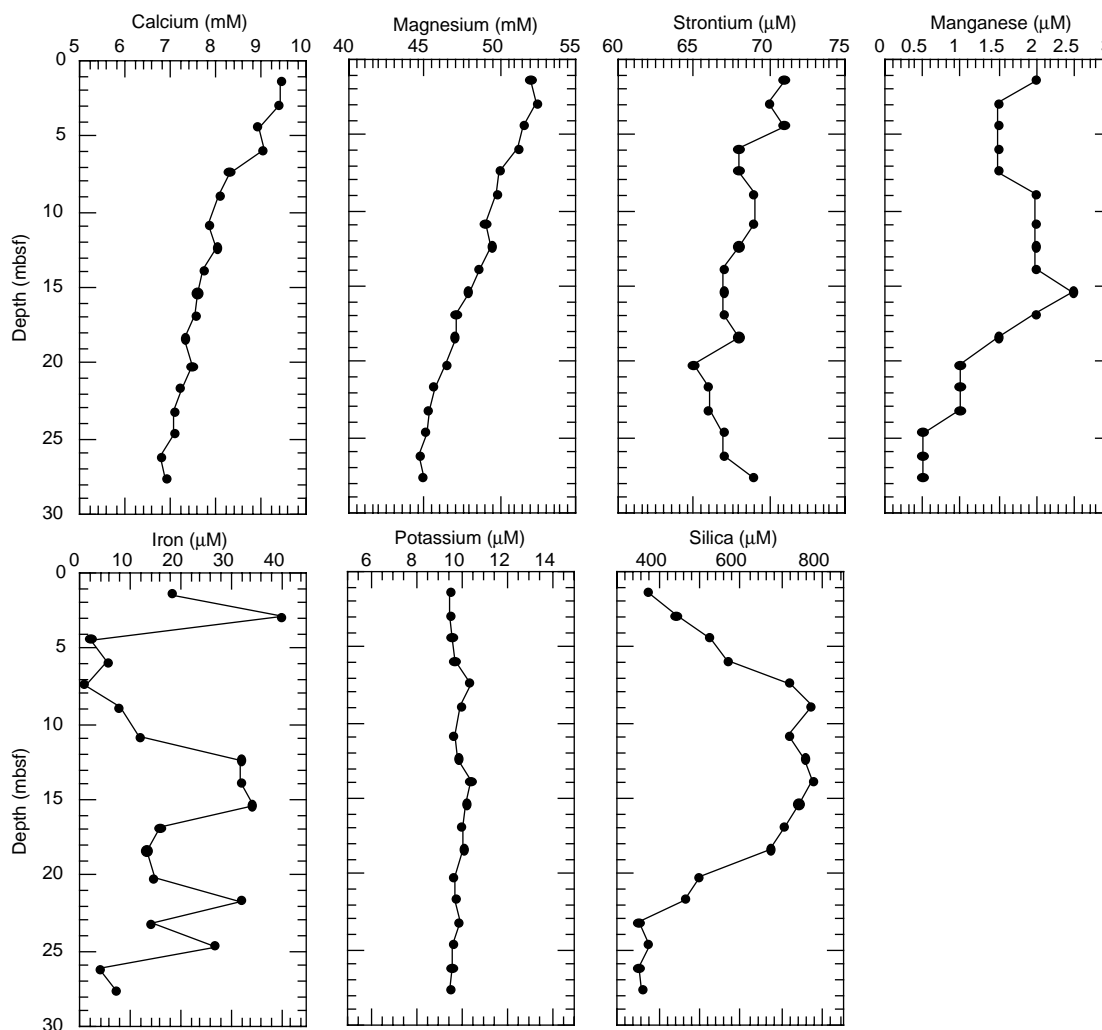


Figure 39. Concentration vs. depth profiles for interstitial waters at Hole 1064A.

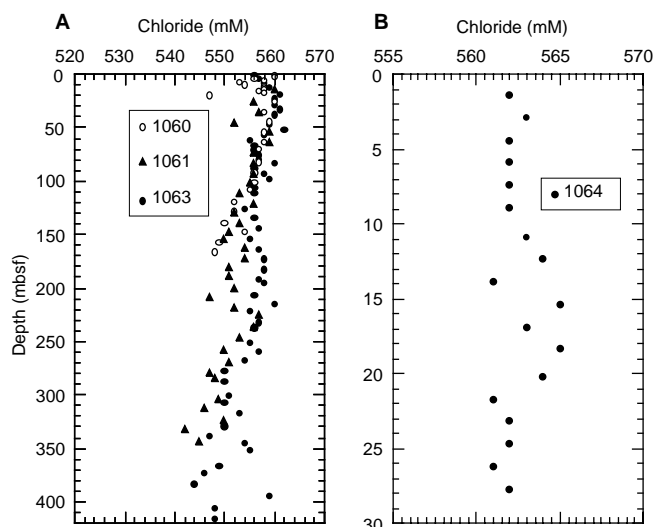


Figure 40. Downhole chloride profiles for (A) Site 1063, with Blake-Bahama Outer Ridge Sites 1060 and 1061 for comparison, and (B) Site 1064.

of the sulfate reduction zone and upper methanogenesis zone. The downhole increase in the concentration of strontium in the methanogenesis zone suggests release of strontium into pore waters by recrystallization or dissolution of biogenic carbonates. The concomitant downcore increase in calcium and decrease in magnesium suggest dolomite formation in the sediment column. The reciprocal relationship between the calcium and strontium concentrations at 270–360 mbsf is probably caused by the reduced amount of biogenic carbonates and increased amount of detrital components of the sediments in this interval (see “Lithostratigraphy” section, this chapter).

Interstitial profiles of iron and manganese are sensitive indicators of redox fronts in a sediment column. These elements are mobilized in the sulfate reduction zone, causing the high concentrations in the interstitial waters. Compared to the Deep Blake-Bahama Outer Ridge sites, the top of the sediment column at Site 1063 contains about twice the amount of dissolved manganese. This is mainly caused by the proximity of the latter site to volcanic sources. At Site 1064, high levels of manganese likely occur in the top of the sulfate reduction zone, but it was not cored. Lower iron concentrations in parts of the sulfate reduction zone at Sites 1063 and 1064 indicate the formation of authigenic iron sulfides, which occur as black mottling or laminae in the sediments (see “Lithostratigraphy” section, this chapter). Low levels of interstitial iron and manganese within the methanogenesis zone at Site 1063 are consistent with their incorporation into newly forming carbonate minerals, such as ankerite and siderite. These conclusions are supported by the common presence of dolomite (and/or

ankerite) in these sediments, as determined by the XRD analysis of bulk samples.

The relatively high levels of dissolved silica in the upper 220 m of the sediment column at Site 1063 suggest dissolution of biogenic silica in the sediments, whereas the markedly reduced silica concentrations in the lower 200 m are the result of the absence of siliceous tests. The downhole decrease in the potassium concentrations at Site 1063 is probably caused by adsorption of potassium ions on clay minerals.

Interstitial Water Chloride and Gas Hydrate

Interstitial water chloride values in the top 10 m of Hole 1063A are slightly lower than the standard seawater (IAPSO) value of 559 mM. The values remain close to the standard seawater value between 13 and 57 mbsf and then show a slight overall downhole freshening trend, amounting to ~3% of the standard seawater value. This trend has an average gradient of approximately -4 mM/100 m and includes some small negative excursions at 61–71, 107–134, 154, 269–340, 360–390, and 407–416 mbsf, with positive excursions at 52, 84, 94, 98, 215, 260, 353, and 396 mbsf.

The interstitial water chloride values at Site 1064 range between 561 and 565 mM, a few mM higher than the standard seawater value. Assuming an overpenetration of about 19 m, the downhole chloride profile at Site 1064 may correspond to the high chloride values in 20–60 mbsf at Site 1063.

Discussion

Chloride values lower than the standard seawater value in the top 10 mbsf, together with a value of 556 mM obtained for the WSTP bottom-water sample, probably reflect the presence of the lower salinity AABW at Site 1063: this water mass has a salinity of 34.88‰ at *Knorr* 140/2 Hydro Station 1.

The overall downhole freshening of chloride values observed at Site 1063 can be explained by a number of different processes: (1) groundwater advection (e.g., Gieskes, 1981); (2) ion filtration by clays (Kastner et al., 1990); (3) mineral dehydration involving clay minerals, opal-A, and other oxy-hydroxides (Kastner et al., 1990; Kastner et al., 1993); and (4) gas hydrate at depth (Hesse and Harrison, 1981; Kvenvolden and Kastner, 1990).

Groundwater advection and clay membrane ion filtration are unlikely processes at Site 1063. The nearest source of freshwater is Bermuda, 350 nmi west-southwest, with a hydrologic head insufficient to supply freshwater to water depths of 4500 m. The process of clay membrane filtration requires a thick sedimentary overburden to supply the necessary filtration pressure. The sediment thickness at Site 1063 is about 1 km and seems insufficient to trap chloride ions within clay minerals. Artificial squeezing effects as induced by Manheim squeezers are also unlikely because squeezing pressures lower than 30,000 psi do not affect interstitial chloride concentrations (Sayles, 1970; Manheim, 1974; Gieskes et al., 1990).

The presence of up to 30% biogenic silica at some levels in the upper 150 m of the sediment section suggests that dissolution and recrystallization of opal-A may release some fresh water and thus freshen the chloride values (e.g., Kastner et al., 1990; Kastner et al., 1993). The dissolution of biogenic silica is supported by increasingly poor preservation of diatoms downhole (see “Biostratigraphy” section, this chapter). Other mineral dehydration reactions as a source for freshwater are not supported by the observed geothermal gradient and interstitial water chemistry. Downhole thermal measurements indicate a bottom-water temperature of 2.34°C and a geothermal gradient of 20°C/km (see “Physical Properties,” section, this chapter). Smectite to illite conversion, which releases water to pore fluids, begins at about 60°C (Hower et al., 1976). Thus, assuming that the measured geothermal gradient and the estimate of sediment thickness are correct, the highest temperatures occurring in the sedimentary section at Site 1063 (20°C per 1000 m of sediment) are insufficient to initialize the clay dewatering process.

The geologic setting of Site 1063 also seems unlikely for gas hydrate formation and occurrence. The site is situated 700 nmi from the North American continent in a basin underlain and partially enclosed by oceanic basement. Reflection seismics suggest that the sediment thickness is only about 1 km; the reflectors are generally flat-lying and attenuate rapidly with increasing depth (see “Site Geophysics” section, this chapter). Furthermore, there is no evidence of a bottom-simulating reflector (BSR), usually indicative of the gas bubbles occurring at the base of gas hydrate stability (see “Inorganic Geochemistry” section, “Deep Blake-Bahama Outer Ridge” chapter, this volume). However, the observed chloride concentrations and chloride gradient are similar to those observed elsewhere on the Deep Blake-Bahama Outer Ridge at locations where the presence of gas hydrate has been suggested (Fig. 40; “Inorganic Geochemistry” section, “Deep Blake-Bahama Outer Ridge” chapter, this volume). Methane concentrations at depth are sufficient to cause sediment expansion, implying that adequate amounts of methane may exist at Site 1063 to produce gas hydrate. Given adequate methane concentration, the pressure and temperature conditions are entirely within the realm of gas hydrate stability. The base of gas hydrate stability at Site 1063 should lie between 1000 and 1250 mbsf, using a bottom-water temperature of 2.34°C, a geothermal gradient of 20°C/km, a water depth of 4595 m, and a hydrate stability equation for seawater (Dickens and Quinby-Hunt, 1994). Thus, a BSR is not expected, nor necessary to indicate the presence of gas hydrate.

The negative and positive excursions of chloride values superimposed on the general trend to decrease downhole has three possible causes. The first possibility is the formation and dissociation of small amounts of gas hydrate in the sediment column (Hesse and Harrison, 1981; Jenden and Gieskes, 1983; Kvenvolden, Kastner, et al., 1990; Paull, Matsumoto, Wallace, et al., 1996). The second possibility is the dissolution or recrystallization of biogenic silica in parts of the sedimentary section, as discussed above. The third explanation for the chloride excursions is that they reflect nonsteady-state conditions induced by glacial-interglacial salinity changes (McDuff, 1985; Schrag and DePaolo, 1993). The depth and geographic position of Site 1063 is such that it has probably been under the influence of mainly AABW during the glacial periods (Boyle and Keigwin, 1987) and mainly NADW during the interglacial periods (Hogg, 1983; Schmitz and McCartney, 1993). Such a switch in the water masses, coupled with increased salinity of the global ocean during the glacial stages, may be reflected in increased chloride values. For example, the increased chloride concentrations at 10–50 mbsf may be the result of the downward diffusion of the last glacial maximum water into the sediment (see “Sedimentation and Mass Accumulation Rates” section, this chapter). However, the chloride data alone do not favor any of the above three possibilities.

PHYSICAL PROPERTIES

Introduction

Site 1063 on the Bermuda Rise shows physical properties similar to the deepest sites on Blake-Bahama Outer Ridge, although noticeable differences exist. Diatom-enriched layers occurring in lithologic Subunit IA (see “Lithostratigraphy” and “Biostratigraphy” sections, this chapter) are clearly recognized at this site as minima in bulk density. On longer time scales, cyclicity in physical properties suggests that sedimentation is orbitally controlled. Site 1064, located on the Sohm Abyssal Plain at a water depth of 5568 m, is a deep-water companion to Site 1063.

MST Measurements

MST data for Holes 1063A and 1064A are on CD-ROM (back pocket, this volume) and presented in Figures 41 and 42. The data were generally collected at 4-cm spacings for magnetic susceptibility to the bottom of each hole and at 50-cm spacings for natural gamma

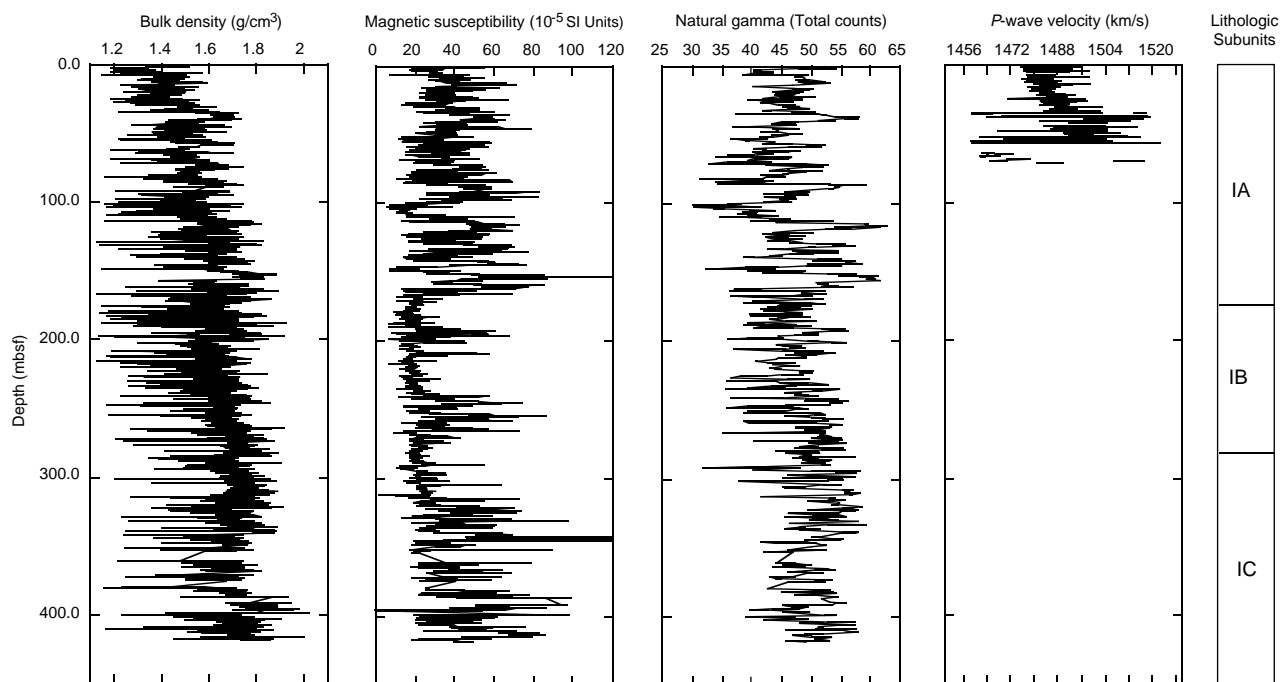


Figure 41. Vertical profiles of MST data from Hole 1063A.

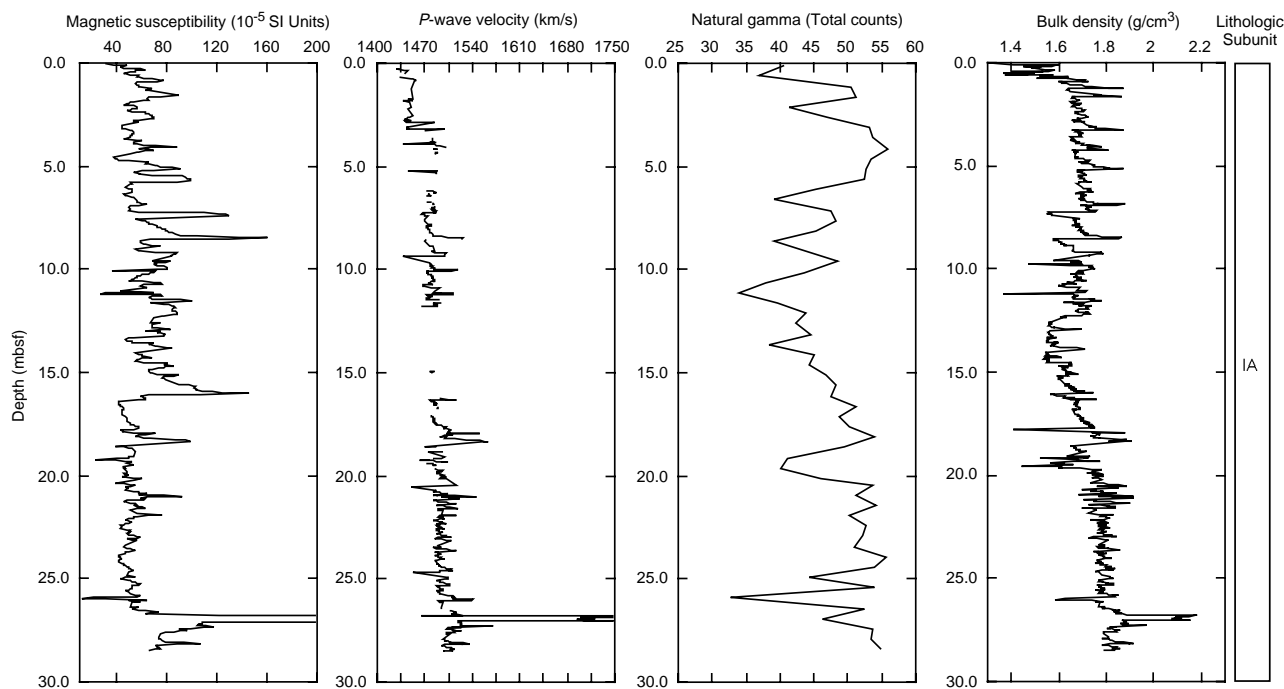


Figure 42. Vertical profiles of MST data from Hole 1064A.

ray (NGR) for Holes 1063A and 1064B. A 2-cm interval was used for the *P*-wave logger (PWL) and GRAPE in the uppermost part of each hole as long as the PWL could collect data. Less sediment distortion and cracking due to interstitial gas at Site 1063 (see “Organic Geochemistry” section, this chapter) allowed for the collection of PWL data to a depth of 50–70 mbsf. All MST sensors provided high quality data to the base of Site 1064 at 28.640 mbsf.

In the interval from 0 to 170 mbsf, which correlates with Subunit IA (see “Lithostratigraphy” section, this chapter), high-amplitude, low-frequency variations in bulk density, magnetic susceptibility, and

natural gamma-ray records are visible. From 170 mbsf to the base of the hole, the properties vary with similar amplitudes, but the variation takes place at a higher frequency. This transition is just below the Brunhes/Matuyama boundary (see “Paleomagnetism” section, this chapter), suggesting that the variability in Subunit IA is driven by 100-k.y. orbital forcing and in Subunits IB and IC by the 40-k.y. orbital forcing.

When examined in detail, the GRAPE-derived bulk densities exhibit decimeter to meter scale variations with values varying between 10% and 20% (Fig. 43). Analyses of a giant piston core (GPC-5) from

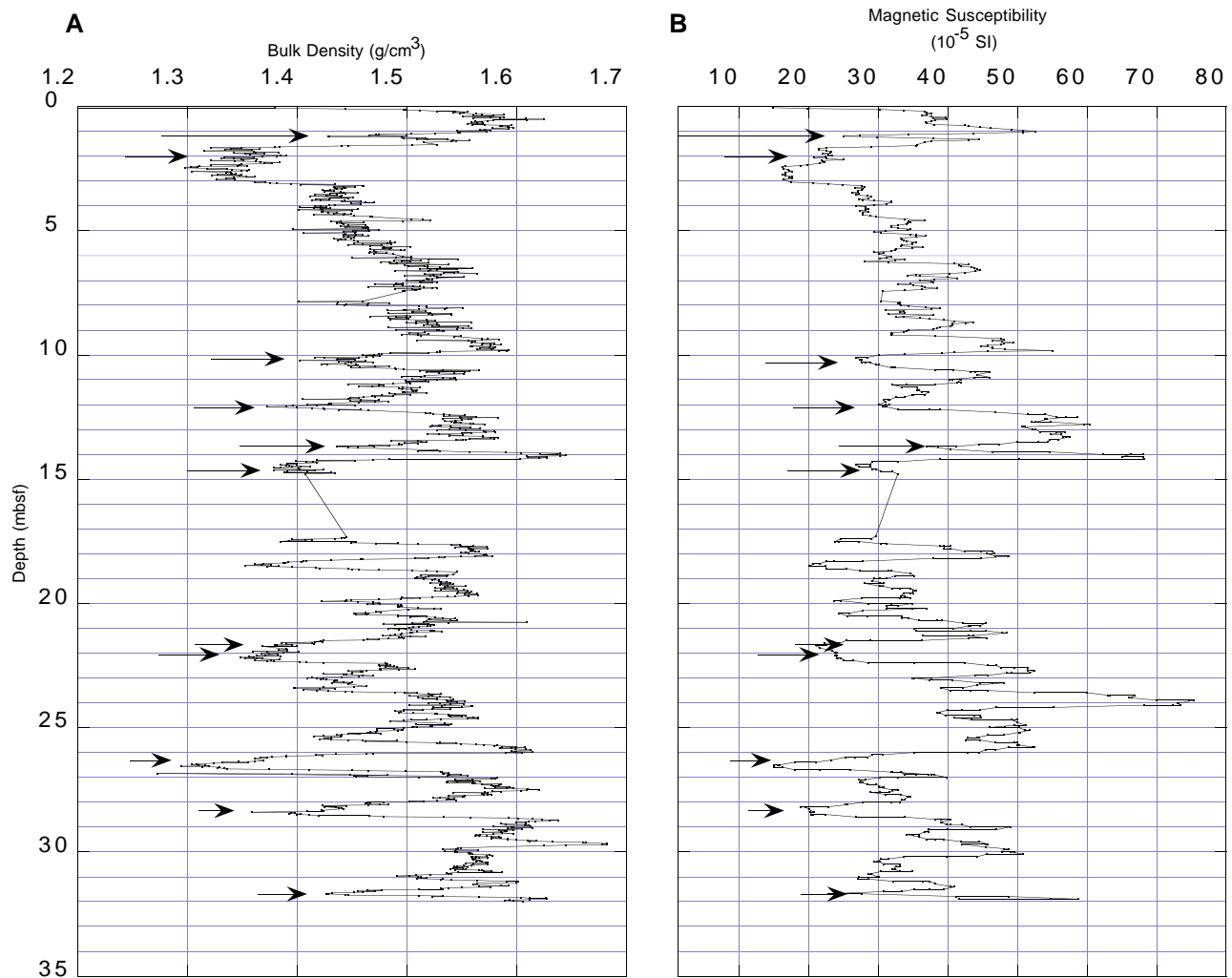


Figure 43. Diatom-rich layers recognizable in (A) bulk density and (B) magnetic susceptibility records for Hole 1063A. Sampled intervals are indicated by arrows.

the northeast Bermuda Rise (Silva et al., 1976; Baker, 1986) suggest that values of lower bulk density at the end of MIS 2 correspond to enrichment of diatoms and radiolarians within the sediments. It was argued that the mixture of abundant sand-sized silica particles with the more predominant clays apparently retarded loss of water through consolidation by holding the pore spaces open with a more rigid structure. Further, it was shown that, in this interval, clay mineralogy did not play a role in creating the higher water contents and consequent lower densities. Additionally, 11 low-density layers within MISs 2 and 3 at Hole 1063B were sampled for bulk density and paleontological analysis to further explore this silica-matrix model for lowered densities (Fig. 43). This reconnaissance showed that these layers were diatom-rich, suggesting that the low-density zones mark episodes of increased diatom productivity and/or preservation (see “Biostratigraphy” and “Lithostratigraphy” sections, this chapter). Furthermore, these layers most likely correlate with the minima in carbonate that occur about every 4 k.y. in core GPC-5 from the northeast Bermuda Rise (Keigwin and Jones, 1994). The general trend of diatom enrichments and carbonate minima are one of the key elements defining sediment lithology within lithologic Unit IA (see “Lithostratigraphy” section, this chapter).

Further investigation of the MST data from Site 1063 shows differing phase relationships between GRAPE and PWL measurements,

again thought to be controlled by the abundance of sand-sized biosilica. In general, compressional wave velocity is observed to increase with increasing bulk density (Hamilton, 1978) resulting in an “in phase” relationship between the two variables. Over the period 80–10 ka in Hole 1063A, 14 “low density” events are noted, yielding an average period of around 4 k.y. between the events (Keigwin and Jones, 1994). Of these 14 events, seven show strongly “out-of-phase” velocity vs. density relationships, where high velocities are associated with low bulk density values (Fig. 44), suggesting that sand-sized biosilica particles become abundant enough in these intervals to increase the shear modulus of the sediment, increasing compressional wave velocity (Hamilton and Bachman, 1982). The seven events noted occur during MISs 2 (2 mbsf and 12–14 mbsf) and 4 (24–28 mbsf), suggesting that diatom productivity and/or preservation potential was highest, although not confined to, these glacial periods. The preliminary stratigraphy used here is based on a comparison of the L^* reflectance parameter with existing oxygen isotope records and percentage carbonate (Adkins et al., 1997).

At Site 1064 P -wave velocity and bulk density increase gradually with depth, although bulk density decreases briefly between 12 and 15 mbsf. Natural gamma reflects the predominantly terrigenous character of the sediments. Higher than usual values of both P -wave velocity and bulk density suggest overpenetration of the corer, although

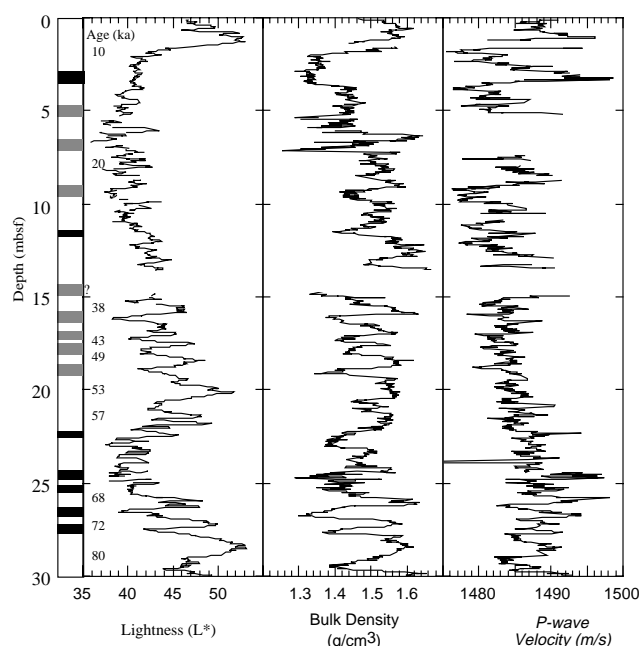


Figure 44. Low bulk density intervals (shaded gray) in Hole 1063A, correlated with P -wave velocity and lightness (L^*). At this site, low bulk density intervals are indicative of high diatom productivity. Seven low-density intervals are correlated with high P -wave velocity (shaded black), and possibly represent sediment where the diatom content is particularly high, imparting a greater “rigidity” to the sediment. Chronology is derived by correlation of gray-scale peaks of known age in piston core MD952036 (J. Adkins et al., unpubl. data).

these high values may be more typical of abyssal plain core tops than the hemipelagic sediments we encountered elsewhere during Leg 172. Although this site is in the Sohm Abyssal Plain, only one major sand layer was sampled at 26.72–27.20 mbsf, presumably because this location is mostly influenced by distal turbidites. The elevated bulk densities and P -wave velocities measured on this sand layer (Fig. 42) are the highest measured during Leg 172.

Index Properties

Index properties samples were taken at a frequency of approximately two per section for Holes 1063A, 1063D, 1064A, and three per core for Hole 1063B, except over the XCB-cored interval where samples were taken at a spacing of one per section. Summary statistics for index properties are presented in Table 22. All collected data for bulk density, grain density, dry density, water content, and porosity at these sites are listed in Tables 23 and 24 and graphically represented in Figures 45 and 46.

In Hole 1063A, bulk density increases from ~ 1.4 g/cm³ at the surface to 1.95 g/cm³ at 400 mbsf. The 100-k.y. cyclicity (based on the biostratigraphic age model; see “Biostratigraphy” section, this chapter) in bulk density is apparent in the upper 170 m (lithostratigraphic Subunit IA). From 170 mbsf to the bottom of the hole, bulk density shows only a slight increase with depth and low-amplitude variability. As at Site 1062, the low amplitude of the bulk density cycles (when compared with those seen on the Blake Outer Ridge) is caused by grain density and porosity values varying “in phase,” where periods of high grain density correspond to periods of high water content and vice versa, thus suppressing the amplitude of bulk density cycles.

Grain density trends at Site 1063 are dominated by long-term variation in sediment supply. From the surface to 70 mbsf, grain density ranges from 2.60 to 2.75 g/cm³, consistent with a significant con-

tribution from biogenic silica (estimates from smear slides suggest up to 25% by area, composed of diatoms, radiolarians, and silicoflagellates—see “Lithostratigraphy” section, this chapter). An abrupt increase at 70 mbsf (~ 340 ka; see “Biostratigraphy” section, this chapter) to 2.85 g/cm³ is possibly related to (1) a reduced supply of biogenic silica below this level; (2) an increased supply of heavy mineral types, characterized by an increased abundance of hematite-bearing lutites (see “Lithostratigraphy” section, this chapter); or (3) a combination of both. From 75 to 160 mbsf (340–875 ka), grain density decreases to 2.75 g/cm³ and fluctuates around this value to the bottom of the hole (>3.12 Ma). It should be noted that Site 1062 shows a similar long-term trend in grain density, suggesting that large-scale ocean circulation changes are the controlling factor.

Values for index properties measurements at Site 1064 (Sohm Abyssal Plain) are notably different from those recorded on the Bermuda Rise at Site 1063. Overall, bulk density is consistently high, with an average value of 1.653 g/cm³ (an average value of 1.435 g/cm³ was obtained for the first 30 m at Site 1063) caused by low porosity (63.4%, compared to 75.27% for the first 30 m at Site 1063) rather than high grain density (although this is also slightly higher than in the first 30 m at Site 1063—2.74 g/cm³ compared with 2.69 g/cm³ at Site 1064). These data concur with the sulfate abundance profiles (see “Inorganic Geochemistry” section, this chapter), which suggest an overpenetration of as much as 20 m. Three physical subdivisions can be made at Site 1064. From the surface to 12 mbsf, bulk and grain densities are more variable than below, reflecting the high frequency of turbidite layers in this interval (see “MST Measurements” above). A zone of higher porosity and lower grain density occurs between 12 and 19 mbsf, suggesting that the pelagic component contains a greater percentage of biogenic silica and/or a decreased heavy mineral component, with variations in grain size perhaps controlling the porosity. From 19 mbsf to the bottom of the hole, sediment becomes homogeneous (with the exception of a single sandy turbidite in Section 172-1064A-3H-6, described in the “Lithostratigraphy” section of this chapter), showing little variation in index properties.

Acoustic Velocity

At Site 1063 (Holes 1063A, 1063B, and 1063D) and Site 1064, longitudinal velocities (perpendicular to bedding, z -direction) and transverse velocities (parallel to bedding, y -direction) have been obtained with the digital sonic velocimeter (DSV) at Site 1063 at a resolution of two measurements each per section (Tables 25, 26). DSV measurements are generally in reasonable agreement with the PWL data for whole-round samples obtained at 2-cm intervals on the MST. Larger offsets between the two data sets occur in the upper part of the records, which is most probably caused by differences in core temperature (18°C at the PWL, 20°C at the DSV), as pore-water velocity changes significantly with temperature. Core temperatures have been monitored for all measured sections, allowing for postcruise temperature corrections of the velocity measurements.

Micropores and macroscopic cracks precluded accurate measurements of sound velocity at Site 1063 below 55 mbsf. Velocity at Hole 1063A (Fig. 47) increases from 1480 m/s at the seafloor to 1500 m/s at 55 mbsf. Significantly higher velocities (1500–1520 m/s) have been measured in an interval between 33 and 40 mbsf, which most likely corresponds to MIS 6.

At Site 1064 (Fig. 48), the general downhole trend of increasing velocity with depth is similar to that observed at Site 1063. However, excursions to higher velocities (>1510 m/s) occur more frequently and are associated with sediments deposited by downslope transport processes (turbidites). Maximum velocities of 1770 m/s measured with the PWL correspond with a sandy layer observed between 26.7 and 27 mbsf, which also shows a high bulk density (2.2 g/cm³; measured by GRAPE; see “MST” above), and therefore most likely represents a prominent seismic reflector.

Table 21. Interstitial water analyses for Sites 1063 and 1064.

Core, section, interval (cm)	Depth (mbsf)	Alkalinity		Cl (mM)	SO ₄ (mM)	PO ₄ (μM)	NH ₄ (μM)	Na (mM)	Mg (mM)	Ca (mM)	K (mM)	SiO ₂ (μM)	Mn (μM)	Fe (μM)	Sr (μM)	
		pH	Salinity													
172-1063A																
1H-1, 140-150	1.40	7.45	4.54	35.0	556	25.89	32	70	449	52.89	10.84	11.9	352	37	0.4	72
1H-3, 140-150	4.40	7.69		35.0	557	22.26	83	530	391	51.52	9.68	11.86	781	25	51.3	69
2H-3, 140-150	8.52	7.51	14.84	35.0	558	14.38	114	1270	365	49.6	7.7	11.65	746	15	29	65
2H-6, 140-150	13.02	7.65	19.66	34.0	559	10.23	171	1580	314	48.79	6.23	11.37	810	9	18	62
3H-3, 140-150	19.20	7.7	24.12	34.0	561	4.48	151	1800	333	46.19	4.21	11.32	812	7.5	3.3	56
3H-6, 140-150	23.70	7.41	22.50	34.0	560	6.17	129	1700	365	46.82	4.36	11.64	790	4.5	12.1	57
4H-3, 140-150	28.70	7.66	22.77	33.5	560	3.61	111	1730	377	44.55	3.53	11.19	759	3.5	10.5	56
4H-6, 140-150	33.20	6.84	22.34	33.5	561	2.29	100	1665	392	43.74	3.43	11.18	733	3	24.2	58
5H-3, 140-150	38.20	7.61	23.57	33.5	560	0.12	96	1610	393	41.38	3.53	10.81	753	3	7.1	72
5H-6, 140-150	42.70	7.51	23.41	33.5												
6H-3, 140-150	47.70	7.16	22.50	33.5	559	0.5	81	1930	412	41.09	3.57	10.26	828	3.5	18	72
6H-6, 140-150	52.20	7.72	21.99	33.5	562	0.2	87	1970	409	40.75	3.22	10.57	781	2	8	73
7H-3, 140-150	57.20	7.69	19.24	33.0	558	0.46	52	1870	439	40.08	3.39	9.97	792	2	6.1	73
7H-6, 140-150	61.70	7.45	19.43	33.0	555	0.35	70	2180	419	39.23	3.71	10.17	876	2.5	23.2	73
8H-3, 140-150	66.70	7.52	17.91	32.5	556	0.25	54	2020	436	38.47	3.64	10.48	885	2	9.1	74
8H-6, 140-150	71.20	7.65	17.88	32.5	556	0.28	48	2180	445	37	3.48	10.57	658	1	2.7	71
9H-3, 140-150	76.20	7.7	17.07	32.5	557	0.16	35	2240	457	37.01	3.98	10.39	753	2.5	2.2	74
9H-6, 140-150	80.70	7.7	16.46	32.5	557	0.15	37	2220	456	36.4	3.98	10.72	770	2	14.4	75
10H-2, 140-150	84.20	7.4	14.97	32.5	560	0.42	26	2330	470	36.21	3.78	10.21	698	1	4.2	75
10H-5, 140-150	88.70	7.59	16.11	32.5	556	0	30	2280	463	34.97	4.56	9.45	768	1	5	79
11H-2, 140-150	93.70	7.69	14.95	32.5	558	0	17	2390	479	34.2	4.44	9.69	808	2	3.3	79
11H-5, 140-150	98.20	7.62	15.00	32.5	559	0	23	2370	471	34.83	5.27	9.78	799	2	16.2	81
12H-5, 135-150	107.11	7.5	13.19	32.0	556	0	13	2490	478	34.39	4.8	9.58	806	2	16.6	80
13H-2, 135-150	112.19	7.75	12.01	32.0	556	0.24	13	2240	478	33.67	5.31	8.68	590	0.5	2.5	81
14H-5, 135-150	126.04	7.61	11.61	32.0	554	0.32	6	2490	483	32.36	6.2	9.02	797	2	9.2	85
15H-4, 135-150	134.19	7.64	11.60	32.0	556	0.14	8	2370	483	31.65	6.59	8.76	792	1	7.1	87
16H-5, 135-150	145.02	7.56	10.33	32.0	557	0.31	2	2610	491	30.89	6.83	8.45	841	1	7.2	86
17H-5, 135-150	154.25	7.51	10.13	32.0	555	0	4	2610	485	30.82	7.35	8.07	608	0.5	3.5	88
18H-5, 135-150	164.10	7.69	11.05	32.0	557	0.19	8	2880	484	30.58	7.67	8.22	792	1.5	9.6	90
19H-5, 139-154	173.54	7.68	9.42	32.0	558	0.41	4	2700	488	30.58	7.44	8.3	676	1	1.1	90
20H-5, 139-159	183.23	7.6	8.82	32.0	558	0	1	2840	490	30.54	7.22	8.14	682	0.5	1.1	89
21H-5, 150-160	192.84	7.7	9.39	32.0	557	0.24	2	2660	487	30.85	7.89	7.5	676	1	2.7	95
22H-1, 70-90	195.80	7.73	6.90	32.0	558	0	2	2760	485	30.95	7.86	7.68	590	0.5	2	92
23X-4, 130-150	207.20	7.78	6.69	32.0	556	0.65	2	2700	485	30.66	7.69	7.15	458	0.5	0.7	95
24X-5, 130-150	214.90	7.63	6.16	32.0	560	0.3	1	2880	488	30.83	7.95	7.08	691	1.5	0.8	96
25X-3, 130-150	221.50	7.66	8.12	32.0	555	0.59	2	2680	483	31.03	8.84	6.45	649	1.5	31	99
26X-4, 130-150	232.60	7.68	5.33	32.0	557	0	1	2140	482	31.01	8.48	6.44	394	1	0	98
27X-1, 130-150	237.65	7.57	4.10	32.0	556	0	1	2660	482	30.66	8.06	5.97	449	1	0	97
28X-4, 130-150	251.80	7.86	4.00	31.5	555	0	2	2430	481	30.25	7.83	4.93	222	0.5	0	97
29X-3, 130-150	259.60	7.92	3.12	31.5	557	0.65	1	2610	485	29.98	7.77	5.01	148	0.5	0	99
30X-3, 130-150	268.62	7.85	3.40	31.5	554	0	1	2410	479	30.3	8.5	4.17	181	0.5	0	96
31X-3, 130-150	277.79	7.86	4.82	31.5	550	0	2	2120	471	31.17	9.88	3.59	233	1	0	102
32X-3, 117-142	288.27	7.66	5.38	31.5	550	0.51	2	2100	473	30.39	10.33	4.05	370	1.5	0	97
33X-5, 125-150	301.05	7.58	4.58	31.5	551	0	1	2120	476	29.5	9.99	3.66	299	1	0	94
34X-3, 125-150	307.75	7.6	4.57	31.5	550	0.08	1	2140	472	30.16	10.53	3.73	313	1	0	96
35X-3, 125-150	317.35	7.7	4.40	31.5	553	0.18	1	2100	476	29.32	11.09	3.72	291	1	0	93
36X-5, 125-150	329.85	7.65	4.48	31.5	550	0	1	2120	474	28.66	10.88	3.4	354	1.5	0	93
37X-5, 125-150	339.45	7.64	4.91	31.0	547	0.17	1	2160	473	28.28	10.91	3.45	302	1.5	0	92
38X-3, 125-150	345.75	7.49	3.66	32.0	554	0.58	1	2220	480	28.09	10.83	3.92	335	1.5	0	92
39X-1, 125-150	352.35	7.74	2.83	31.5	555	0.88	1	2120	480	28.93	10.44	3.5	216	1	0	95
40X-4, 125-150	366.45	8.06	2.42	31.0	549	0.42	1	2120	474	28.71	10.05	3.41	154	1	0	96
41X-2, 125-150	373.05	8.26	3.22	31.0	546	0.32	1	1850	467	30.31	10.38	2.9	99	0.5	0	105
42X-3, 125-150	384.15	7.5	2.12	31.0	544	0.45	2	1750	464	30.45	9.93	3.07	101	0.5	0	103
43X-4, 120-150	395.20	8.13	3.00	32.0	559	0.34	1	2240	489	27.72	8.39	3.85	145	0.5	0	97
44X-5, 120-150	406.30	8.08		31.0	548	0	1	1420	464	31.18	10.09	2.78	126	0.5	0	103
45X-5, 120-150	415.90	7.73	3.71	31.0	548	0.15	2	1970	473	29.08	9.54	3.32	181	1.1	0	101
1072-1064A																
1H-1, 140-150	1.40	7.23	10.60	35.0	562	20.17	4	1040	480	52.04	9.45	9.57	378	2	18.3	71
1H-2, 140-150	2.90	7.66	11.98	35.0	563	19.43	7	1120	481	52.45	9.42	9.52	444	1.5	40.2	70
1H-3, 140-150	4.40	7.68	11.67	35.0	562	19.03	4	1250	481	51.55	8.95	9.62	527	1.5	2.3	71
1H-4, 140-150	5.90	7.57	12.27	35.0	562	18.66	4	1270	481	51.21	9.06	9.73	569	1.5	5.6	68
1H-5, 140-150	7.40	7.62	12.82	35.0	562	17.44	4	1290	483	50.03	8.31	10.4	720	1.5	1	68
1H-6, 140-150	8.90	7.57	12.74	35.0	562	17.28	12	1340	483	49.82	8.09	10.04	773	2	8	69
2H-1, 140-150	10.90	7.52	12.83	35.0	563	16.58	17	1340	485	49.05	7.86	9.7	718	2	12	69
2H-2, 140-150	12.40	7.62	12.94	34.5	564	16.27	25	1210	485	49.5	8.04	9.88	757	2	32.1	68
2H-3, 140-150	13.90	7.6	12.61	34.5	561	15.91	30	1290	482	48.66	7.74	10.43	777	2	32.2	67
2H-4, 140-150	15.40	7.63	12.77	35.0	565	15.01	24	1290	486	47.96	7.61	10.25	742	2.5	34.4	67
2H-5, 140-150	16.90	7.17	12.50	34.5	563	14.63	10	1250	485	47.12	7.57	10.06	707	2	16	67
2H-6, 140-150	18.40	7.65	12.01	34.5	565	14.37	7	1100	487	47.08	7.33	10.11	672	1.5	13.4	68
3H-1, 140-150	20.20	7.63	11.75	34.0	564	13.44	5	1230	485	46.48	7.48	9.72	501	1	14.9	65
3H-2, 140-150	21.70	7.65	11.46	34.0	561	12.72	5	960	482	45.63	7.24	9.77	466	1	32	66
3H-3, 140-150	23.20	7.67	11.23	34.0	562	12.48	5	1310	484	45.28	7.1	9.93	354	1	14.3	66
3H-4, 140-150	24.70	7.62	11.35	34.0	562	11.67	9	1250	483	45.13	7.1	9.64	378	0.5	27	67
3H-5, 140-150	26.20	7.63	11.35	34.0	561	11.63	7	1100	483	44.66	6.81	9.61	354	0.5	4.1	67
3H-6, 140-150	27.70	7.65	11.86	34.0	562	10.35	7	1270	481	44.95	6.93	9.54	363	0.5	7.4	69

Note: Blank values in the table indicate that measurements were not made.

Shear Strength

At Holes 1063A and 1063D and Hole 1064A, measurements of undrained shear strength (Tables 27, 28) were taken at the rate of two per section using the vane shear device and the pocket penetrometer (see “Explanatory Notes” chapter, this volume) in

Table 22. Average values and standard deviation of index properties measured at Sites 1063-1064.

Hole		Water content wet (%)	Water content dry (%)	Wet bulk density (g/cm ³)	Grain density (g/cm ³)	Dry density (g/cm ³)	Porosity (%)	Void ratio
1063A/B/D	Mean	38.579	66.767	1.675	2.732	1.041	61.941	1.775
	SD	8.616	28.893	0.143	0.081	0.223	7.915	0.743
1064A	Mean	39.489	66.231	1.653	2.742	1.004	63.412	1.771
	SD	4.595	13.242	0.080	0.034	0.123	4.213	0.339

Note: SD = standard deviation.

Table 23. Index properties of samples from Site 1063.

Leg	Site	Hole	Core	Type	Section	Top (cm)	Bottom (cm)	Depth (mbsf)	Water content wet (%)	Water content dry (%)	Wet bulk density (g/cm ³)	Grain density (g/cm ³)	Dry density (g/cm ³)	Porosity (%)	Void ratio
172	1063	A	1	H	1	24	26	0.24	49.897	99.589	1.474	2.622	0.739	71.833	2.55
172	1063	A	1	H	1	106	108	1.06	45.728	84.258	1.568	2.841	0.851	70.037	2.337
172	1063	A	1	H	2	58	60	2.08	62.308	165.3	1.33	2.69	0.5	81.32	4.35
172	1063	A	1	H	2	120	122	2.7	62.102	163.86	1.33	2.65	0.5	80.94	4.24
172	1063	A	1	H	3	18	20	3.18	65.69	191.45	1.29	2.63	0.44	83.15	4.93
172	1063	A	1	H	3	98	100	3.98	60.078	150.48	1.37	2.78	0.54	80.36	4.09
172	1063	A	1	H	4	26	28	4.76	57.962	137.87	1.39	2.74	0.58	78.73	3.7
172	1063	A	2	H	1	36	38	5.66	49.536	98.162	1.493	2.716	0.754	72.248	2.603
172	1063	A	2	H	2	46	48	6.4	48.799	95.309	1.503	2.71	0.769	71.611	2.523
172	1063	A	2	H	2	106	108	7	50.969	103.95	1.47	2.73	0.72	73.54	2.78

This is a sample of the table that appears on the volume CD-ROM.

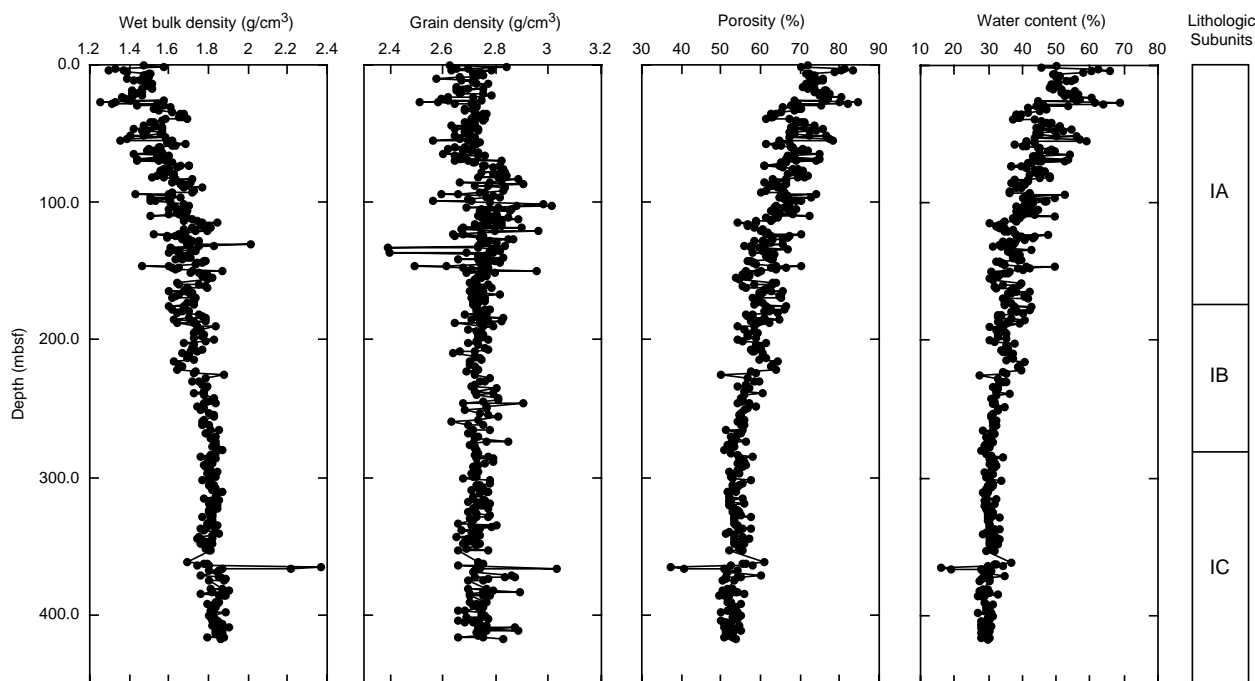


Figure 45. Index properties measurements of wet bulk density, grain density, porosity, and water content vs. depth for Hole 1063A.

Thermal Conductivity and Heat Flow

At Holes 1063A, 1063B, and 1064A, thermal conductivity was measured at a resolution of one to three measurements per core (Tables 29, 30). At Site 1063, thermal conductivity increases with depth (Fig. 50). Linear least squares approximations to the increase in conductivity with depth result in: $k = 0.96 + 0.0002z$, where k is thermal conductivity (W/[m²K]) and z is depth in mbsf. A higher gradient (0.004 W/[m²K]) is observed in the upper 40 mbsf in the sediment column. Superimposed on the general trend are cyclic changes (~0.1 W/[m²K]) of thermal conductivity. At Site 1064, thermal conductivity increases from 0.95 at 1 mbsf to 1.02 at 25 mbsf (Fig. 51).

To calculate heat flow at the Bermuda Rise, in situ temperature was measured at Hole 1063B using the Adara temperature shoe on four of the APC cores (Cores 172-1063B-8H, 10H, 12H, and 15H). Only the two deeper measurements show reliable results and were used to calculate equilibrium temperatures extrapolated from transient temperature data. Temperatures were 8.51°C at 112.3 mbsf and 9.08°C at 140.8 mbsf. The linear temperature gradient calculated from these in situ temperatures is 0.02°C/m. Additionally, a mudline temperature of 2.34°C was obtained with the Adara tool on the WSTP. Combining the average thermal conductivity of 0.99 ± 0.07 W/(m²K) at Site 1062 with the temperature gradient results in a heat flow of 19.8 mW/m².

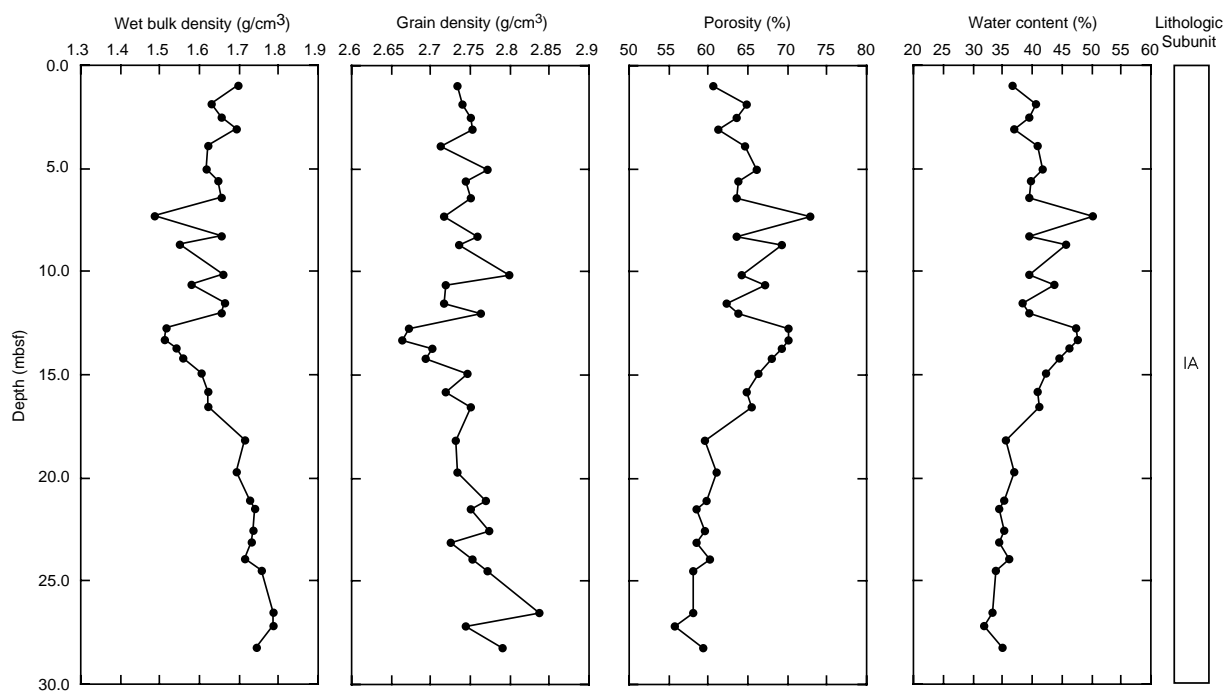


Figure 46. Index properties measurements of wet bulk density, grain density, porosity, and water content vs. depth for Hole 1064A.

Table 24. Index properties of samples from Site 1064.

Leg	Site	Hole	Core	Type	Section	Top (cm)	Bottom (cm)	Depth (mbsf)	Water content wet (%)	Water content dry (%)	Wet bulk density (g/cm ³)	Grain density (g/cm ³)	Dry density (g/cm ³)	Porosity (%)	Void ratio
172	1064	A	1	H	1	95	97	0.95	36.591	57.706	1.697	2.734	1.076	60.642	1.541
172	1064	A	1	H	2	40	42	1.9	40.698	68.628	1.629	2.74	0.966	64.74	1.836
172	1064	A	1	H	2	100	102	2.5	39.316	64.787	1.654	2.75	1.004	63.503	1.74
172	1064	A	1	H	3	12	14	3.12	36.995	58.718	1.694	2.752	1.068	61.213	1.578
172	1064	A	1	H	3	89	91	3.89	40.783	68.869	1.622	2.713	0.96	64.598	1.825
172	1064	A	1	H	4	55	57	5.05	41.75	71.674	1.618	2.771	0.943	65.984	1.94
172	1064	A	1	H	4	108	110	5.58	39.703	65.846	1.646	2.743	0.992	63.814	1.764
172	1064	A	1	H	5	39	41	6.39	39.372	64.941	1.653	2.75	1.002	63.558	1.744
172	1064	A	1	H	5	128	130	7.28	50.227	100.912	1.484	2.717	0.739	72.811	2.678
172	1064	A	1	H	6	76	78	8.26	39.334	64.837	1.655	2.758	1.004	63.584	1.746
172	1064	A	1	H	6	119	121	8.69	45.761	84.368	1.55	2.736	0.841	69.273	2.254
172	1064	A	2	H	1	66	68	10.16	39.513	65.325	1.661	2.799	1.005	64.097	1.785
172	1064	A	2	H	1	114	116	10.64	43.583	77.251	1.579	2.718	0.891	67.216	2.05
172	1064	A	2	H	2	55	57	11.55	38.343	62.189	1.663	2.716	1.025	62.258	1.65
172	1064	A	2	H	2	96	98	11.96	39.546	65.414	1.653	2.762	0.999	63.824	1.764
172	1064	A	2	H	3	21	23	12.71	47.296	89.738	1.517	2.672	0.8	70.074	2.342
172	1064	A	2	H	3	77	79	13.27	47.473	90.378	1.513	2.664	0.795	70.158	2.351
172	1064	A	2	H	3	119	121	13.69	46.058	85.385	1.54	2.701	0.831	69.254	2.252
172	1064	A	2	H	4	21	23	14.21	44.633	80.613	1.559	2.694	0.863	67.96	2.121
172	1064	A	2	H	4	92	94	14.92	42.333	73.41	1.604	2.746	0.925	66.312	1.968
172	1064	A	2	H	5	28	30	15.78	40.983	69.443	1.62	2.719	0.956	64.84	1.844
172	1064	A	2	H	5	107	109	16.57	41.256	70.231	1.622	2.75	0.953	65.348	1.886
172	1064	A	2	H	6	116	118	18.16	35.599	55.278	1.714	2.73	1.104	59.577	1.474
172	1064	A	3	H	1	68	70	19.68	36.922	58.534	1.691	2.733	1.067	60.972	1.562
172	1064	A	3	H	2	75	77	21.05	35.341	54.657	1.728	2.769	1.118	59.649	1.478
172	1064	A	3	H	2	118	120	21.48	34.36	52.347	1.741	2.749	1.143	58.428	1.405
172	1064	A	3	H	3	74	76	22.54	35.095	54.071	1.734	2.774	1.125	59.426	1.465
172	1064	A	3	H	3	129	131	23.09	34.497	52.664	1.732	2.724	1.135	58.347	1.401
172	1064	A	3	H	4	61	63	23.91	35.987	56.219	1.713	2.753	1.096	60.185	1.512
172	1064	A	3	H	4	120	122	24.5	33.793	51.042	1.758	2.772	1.164	58.011	1.382
172	1064	A	3	H	6	18	20	26.48	33.275	49.868	1.785	2.836	1.191	57.999	1.381
172	1064	A	3	H	6	87	89	27.17	31.905	46.854	1.786	2.743	1.216	55.656	1.255
172	1064	A	3	H	7	41	43	28.21	34.822	53.427	1.743	2.79	1.136	59.28	1.456

This table also appears on the volume CD-ROM.

Resistivity

Resistivity at Sites 1063 and 1064 was measured using the Wayne-Kerr Precision Component Analyzer with a four-electrode probe (see “Physical Properties” section, “Explanatory Notes” chapter, this volume). Two measurements per section were made in APC-ored sections (Tables 31, 32; Fig. 52). A comparison of resistivity

measurements at Hole 1063A with downhole logging measurements (see “Downhole Logging” section, this chapter) shows that the two data sets correspond in terms of amplitude and wavelength over the common measurement interval (80–200 mbsf). In general, resistivity varies as a function of porosity, and the cyclicity shown matches the index property measurements discussed above. No trends in resistivity are apparent at Site 1064.

Table 25. Compressional wave velocity measurements from Site 1063.

Leg	Site	Hole	Core	Type	Section	Interval (cm)	Depth (mbsf)	Temp. (° C)	Velocity 1	Velocity 2	Velocity 3
									Z-direction (m/s)	Y-direction (m/s)	X-direction (m/s)
172	1063	A	1	H	1	24	0.24	19.9	1488		
172	1063	A	1	H	1	106	1.06	19.9	1492		
172	1063	A	1	H	2	60	2.1	19.9	1478	1490	
172	1063	A	1	H	2	120	2.7	19.9	1482	1483	
172	1063	A	1	H	3	20	3.2	19.1	1488	1486	
172	1063	A	1	H	3	100	4	19.1	1487	1486	
172	1063	A	1	H	4	26	4.76	19.7		1479	
172	1063	A	2	H	1	36	5.66	17.3	1473	1466	
172	1063	A	2	H	2	48	6.42	18.1	1472	1464	
172	1063	A	2	H	3	28	7.4	18.2	1466	1466	

This is a sample of the table that appears on the volume CD-ROM.

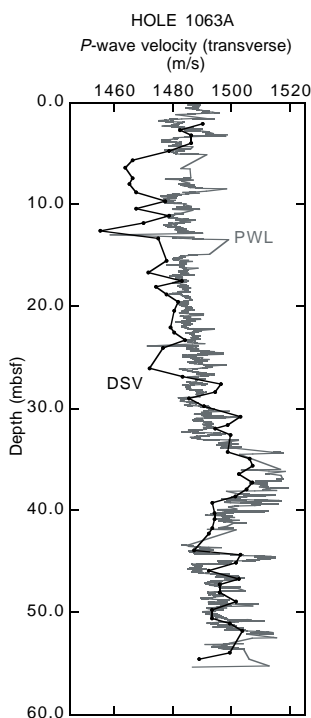


Figure 47. Comparison of compressional wave velocity measurements (PWL and DSV) for Hole 1063A.

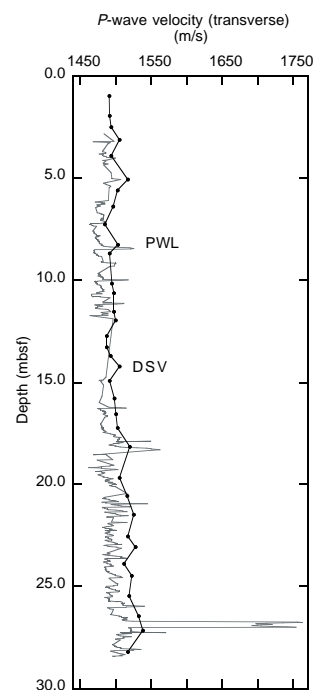


Figure 48. Comparison of compressional wave velocity measurements (PWL and DSV) for Hole 1064A.

DOWNHOLE LOGGING

Logging Operations

Hole 1063A was logged with the triple combination tool and the Formation MicroScanner (FMS)-Sonic logging tool (see “Downhole Logging” section, “Explanatory Notes” chapter, this volume), after the hole had been reamed and flushed of debris. Logging operations started at 0145 on 28 March and finished at 2300 the same day (see “Operations” section, this chapter). We ran one main triple combination pass, with a repeat of the upper section, and two full passes of the FMS-Sonic tool (see Fig. 53). The wireline heave compensator was used for all passes.

The depth to the logged measurements is calculated from the length of cable played out minus the cable length to the seafloor (taken to be the step reduction in gamma-ray log at the sediment/water boundary). Differences between the drill-pipe measurement (DPM) and the log measurement occur as a result of such factors as core expansion and incomplete recovery, in the case of the DPM, and cable stretch (~1 m/km), in the case of the logs. Hence, there can be small but significant offsets between the two, and this should be taken

into account when looking at the figures. To prevent confusion, log measurements are always on the log depth scale, and core measurements are always on the core depth scale.

Log Quality

Borehole caliper measurements showed that the hole’s narrowest diameter is ~12 in (except where there are bridges), but often contains narrow washouts, increasing in frequency, size, and thickness uphole (Fig. 54). From 190 mbsf to the pipe, the hole was wider than the maximum extent of the caliper (17 in) for at least 50% of the interval. The narrow washouts resulted in poor contact with the borehole wall and hence spikes in some of the logs. For example, the array porosity (limestone corrected; APLC) reads 100% (i.e., borehole fluid) in places. Bulk density, shallow resistivity (spherically focused resistivity measurement [SFLU]), and natural gamma display similar spikes. In some places in the upper section, for example between 125 and 135 mbsf, the accelerator porosity sonde (APS) and hostile environment litho-density (HLDT) tools give out-of-range readings, probably because of borehole roughness. Although some of the washouts are likely caused by the drill bit rotating at the same depth for a period

Table 26. Compressional wave velocity measurements from Site 1064.

Leg	Site	Hole	Core	Type	Section	Interval (cm)	Depth	Temp. (°C)	Velocity 1 Z-direction (m/s)	Velocity 2 Y-direction (m/s)	Velocity 3 X-direction (m/s)
172	1064	A	1	H	1	96	0.96	21.1	1486	1491	
172	1064	A	1	H	2	44	1.94	20.6	1491	1492	
172	1064	A	1	H	2	101	2.51	20.8	1493	1494	
172	1064	A	1	H	3	13	3.13	21.1	1507	1506	
172	1064	A	1	H	3	90	3.9	21.2	1493	1494	
172	1064	A	1	H	4	56	5.06	20.9	1514	1518	
172	1064	A	1	H	4	109	5.59	21.2	1502	1503	
172	1064	A	1	H	5	39	6.39	20.3	1493	1497	
172	1064	A	1	H	5	128	7.28	20	1483	1485	
172	1064	A	1	H	6	76	8.26	19.9	1497	1504	
172	1064	A	1	H	6	120	8.7	19.8	1488	1492	
172	1064	A	2	H	1	67	10.17	19.9	1493	1496	
172	1064	A	2	H	1	114	10.64	19.8	1496	1498	
172	1064	A	2	H	2	55	11.55	19.7	1501	1498	
172	1064	A	2	H	2	97	11.97	20	1492	1500	
172	1064	A	2	H	3	23	12.73	19.7	1485	1488	
172	1064	A	2	H	3	78	13.28	20.3	1486	1488	
172	1064	A	2	H	3	121	13.71	20.1	1488	1493	
172	1064	A	2	H	4	23	14.23	19.9	1493	1506	
172	1064	A	2	H	4	93	14.93	20.4	1487	1492	
172	1064	A	2	H	5	29	15.79	19.5	1493.6	1498	
172	1064	A	2	H	5	108	16.58	20.3	1494.8	1501	
172	1064	A	2	H	6	24	17.24	19.1	1497.4	1503	
172	1064	A	2	H	6	117	18.17	20.2	1515	1520	
172	1064	A	3	H	1	69	19.69	19.3	1507.8	1506	
172	1064	A	3	H	2	28	20.58	20.7	1509.7	1516	
172	1064	A	3	H	2	118	21.48	20.6	1520.3	1526	
172	1064	A	3	H	3	75	22.55	21.1	1512	1518	
172	1064	A	3	H	3	129	23.09	21.3	1514.3	1528	
172	1064	A	3	H	4	61	23.91	21.2	1506.6	1512	
172	1064	A	3	H	4	119	24.49	21.1	1518.3	1523	
172	1064	A	3	H	5	67	25.47	21.5	1513.7	1519	
172	1064	A	3	H	6	18	26.48	20.8	1519	1532	
172	1064	A	3	H	6	87	27.17	21.4	1534.4	1539	
172	1064	A	3	H	7	42	28.22	21.1	1513	1518	

This table also appears on the volume CD-ROM.

Table 27. Undrained-shear strength measurements from Site 1063.

Leg	Site	Hole	Core	Type	Section	Interval (cm)	Depth (mbsf)	Method	Spring no.	Undrained shear strength (kPa)	Residual strength (kPa)
172	1063	A	1	H	1	32	0.32	Vane	B-4	5.2	2.1
172	1063	A	1	H	1	114	1.14	Vane	B-4	4.5	1.7
172	1063	A	1	H	2	52	2.02	Vane	B-4	2.7	1.4
172	1063	A	1	H	2	128	2.78	Vane	B-4	2.4	1
172	1063	A	1	H	3	110	4.1	Vane	B-1	2.1	0.8
172	1063	A	1	H	3	122	4.22	Vane	B-1	2.3	1.6
172	1063	A	1	H	4	45	4.95	Vane	B-1	2.6	1.3
172	1063	A	2	H	1	44	5.74	Vane	B-1	3	1.8
172	1063	A	2	H	2	70	6.64	Vane	B-1	3.2	1.7
172	1063	A	2	H	3	38	7.5	Vane	B-1	4.2	2.3

This is a sample of the table that appears on the volume CD-ROM.

of time (e.g., between taking cores), they are probably also lithologically controlled. The more deeply penetrating logs, such as medium resistivity, are much less affected by borehole roughness. Hole 1063A was rougher than Hole 1061A.

Between 275 and 287 mbsf, Hole 1063A had closed in, forming a bridge that was passable with the tool strings. Further bridges were encountered between 380 and 389 mbsf and 397 and 400 mbsf. Anomalously high gamma-ray measurements and bad sonic velocities occurred in these intervals. The absolute values of the density and density-derived porosity matched the index physical properties of the cores well, apart from the many anomalous density lows at washouts. The core natural gamma profile tracks the downhole natural gamma well.

As at Hole 1061A, the initial sonic velocities derived from each of the interval transit times (Δt) at Hole 1063A gave logs that were offset from each other. The Δt for the two 3-m transits (lower transmitter to lower receiver and upper transmitter to upper receiver), which should be the same, were offset from each other by a time

equivalent to an extra separation of 15 cm (the distance to the next highest receiver on the tool). Recalculating the velocities so that they took into account these 15 cm yielded logs that overlay each other much better, and examples of these velocities are shown in Figure 54. Anomalous spikes in the log are caused by cycle skipping (misreading the first arrival at the receiver) and will be removed during on-shore processing.

Both the triple combo and the FMS-Sonic tool reached to within 2 m of the bottom of the hole, probably because any material that fell down the hole was caught on the bridges.

Logging Units

The sedimentary sequence could be divided into four distinct units on the basis of changes in the character of the downhole logs, particularly resistivity (Figs. 54, 55). Overall, there is a downhole compaction trend to most of the logs; sonic velocity, resistivity, and density all increase downhole, whereas porosity decreases.

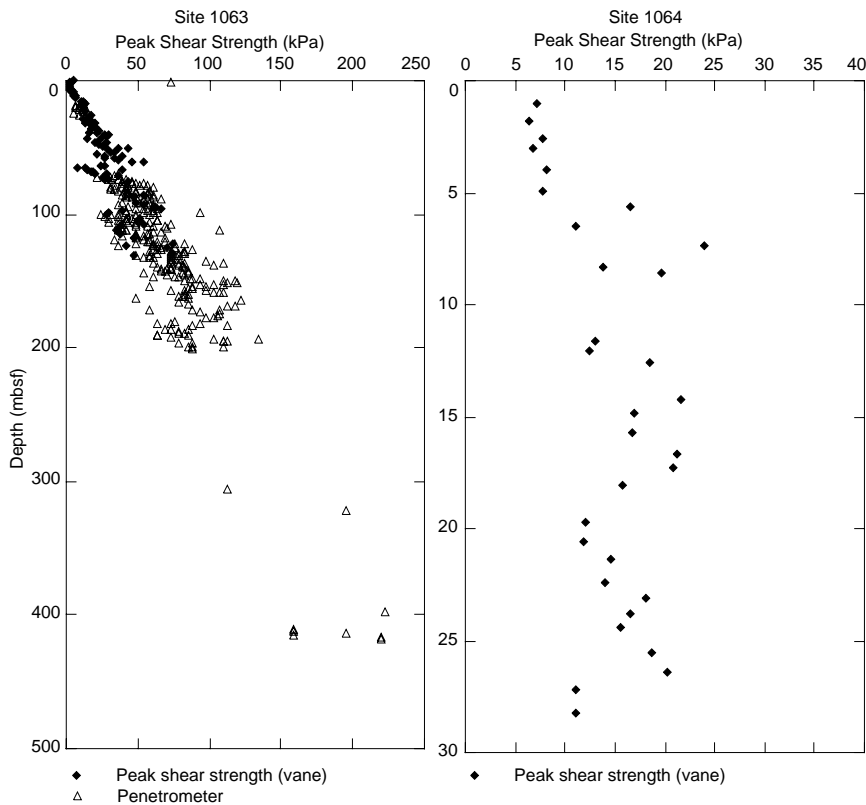


Figure 49. Vertical profiles of undrained shear strength for Sites 1063 and 1064.

Table 28. Undrained shear-strength measurements from Site 1064.

Leg	Site	Hole	Core	Type	Section	Interval (cm)	Depth (mbsf)	Method	Spring no.	Undrained shear strength (kPa)	Residual strength (kPa)
172	1064	A	1	H	1	105	1.05	Vane	B-1	7.3	
172	1064	A	1	H	2	33	1.83	Vane	B-1	6.4	3.2
172	1064	A	1	H	2	110	2.6	Vane	B-1	7.8	
172	1064	A	1	H	3	5	3.05	Vane	B-1	6.8	2.9
172	1064	A	1	H	3	5	3.05	Vane	B-1	6.8	2.9
172	1064	A	1	H	3	102	4.02	Vane	B-1	8.1	4
172	1064	A	1	H	4	49	4.99	Vane	B-1	7.9	3.2
172	1064	A	1	H	4	117	5.67	Vane	B-1	16.6	7.4
172	1064	A	1	H	5	48	6.48	Vane	B-1	11.1	4.6
172	1064	A	1	H	5	136	7.36	Vane	B-1	24	11.4
172	1064	A	1	H	5	136	7.36	Vane	B-1	24	11.4
172	1064	A	1	H	6	84	8.34	Vane	B-1	13.9	7.8
172	1064	A	1	H	6	113	8.63	Vane	B-1	19.8	10.3
172	1064	A	2	H	2	65	11.65	Vane	B-1	13	5.3
172	1064	A	2	H	2	108	12.08	Vane	B-1	12.5	5
172	1064	A	2	H	3	14	12.64	Vane	B-1	18.6	8.6
172	1064	A	2	H	4	30	14.3	Vane	B-1	21.6	
172	1064	A	2	H	4	84	14.84	Vane	B-2	17	8.5
172	1064	A	2	H	5	21	15.71	Vane	B-2	16.8	8.1
172	1064	A	2	H	5	116	16.66	Vane	B-2	21.2	9.5
172	1064	A	2	H	6	33	17.33	Vane	B-2	20.8	10.1
172	1064	A	2	H	6	107	18.07	Vane	B-2	15.9	8.6
172	1064	A	3	H	1	77	19.77	Vane	B-2	12.1	6.209
172	1064	A	3	H	2	29	20.59	Vane	B-2	11.93	6.007
172	1064	A	3	H	2	111	21.41	Vane	B-2	14.68	8.464
172	1064	A	3	H	3	67	22.47	Vane	B-2	14.07	7.224
172	1064	A	3	H	3	136	23.16	Vane	B-2	18.22	9.841
172	1064	A	3	H	4	54	23.84	Vane	B-2	16.61	7.365
172	1064	A	3	H	4	112	24.42	Vane	B-2	15.64	6.466
172	1064	A	3	H	5	75	25.55	Vane	B-2	18.67	8.401
172	1064	A	3	H	6	95	27.25	Vane	B-2	11.09	5.322
172	1064	A	3	H	6	11	26.41	Vane	B-2	20.2	9.944
172	1064	A	3	H	7	50	28.3	Vane	B-2	11.17	5.287

This table also appears on the volume CD-ROM.

Table 29. Thermal conductivity measurements from Site 1064.

Leg	Site	Hole	Core	Type	Section	Interval (cm)	Depth (mbsf)	Thermal conductivity (W/[m·K])
172	1064	A	1	H	1	60	0.6	0.95
172	1064	A	1	H	3	60	3.6	0.978
172	1064	A	1	H	5	60	6.6	0.96
172	1064	A	2	H	1	70	10.2	0.947
172	1064	A	2	H	3	50	13	0.91
172	1064	A	2	H	5	60	16.1	1.02
172	1064	A	3	H	1	60	19.6	0.973
172	1064	A	3	H	3	50	22.3	0.969
172	1064	A	3	H	5	60	25.4	1.022

This table also appears on the volume CD-ROM.

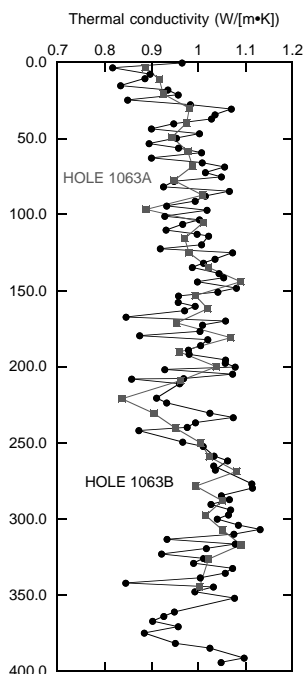


Figure 50. Thermal conductivity vs. depth at Holes 1063A and 1063B.

Table 31. Resistivity measurements from Site 1063.

Leg	Site	Hole	Core	Core type	Section	Interval (cm)	Depth (mbsf)	Sed temp (°C)	Resistance Z-direction (Ω)	Resistance Y-direction (Ω)	Resistivity Z-direction (Ωm)	Resistivity Y-direction (Ωm)	Comments
172	1063	A	1	H	1	98	0.98	20	6.925	6.6	0.545	0.54516	
172	1063	A	1	H	1	16	0.16	20	6.225	5.927	0.48991	0.48957	
172	1063	A	1	H	2	40	1.9	19.9	5.1495	4.9545	0.40527	0.40924	
172	1063	A	1	H	2	114	2.64	19.9	4.821	4.958	0.37941	0.40953	
172	1063	A	1	H	3	40	3.4	19.9	4.74	4.75	0.37304	0.39235	
172	1063	A	1	H	3	116	4.16	19.9	5.8515	5.4085	0.46051	0.44674	
172	1063	A	1	H	4	56	5.06	19.7	5.375	5.17	0.42301	0.42704	
172	1063	A	2	H	1	52	5.82	17.3	7.75	9.95	0.60993	0.82187	
172	1063	A	2	H	2	82	6.76	18.1	5.792	7.9315	0.45583	0.65514	
172	1063	A	2	H	2	24	6.18	18.1	7.4415	6.87	0.58565	0.56746	

This is a sample of the table that appears on the volume CD-ROM.

Unit 1 (162 mbsf)

The uppermost unit is characterized by a strong long-wavelength cyclicity of the natural gamma, resistivity, and velocity logs. The peaks in total gamma are caused by increased clay contents in the sediment, and they correspond to peaks in resistivity, density, and sonic velocity, and lows in porosity. The resistivity highs are probably caused by the reduced porosity of the clay-rich layers; the cycles are seen most clearly in the medium-resistivity record. The lowest re-

sistivity values of the whole log are recorded close to the boundary between Units 1 and 2, at 159 mbsf.

Unit 2 (162–250 mbsf)

The top of Unit 2 is marked by a downhole step decrease in resistivity values, in contrast to the expected general downhole compaction trend. The long-wavelength cycles of Unit 1 are replaced by shorter cycles of lesser amplitude. The regularity of these cycles is

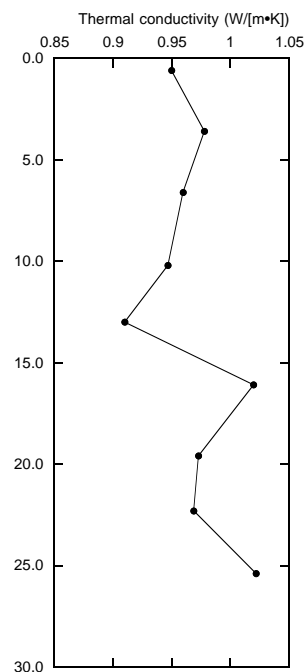


Figure 51. Thermal conductivity vs. depth at Hole 1064A.

Table 30. Thermal conductivity measurements from Site 1063.

Leg	Site	Hole	Core	Type	Section	Interval (cm)	Depth (mbsf)	Thermal conductivity (W/[m·K])
172	1063	A	1	H	1	50	0.5	0.965
172	1063	A	1	H	3	50	3.5	0.817
172	1063	A	2	H	3	50	7.62	0.897
172	1063	A	2	H	5	50	10.62	0.886
172	1063	A	3	H	1	50	15.3	0.834
172	1063	A	3	H	3	50	18.3	0.935
172	1063	A	3	H	5	50	21.3	0.957
172	1063	A	4	H	1	50	24.8	0.849
172	1063	A	4	H	3	50	27.8	0.983
172	1063	A	4	H	5	50	30.8	1.07

This is a sample of the table that appears on the volume CD-ROM.

Table 32. Resistivity measurements from Site 1064.

Leg	Site	Hole	Core	Core type	Section	Interval (cm)	Depth (mbsf)	Sed temp (°C)	Resistance Z-direction (Ω)	Resistance Y-direction (Ω)	Resistivity Z-direction (Ωm)	Resistivity Y-direction (Ωm)
172	1064	A	1	H	1	102	1.02	21.4	7.6825	7.536	0.60461	0.62247
172	1064	A	1	H	2	95	2.45	21	7.856	7.525	0.61827	0.62157
172	1064	A	1	H	3	35	3.35	21	8.5245	8.508	0.67088	0.70276
172	1064	A	1	H	4	102	5.52	20.7	7.4745	7.2615	0.58824	0.5998
172	1064	A	1	H	5	135	7.35	20.8	6.41	6.231	0.50447	0.51468
172	1064	A	1	H	6	128	8.78	19.8	7.3025	7.1865	0.57471	0.5936
172	1064	A	2	H	1	117	10.67	20	8.4285	8.7085	0.66332	0.71932
172	1064	A	2	H	2	104	12.04	19.9	7.464	7.8355	0.58742	0.64721
172	1064	A	2	H	3	115	13.65	20.2	7.223	6.8955	0.56845	0.56957
172	1064	A	2	H	4	102	15.02	20.3	7.5285	7.5675	0.59249	0.62508
172	1064	A	2	H	5	102	16.52	20	8.2145	8.313	0.64648	0.68665
172	1064	A	2	H	6	126	18.26	19.9	10.394	9.973	0.81801	0.82377
172	1064	A	3	H	1	82	19.82	19.5	8.86	8.86	0	0.73184
172	1064	A	3	H	2	124	21.54	21.2	9.546	9.841	0.75127	0.81287
172	1064	A	3	H	3	128	23.08	21.2	9.647	9.875	0.75922	0.81568
172	1064	A	3	H	4	129	24.59	21.5	9.176	9.702	0.72215	0.80139
172	1064	A	3	H	5	81	25.61	21.1	8.8095	8.9265	0.69331	0.73733
172	1064	A	3	H	6	101	27.31	21.3	21.67	22.792	1.70543	1.88262
172	1064	A	3	H	7	35	28.15	21.1	9.4285	9.232	0.74202	0.76256

This table also appears on the volume CD-ROM.

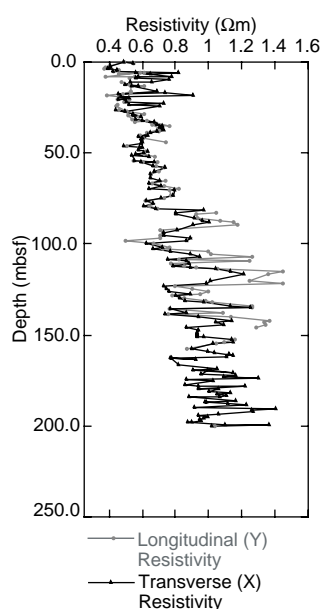


Figure 52. Resistivity measurements at Site 1063.

particularly evident in the computed gamma-ray (HCGR) log (the portion of the gamma-ray signal caused by K and Th, which are contained in the clay fraction). There is a complex relationship between HCGR and resistivity; between 160 and 200 mbsf there is correlation, whereas between 215 and 250 mbsf there is anti-correlation. The uranium log and Th/K value are also complex, showing large amplitude variations, but no consistent relationship with each other or the total gamma logs.

Unit 3 (250–329 mbsf)

Unit 3 was selected on the basis of a downhole increase in density, resistivity, and velocity over an interval of about 10 m. The gamma-ray logs show a continuation of the Unit 2 variations, but are obscured between 275 and 287 mbsf by the effect of a thick bridge in the hole.

Unit 4 (329 mbsf–bottom of hole)

This lowermost unit was selected on the basis of a distinctive, sharp drop in resistivity at 329 mbsf (very similar to the Unit 3/Unit

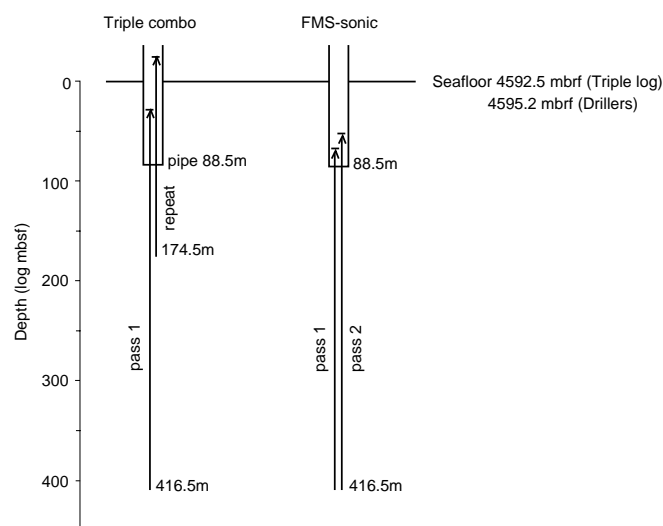


Figure 53. Graphic summary of downhole logging operations at Hole 1063A. Seafloor was selected on the basis of the step in the natural gamma logs at the sediment/water boundary.

4 boundary seen at Hole 1061A), which the other logs do not show at this boundary.

Porosity Measurements

The APS tool derives its porosity measurement from the slowing of fast neutrons by hydrogen in the formation. It assumes that all the formation's hydrogen is in pore water (and that the matrix is limestone in the case of APLC, the main porosity measurement given by the APS) and does not account for the hydrogen in the bound water of clays. This results in an overestimate of porosity for the clay-rich sediments of Hole 1063A.

An improved estimate of porosity (Φ) was derived from the bulk density log (RHOB) using the following equation:

$$\Phi = (\rho_{gr} - \rho_b) / (\rho_{gr} - \rho_w),$$

where the mean grain density of the index physical properties measurements ($2.734 \pm 0.099 \text{ g/cm}^3$) was used for the grain density (ρ_{gr}), 1.03 g/cm^3 for pore-water density (ρ_w), and RHOB for the bulk density (ρ_b). The density-derived porosity estimates are very close to the

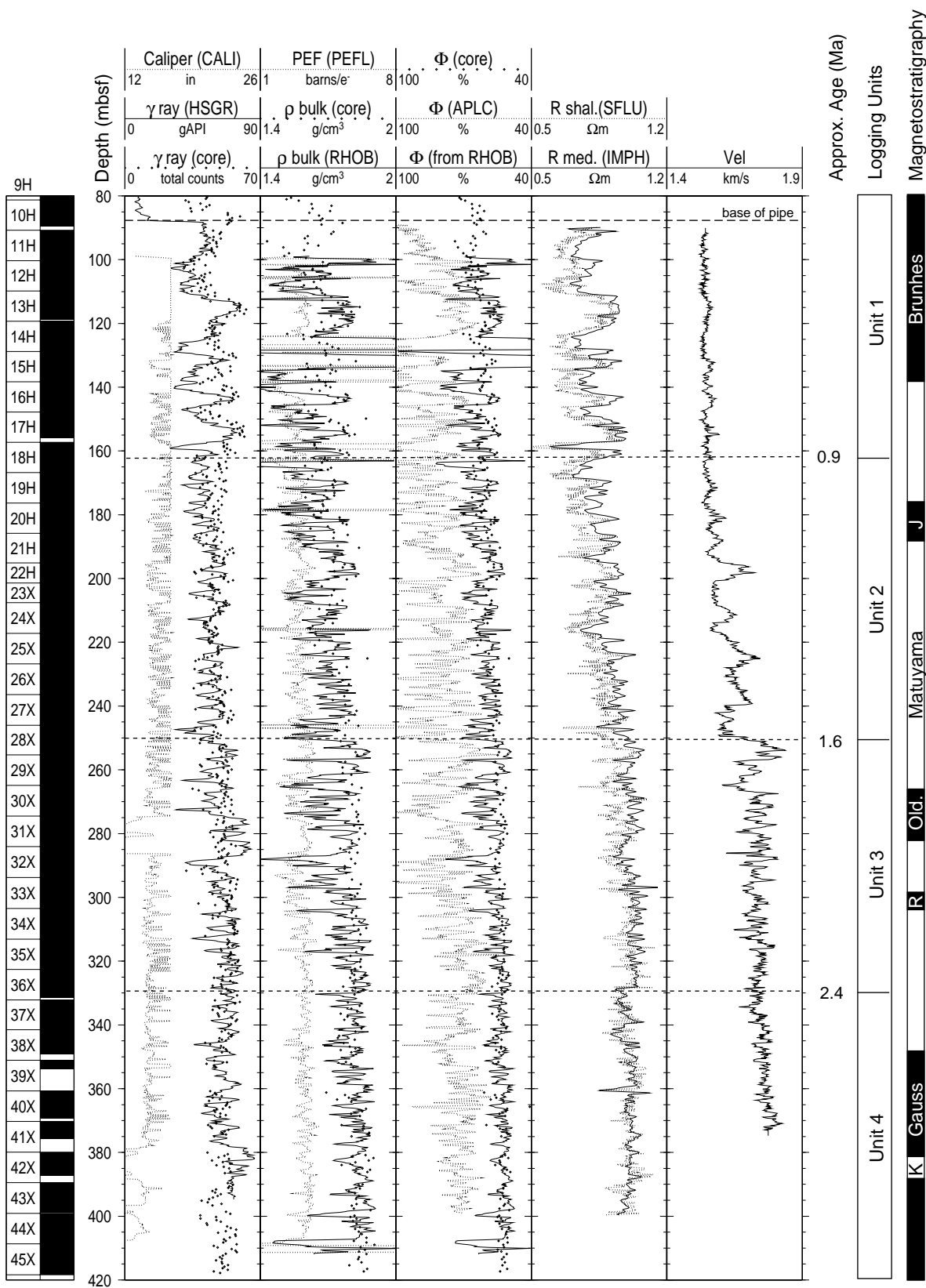


Figure 54. Downhole logs of caliper (CALI), total natural gamma (γ), photoelectric factor (PEF), bulk density (ρ), porosity (Φ), resistivity (R), and velocity (Vel) from Hole 1063A, with core measurements of bulk density and porosity (index properties) and natural gamma (MST). Logging units were chosen on the basis of the logs; their approximate ages were taken from chronostratigraphy (see “Paleomagnetism” and “Biostratigraphy” sections, this chapter).

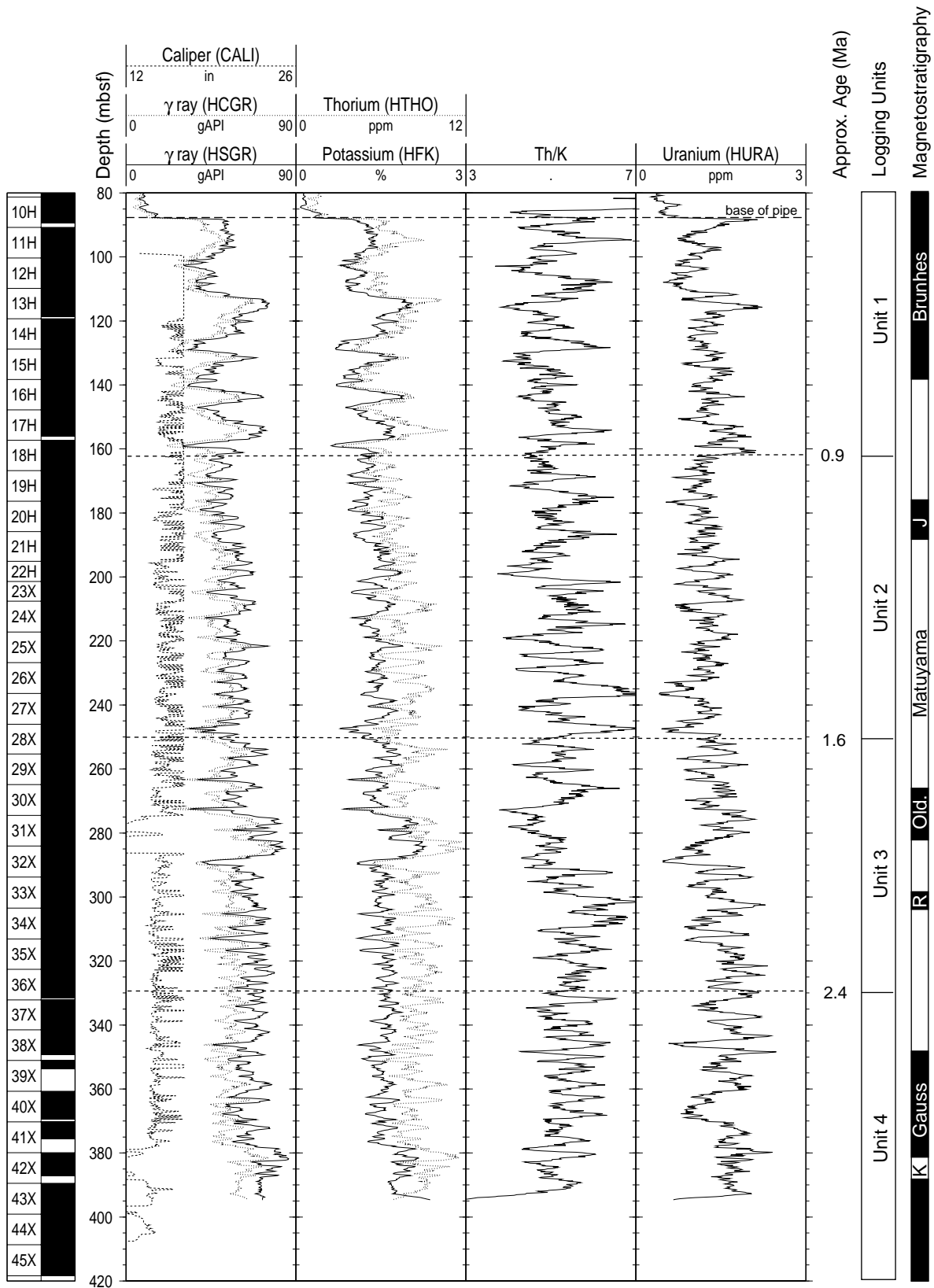


Figure 55. Downhole logs from the hostile environment natural gamma-ray sonde (HNGS) tool. Logging units were chosen on the basis of the logs; their approximate ages were taken from chronostratigraphy (see “Paleomagnetism” and “Biostratigraphy” sections, this chapter).

core index properties porosities, except in the thin washed-out layers where tool contact with the borehole wall was poor.

Clay Lithology

Clays form the major component of the sediment at Site 1063 (see “Lithostratigraphy” section, this chapter). From the potassium content (Fig. 55), illite comprises between 12% and 40% of the bulk sediment and between 22% and 73% of the sediment itself, assuming an average porosity of 55% (see “Downhole Logging” section, “Deep Blake-Bahama Outer Ridge” chapter, this volume). From Figure 56, the rest of the clay fraction seems to be mostly kaolinite and/or montmorillonite rather than chlorite.

FMS

There is very little layering apparent in the FMS images from Hole 1063A, and by far the clearest layered feature in the log is the resistive layer at 100.4 mbsf (Fig. 57). This probably corresponds to the silt layer seen in the cores (see “Lithostratigraphy” section, this chapter) at the equivalent core depth. A hiatus has been suspected at roughly this depth on the basis of (1) the seismic section (see “Site Geophysics” section, this chapter), (2) the correlation of magnetic susceptibilities with the marine $\delta^{18}O$ record (see “Sedimentation and Mass Accumulation Rates” section, this chapter), and (3) evidence as shown in Figure 58, where the log peak interpreted as $\delta^{18}O$ Stage 14 is thinner than might be expected.

Black spots with sharp edges appear on the FMS images throughout the sequence (Fig. 57). These are interpreted to be iron sulfide (e.g., pyrite) concretions, because they are much more conductive than the surrounding clay and conductive features appear dark on the FMS image. Also, concretions are present in the core. The mottled appearance of the image around the black spots might be because of inhomogeneously distributed iron sulfide.

The overall quality of the FMS data was poor, because the roughness of the borehole wall caused bad pad contact through much of the interval. Also, the maximum extension of the FMS calipers is 15 in, and the borehole was often wider than this in its upper section.

Comparison of Hole 1063A with Hole 1061A

Figure 58 compares several aspects of the logging results: Unit 1 is compared with Unit 2; the HCGR is compared with the medium penetration resistivity (IMPH); the resistivity at Site 1063 is compared with the resistivity at Site 1061; and the logs are compared with

the SPECMAP $\delta^{18}O$ record. The resistivity log from Hole 1061A was put onto the depth scale of Hole 1063A to facilitate comparison between the two logs. The downhole logs from Hole 1061A and 1063A, along with lithologic age data, are shown on the back-pocket foldout (Fig. 26, “Carolina Slope” Chapter, in the back pocket of this volume; Fig. 59).

The contrast between Units 1 and 2 is best seen in the natural gamma log. Above ~162 mbsf, HCGR has long-wavelength cycles, compared to the shorter wavelength cycles of lesser amplitude below. HCGR tracks the change in dominant glacial–interglacial cyclicity from 40 to 100 k.y. (the middle Pleistocene climatic shift; Berger and Jansen, 1994).

There is a remarkable match in resistivity (and other logs) between the two holes, considering they are separated by 1500 km. Not only do the trend and detail of the peaks and troughs match, but so do their amplitudes. The small amplitude offset in Unit 1 is likely the result of the greater range of variation in clay content at Hole 1063A.

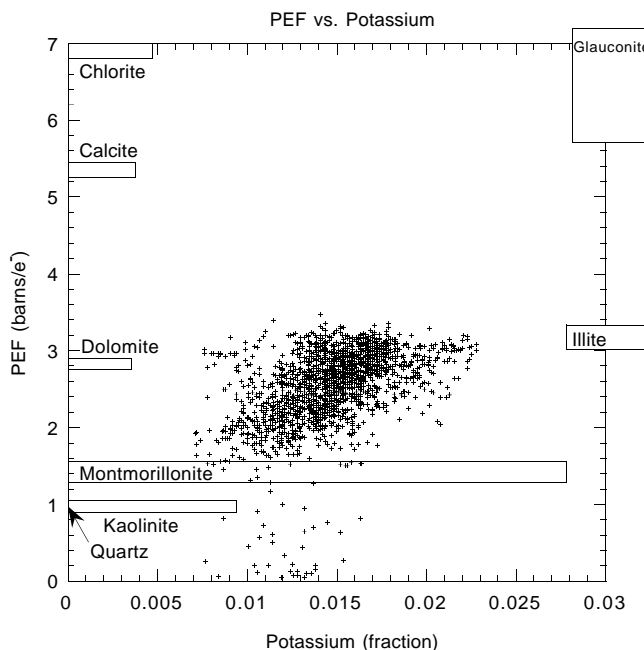


Figure 56. Crossplot of PEF (photoelectric factor) vs. potassium in Hole 1063A. Fields are given for various clays and other minerals.

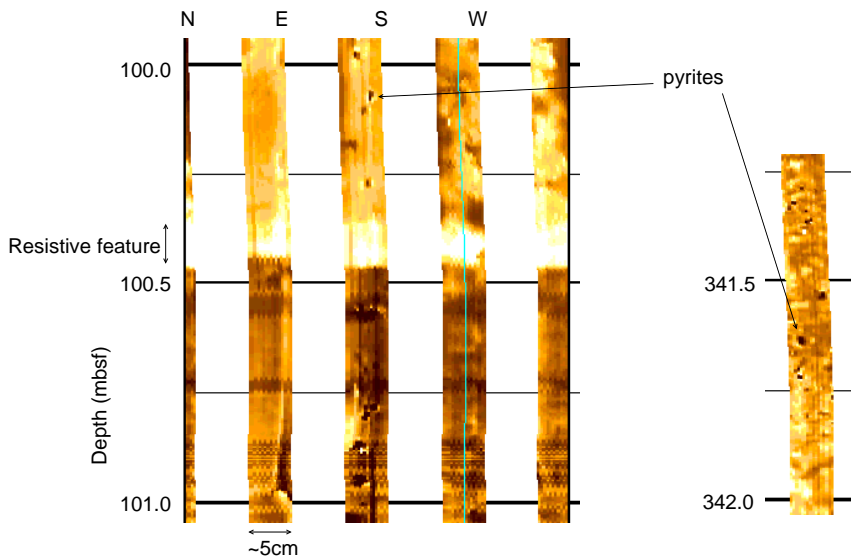


Figure 57. FMS microresistivity image of a resistive feature at 100.4 mbsf. The feature has a flat base and a graded top, and is likely to be the same as the silt layer seen at an equivalent mbsf depth in the cores (see “Lithostratigraphy” section, this chapter). Also shown are examples of images of pyrite concretions, which are relatively conductive and appear as dark spots throughout the sequence.

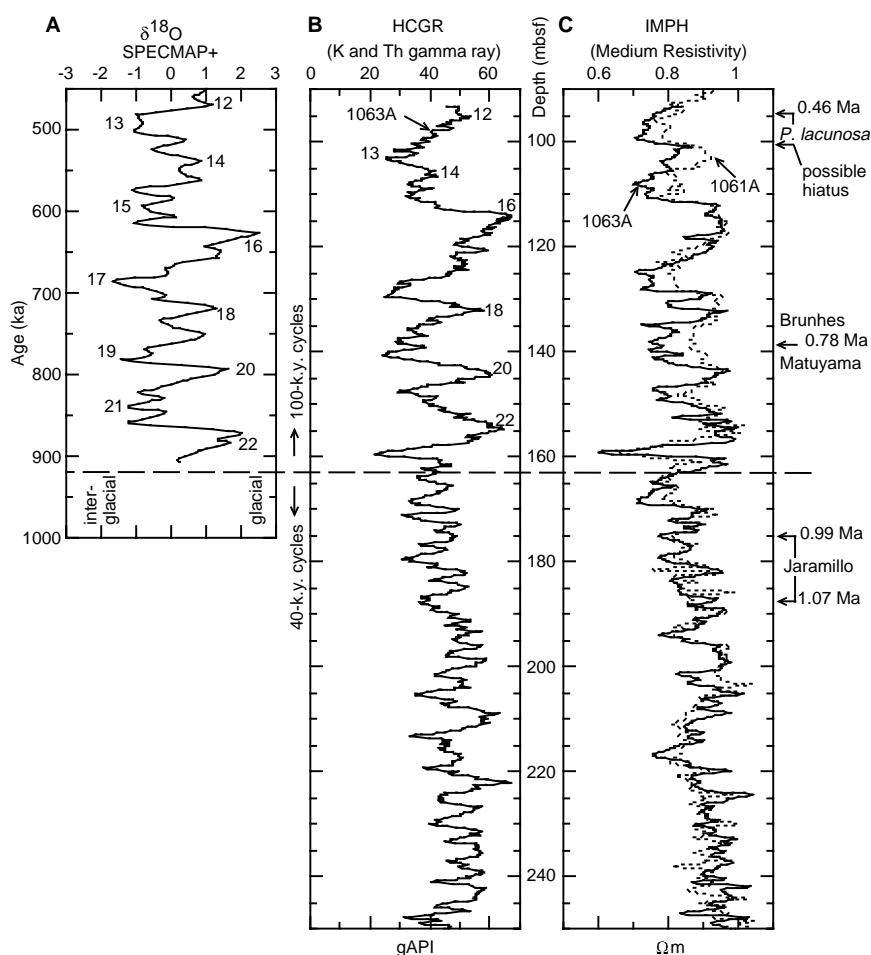


Figure 58. Comparison of (A) the generalized SPEC-MAP oxygen isotope stratigraphy and (B) computed gamma-ray (HCGR) log results from Bermuda Rise Site 1063, with (C) the medium penetration resistivity (IMPH) log results from Blake Outer Ridge Site 1061, scaled to results from Site 1063. HCGR is a measure of clay content, because it is the gamma radiation caused by K and Th, which are present in clay minerals. Chronostratigraphic markers are detailed in the “Paleomagnetism” and “Biostratigraphy” sections (this chapter).

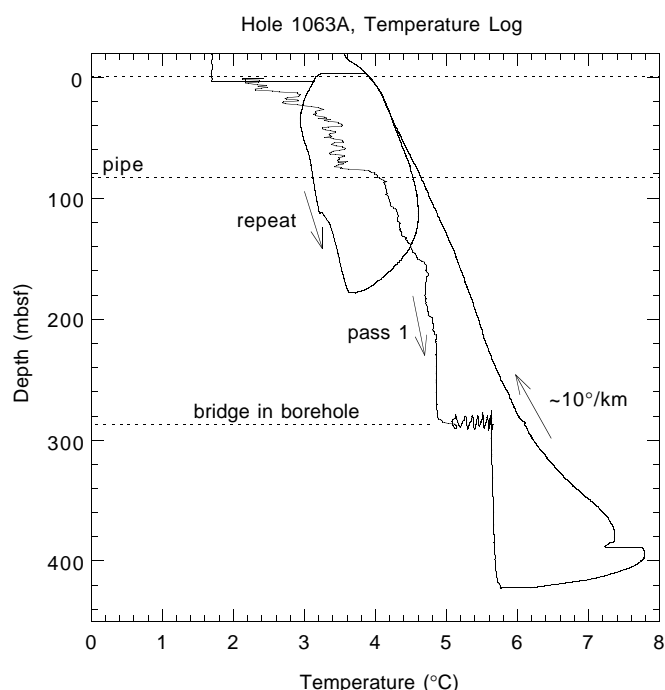


Figure 59. Temperature log from Hole 1063A obtained with the Lamont temperature tool, at the base of the triple combination tool string.

The match continues to be good to the base of Unit 3 (not shown in Fig. 58). The implication is that the same root paleoceanographic changes are responsible for the log (and lithologic) variations seen at both sites.

In Unit 1, the natural gamma log shows a strong positive correlation with resistivity, with perhaps a (unexplained) slight lag in the resistivity. HCGR, the gamma radiation caused by K and Th, is taken to be a measure of total clay content (although chlorite contains little of either K or Th, and so does not contribute much to HCGR), and the IMPH resistivity is related to the clay content through porosity, giving the observed HCGR-IMPH match. However, the story is more complex in Unit 2, where the upper part shows HCGR-IMPH correlation, but the lower part shows anti-correlation.

Both gamma-ray and resistivity logs clearly follow the known glacial-interglacial stages of the $\delta^{18}\text{O}$ isotope record. Stage 19 is pinned by the Brunhes/Matuyama boundary to 138.5 mbsf, and Stage 12 by the disappearance of *P. lacunosa* to 95.8 mbsf, and between these ties, the pattern of the log falls neatly against the pattern of the isotope stages. The shape of the glacial and interglacials match well; glacial Stages 16 and 20 are more prominent than the others in both $\delta^{18}\text{O}$ and HCGR. This match also confirms that the Unit 1 peaks in gamma-ray counts, and hence clay content, represent sediment deposited during glacials.

There is an intriguing event at 160 mbsf, near the Unit 1/2 boundary in Holes 1063A and 1061A: a marked resistivity and gamma low. This level corresponds to a carbonate-rich layer in both holes (see “Lithostratigraphy” section, this chapter). At this level in Hole 1063A there is a washout in the hole, which lowered the gamma-ray and resistivity values further. The repetition of the event at the two sites means that it is probably not just an isolated sedimentary inci-

dent, but more likely the result of a paleoceanographic transition/reorganization at the change from 40- to 100-k.y. dominated cycles. The character of the event in the logs seems to indicate that the dominant 40-k.y. periodicity carries on for a cycle after the 100-k.y. cycle has taken hold.

At both Holes 1061A and 1063A, the Unit 3/4 boundary was chosen at a distinctive step up (uphole) in the resistivity logs. From the chronostratigraphies, these appear to be the same age, about 2.4 Ma. The other logs do not show distinctive patterns at this boundary.

SITE GEOPHYSICS

Separate site surveys were done for Sites 1063 and 1064 (Figs. 60, 61). For both, the generator injectorgun was used as the sound source and the Teledyne single channel hydrophone array was used as the receiver. Postprocessing was similar to that done at earlier sites (see “Explanatory Notes” chapter, this volume). In addition, 3.5-kHz echograms were recorded during both surveys and along the transit line between sites. At the end of Site 1063, 1 hr of onsite 3.5-kHz echograms was recorded digitally for later processing to improve signal-to-noise ratio and to better resolve deeper reflectors.

Site 1063

A 1.5-hr, seismic survey was performed at Site 1063 on 24 March 1997, between 02:39:28 and 04:08:38 UTC (Line 8). The seismic profile crossing Site 1063 (Fig. 62) contains a high-amplitude sequence of bottom parallel, continuous, seismic laminations from the seafloor to 0.28 s TWT, named seismic Unit 1. A deeper sequence of lower amplitude, continuous, parallel reflectors which comprise seismic Unit 2 can be traced to about 0.45 s TWT, at which point they fade from view. An acoustically transparent interval, here termed Unit 3, extends from 0.45 s TWT to the basement at 1.55 s TWT. Seismic Unit 1 can be subdivided into two subunits. Seismic Subunit 1A extends from the seafloor to 0.20 s TWT and is characterized by high-amplitude, low-frequency parallel reflectors relative to the unit below. Unit 1B extends from 0.20 s to 0.28 s TWT and is characterized by more closely spaced parallel reflectors. There is good correlation between seismic Subunit 1A and lithologic Subunit IA (Fig. 63). This interval of high-amplitude, low-frequency reflectors corresponds with the zone of diatom-rich, nannofossil clays. The long-

wavelength, high-amplitude variability in the density of these clays (see “Physical Properties” section, this chapter) is consistent with the seismic character. The transition from lithologic Subunit IA to IB is marked by a disappearance of the silica-rich, high water-content layers. The variability in the water-content record is lower and at a higher frequency, which is also consistent with the seismic character of seismic Subunit 1B.

Preliminary analysis of the interval velocity of the sediments using the well-logging measurements at Hole 1063A suggests that this

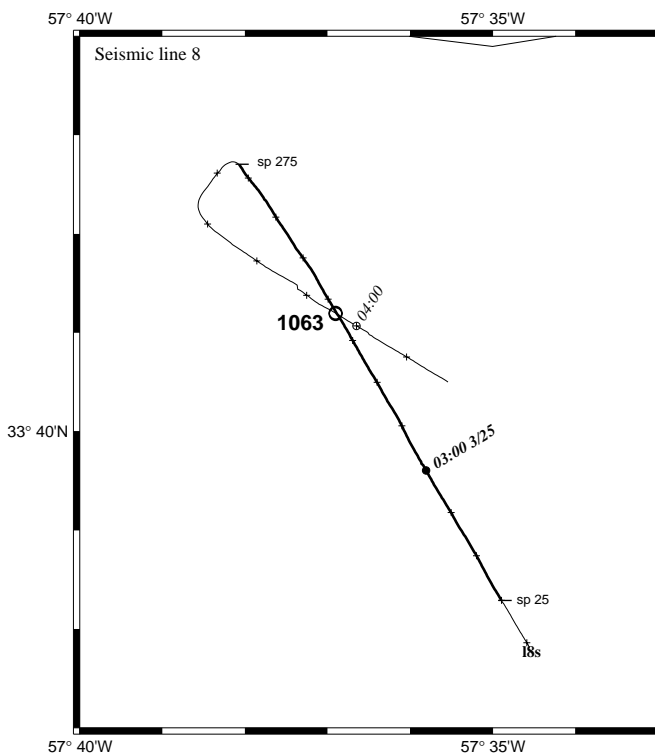


Figure 60. Survey track over Site 1063, with dates, times (UTC), and selected shotpoints given by the numbers along the survey line. Track for seismic profile in Figure 62 is thicker.

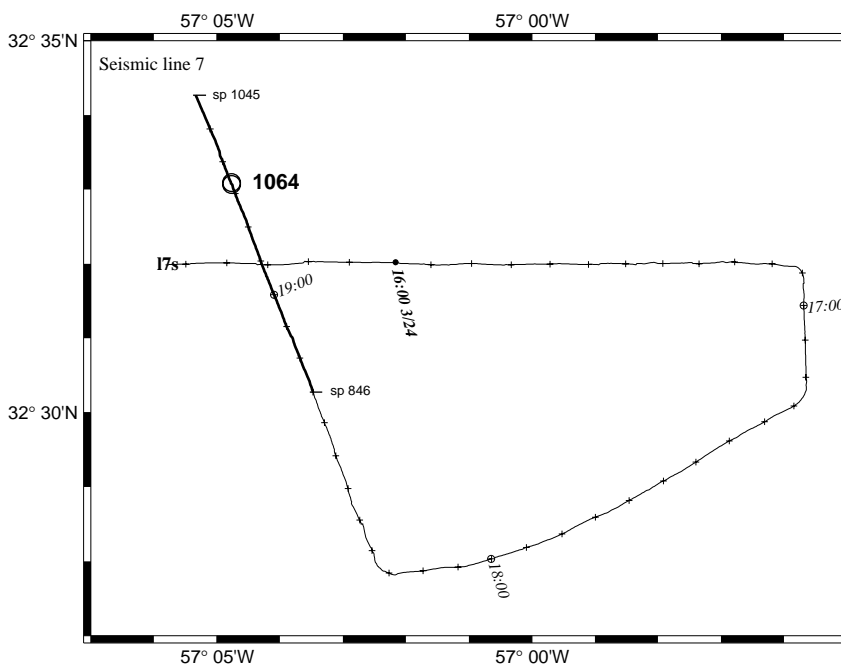


Figure 61. Survey track over Site 1064, with dates, times (UTC), and selected shotpoints given by the numbers along the survey line. Track for seismic profile in Figure 64 is thicker.

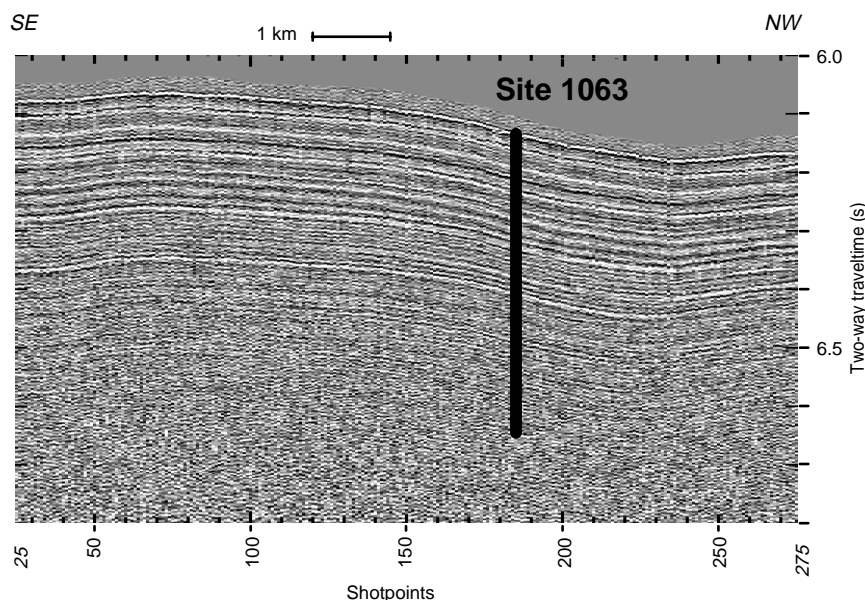


Figure 62. Seismic profile of Site 1063, Bermuda Rise.

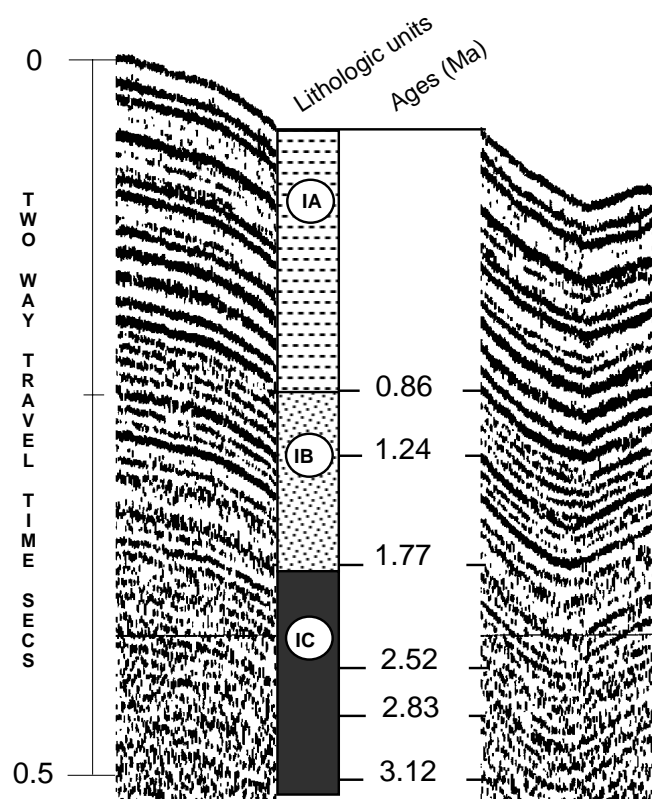


Figure 63. Seismic profile of Site 1063 showing lithologic units and ages. Depths of stratigraphic horizons were determined from interval velocities calculated from well-logging of Hole 1063A.

transition from low-frequency (widely spaced) to high-frequency (closely spaced) reflectors takes place ~165 mbsf. Stratigraphic analysis at Site 1063 places this depth at ~0.86 Ma, very close to the switchover between climate dominated by 100-k.y. orbital forcing to climate dominated by 40-k.y. forcing. This switchover and these cycles can be seen in the well logging of the sediments as well as the bulk density measurements provided by the GRAPE. The properties of sediments younger than 0.86 Ma vary, with conspicuously longer wavelengths than those of older sediments. Thus, it appears that the

characteristics of the seismic profile at Site 1063 dramatically reflect (pun intended) the influence of 100- and 40-k.y. climatic cycles on the nature and composition of the sediments of the Northern Bermuda Rise. Widely spaced reflectors correlate with the period of 100-k.y. climate variation and more closely spaced reflectors correlate with the 40-k.y.-period of variation.

A second important result is that the seismically high-amplitude (seismically bright) sediments of the northern Bermuda Rise have accumulated very continuously since ~1.5 Ma. The reflectors older than 1.5 Ma are much lower in amplitude and fade gradually as they grow older until they are barely noticeable at 2.52 Ma. Ignoring the loss of seismic energy that occurs with depth, this suggests that, although the onset of Northern Hemisphere glaciation contributed large volumes of sediment to the Northern Bermuda Rise and the sedimentation rates were high, the onset itself did not create seismically bright sediments. The influence of the climatic system on the seismic characteristics of the sediments of the Northern Bermuda Rise must have evolved over time until ~1.5 Ma when conditions were right to create seismically well-stratified sediments. From 1.5 to 0.86 Ma the climatic system imprinted a 40-k.y. variability into the sediments, which is reflected in the seismic records. At 0.86 Ma, the switchover to 100-k.y. cycles began to leave its mark. Determining the reasons for these changes will require further study.

Site 1064

The survey for Site 1064 was carried out from 1543 to 1930 hr UTC on 24 March 1997 (Line 7). This survey was extensive because we planned to propose a new site for drilling at this location to take advantage of the time saved during the Blake-Bahama Outer Ridge operations. Site 1064 is located at 32°32.72'N, 57°04.59'W at a water depth of 5500 m.

Site 1064 is located on the floor of the southeastern arm of the Sohm Abyssal Plain in a region flanked by abyssal hills. The site survey suggests that these hills trend northeast-southwest, probably parallel to the original spreading direction. With this orientation, the flow of turbidites from the Laurentian Fan source region to Site 1064 is unobstructed. The seismic profile (Fig. 64) shows that seismically stratified sediments are at least 0.6 s TWT thick at this site, with closely spaced continuous reflectors in the upper 60 m and a deeper continuous reflector at ~85 m. The 3.5-kHz sonar penetrated to 100 m, revealing alternating intervals of weak and strong reflectors (Fig. 65). This deep penetration of the 3.5 kHz along with reflectors observed to 30 m in the 12 kHz suggested that the sediments are rela-

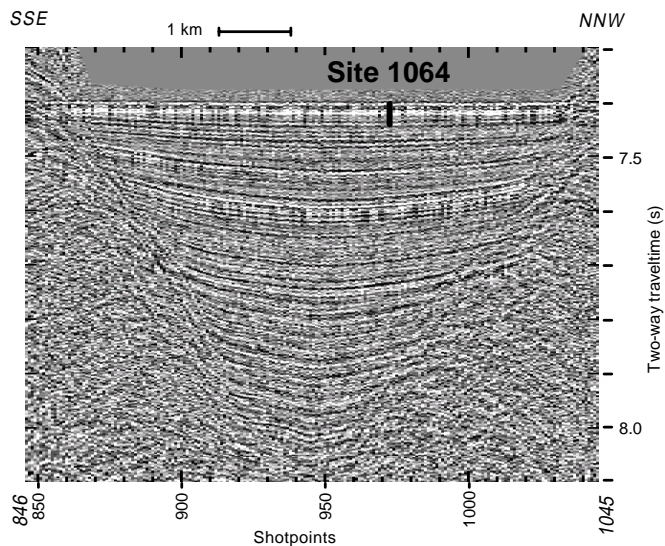


Figure 64. Seismic profile of Site 1064, southeastern Sohm Abyssal Plain.

tively fine-grained. A particularly strong reflector was observed at 0.05 s TWT, at ~37 m.

The region is well known from previous expeditions. Four piston cores were recovered by the *CSS Hudson* in 1980 as part of the seabed nuclear waste disposal program. Vilks et al. (1985) reported that the cores consist almost exclusively of muds, except for silty sands near the bottom of each core. Within each 10-m core, 39 distinct color changes were recognized and correlated. Foraminifer biostratigraphy and stable isotope stratigraphy showed that the upper 1.5 m was Holocene and that the previous interglacial was ~10 mbsf.

Very high P -wave velocities (1770 m/s), bulk densities (2.2 g/cm^3), and densities were measured in a sandy turbidite layer between 26.72 and 27.20 mbsf at Site 1064. This turbidite should appear as a prominent reflector in the 3.5-kHz echograms. There are two possibilities shown in the 3.5-kHz echograms (Fig. 65). A sequence of moderate intensity, semi-continuous reflectors begins about 0.025 s of TWT and a strong, continuous reflector begins at 0.05 s TWT. If the shallower reflector at 0.025 s TWT correlates with this sandy bed at 27 mbsf, then the interval velocity to this bed is about 1080 m/s, much lower than the P -wave velocities measured by the PWL, the MST, or by the DSV. The average P -wave velocity to this layer measured by the PWL is 1484 m/s. If the turbidite correlates with the deeper reflector appearing at 0.05 s TWT, then the interval velocity is 2160 m/s. This is about 45% higher than the average velocity to the sand layer. If, however (see "Physical Properties" and "Inorganic Geochemistry" sections, this chapter), the first core at Site 1064 overpenetrated, a more firm correlation can be made. Assuming an interval velocity of 1484 m/s and using a TWT of 0.05 s to the sandy turbidite/strong reflector, its depth is calculated as 37.1 mbsf. If the correlation between the sandy bed and strong reflector is correct, it suggests that the first core overpenetrated ~10 m.

REFERENCES

- Adkins, J., Boyle, E.A., Keigwin, L.D., Cortijo, E., 1997. Variability Of the north Atlantic thermohaline circulations during the last interglacial period. *Nature*, 390:154–156.
- Bacon, M.P., and Rosholt, J.P., 1982. Accumulation rates of the ^{230}Th , ^{231}Pa and some transition metals on the Bermuda Rise. *Geochim. Cosmochim. Acta*, 46:651–666.
- Baker, M.J., 1986. Sedimentation of the Northern Bermuda Rise [Master of Sci. thesis]. Univ. of Rhode Island, Narragansett, RI.
- Baldauf, J.G., 1984. Cenozoic diatom biostratigraphy and paleoceanography of the Rockall Plateau region, North Atlantic, Deep Sea Drilling Project Leg 81. In Roberts, D.G., Schnitker, D., et al., *Init. Repts. DSDP*, 81: Washington (U.S. Govt. Printing Office), 439–478.
- Barranco, F.T., Jr., Balsam, W.L., and Deaton, B.C., 1989. Quantitative reassessment of brick red lutites: evidence from reflectance spectrophotometry. *Mar. Geol.*, 89:299–314.
- Barron, J.A., 1985. Late Eocene to Holocene diatom biostratigraphy of the equatorial Pacific Ocean, Deep Sea Drilling Project Leg 85. In Mayer, L., Theyer, F., Thomas, E., et al., *Init. Repts. DSDP*, 85: Washington (U.S. Govt. Printing Office), 413–456.
- Berger, W.H., and Jansen, E., 1994. Mid-Pleistocene climate shift: the Nansen connection. In Johannessen, O.M., Muensch, R.D., and Overland, J.E. (Eds.), *The Role of the Polar Oceans in Shaping the Global Environment*. Geophys. Monogr., Am. Geophys. Union, 85:295–311.
- Berner, R.A., 1980. *Early Diagenesis: A Theoretical Approach*. Princeton, NJ (Princeton Univ. Press).
- Biscaye, P.E., Gardner, W.D., Zaneveld, J.R.V., Pak, H., and Tucholke, B., 1980. Nephels! Have we got Nephels! *Eos*, 61:1014.
- Boyle, E.A., and Keigwin, L.D., 1987. North Atlantic thermohaline circulation during the past 20,000 years linked to high-latitude surface temperature. *Nature*, 330:35–40.
- Claypool, G.E., and Kaplan, I.R., 1974. The origin and distribution of methane in marine sediments. In Kaplan, I.R. (Ed.), *Natural Gases in Marine Sediments*. New York (Plenum), 99–139.
- Corliss, B.H., and Honjo, S., 1981. Dissolution of deep-sea benthonic foraminifera. *Micropaleontology*, 27:356–378.
- Denham, C.R., and Cox, A., 1971. Evidence that the Laschamp polarity event did not occur 13,300–30,400 years ago. *Earth Planet. Sci. Lett.*, 13:181–190.
- Dickens, G.R., Paull, C.K., Wallace, P., and the ODP Leg 164 Scientific Party, 1996. Direct measurement of in situ methane quantities in a large gas-hydrate reservoir. *Nature*, 385:426–428.
- Dickens, G.R., and Quinby-Hunt, M.S., 1994. Methane hydrate stability in seawater. *Geophys. Res. Lett.*, 21:2115–2118.
- Druffel, E., 1997. Pulses of rapid ventilation in the North Atlantic surface ocean during the past century. *Science*, 275:1454–1457.
- Emerson, S., and Hedges, J.I., 1988. Processes controlling the organic carbon content of open ocean sediments. *Paleoceanography*, 3:621–634.
- Espitalié, J., Deroo, G., and Marquis, F., 1986. La pyrolyse Rock-Eval et ses applications, Partie III. *Rev. Inst. Fr. Pet.*, 41:73–89.
- Gieskes, J.M., 1981. Deep-sea drilling interstitial water studies: implications for chemical alteration of the oceanic crust, layers I and II. In Warne, J.E., Douglas, R.G., and Winterer, E.L. (Eds.), *The Deep Sea Drilling Project: A Decade of Progress*. Spec. Publ.—Soc. Econ. Paleontol. Mineral., 32:149–167.
- Gieskes, J.M., Blanc, G., Vrolijk, P., Elderfield, H., and Barnes, R., 1990. Interstitial water chemistry—major constituents. In Moore, J.C., Mascle, A., et al., *Proc. ODP, Sci. Results*, 110: College Station, TX (Ocean Drilling Program), 155–178.
- Hamilton, E.L., 1978. Sound velocity-density relations in sea-floor sediments and rocks. *J. Acoust. Soc. Am.*, 63:366–377.
- Hamilton, E.L., and Bachman, R.T., 1982. Sound velocity and related properties of marine sediments. *J. Acoust. Soc. Am.*, 72:1891–1904.
- Hesse, R., and Harrison, W.E., 1981. Gas hydrates (clathrates) causing pore-water freshening and oxygen isotope fractionation in deep-water sedimentary sections of terrigenous continental margins. *Earth Planet. Sci. Lett.*, 55:453–462.
- Hogg, N.G., 1983. A note on the deep circulation of the Western North Atlantic: its nature and causes. *Deep-Sea Res. Part A*, 9:945–961.
- Hollister, C.D., and McCave, I.N., 1984. Sedimentation under deep sea storms. *Nature*, 309:220–225.
- Hower, J., Eslinger, E.V., Hower, M.E., and Perry, E.A., 1976. Mechanism of burial metamorphism of argillaceous sediment. 1. Mineralogical and chemical evidence. *Geol. Soc. Am. Bull.*, 87:725–737.
- Jenden, P.D., and Gieskes, J.M., 1983. Chemical and isotopic composition of interstitial water from Deep Sea Drilling Project Sites 533 and 534. In Sheridan, R.E., Gradstein, F.M., et al., *Init. Repts. DSDP*, 76: Washington (U.S. Govt. Printing Office), 453–461.
- Jenkins, W.J., 1982. On the climate of a subtropical ocean gyre: decade timescale variation in water mass renewal in the Sargasso Sea. *Science*, 40:265–290.
- Kastner, M., Elderfield, H., Jenkins, W.J., Gieskes, J.M., and Gamo, T., 1993. Geochemical and isotopic evidence for fluid flow in the western Nankai subduction zone, Japan. In Hill, I.A., Taira, A., Firth, J.V., et al., *Proc. ODP, Sci. Results*, 131: College Station, TX (Ocean Drilling Program), 397–413.

- Kastner, M., Elderfield, H., Martin, J.B., Suess, E., Kvenvolden, K.A., and Garrison, R.E., 1990. Diagenesis and interstitial-water chemistry at the Peruvian continental margin—major constituents and strontium isotopes. *In* Suess, E., von Huene, R., et al., *Proc. ODP, Sci. Results*, 112: College Station, TX (Ocean Drilling Program), 413–440.
- Keigwin, L.D., 1987. Pliocene stable-isotope record of Deep Sea Drilling Project Site 606: sequential events of ^{18}O enrichment beginning at 3.1 Ma. *In* Ruddiman, W.F., Kidd, R.B., Thomas, E., et al., *Init. Repts. DSDP*, 94 (Pt. 2): Washington (U.S. Govt. Printing Office), 911–920.
- , 1996. The Little Ice Age and the medieval warm period in the Sargasso Sea. *Science*, 274:1504–1508.
- Keigwin, L.D., and Jones, G.A., 1989. Glacial-Holocene stratigraphy, chronology, and paleoceanographic observations on some North Atlantic sediment drifts. *Deep-Sea Res.*, 36:845–867.
- , 1994. Western North Atlantic evidence for millennial-scale changes in ocean circulation and climate. *J. Geophys. Res.*, 99:12397–12410.
- , 1995. The marine record of deglaciation from the continental margin off Nova Scotia. *Paleoceanography*, 10:973–985.
- Kendrick, J.W., 1979. Geochemical studies of black clays from Leg 43, Deep Sea Drilling Project. *In* Tucholke, B.E., Vogt, P.R., et al., 1979. *Init. Repts. DSDP*, 43: Washington (U.S. Govt. Printing Office), 633–642.
- Kendrick, J.W., Hood, A., and Castano, J.R., 1979. Petroleum-generating potential of Cretaceous sediments from Leg 42, Deep Sea Drilling Project. *In* Tucholke, B.E., Vogt, P.R., et al., 1979. *Init. Repts. DSDP*, 43: Washington (U.S. Govt. Printing Office), 663–668.
- Kvenvolden, K.A., and Kastner, M., 1990. Gas hydrates of the Peruvian outer continental margin. *In* Suess, E., von Huene, R., et al., *Proc. ODP, Sci. Results*, 112: College Station, TX (Ocean Drilling Program), 517–526.
- Laine, E.P., Gardner, W.D., Richardson, M.J., and Kominz, M.A., 1994. Abyssal currents and advection of resuspended sediment along the northeastern Bermuda Rise. *Mar. Geol.*, 119:159–171.
- Laine, E.P., and Hollister, C.D., 1981. Geological effects of the Gulf Stream system on the northern Bermuda Rise. *Mar. Geol.*, 39:277–310.
- Liddicoat, J.C., and Coe, R.S., 1979. Mono Lake geomagnetic excursion. *J. Geophys. Res.*, 84:261–271.
- Mackin, J.E., and Aller, R.C., 1984. Ammonium adsorption in marine sediments. *Limnol. Oceanogr.*, 29:250–257.
- Malmgren, B.A., and Kennett, J.P., 1981. Phyletic gradualism in a Late Cenozoic planktonic foraminiferal lineage, DSDP Site 284: southwest Pacific. *Paleobiology*, 7:230–240.
- Manheim, F.T., 1974. Comparative studies on extraction of sediment interstitial waters: discussion and comment on the current state of interstitial water studies. *Clays Clay Miner.*, 22:337.
- McCave, I.N., 1979. Depositional features of organic-carbon-rich black and green mudstones at DSDP Sites 386 and 387, western North Atlantic. *In* Tucholke, B.E., Vogt, P.R., et al., *Init. Repts. DSDP*, 43: Washington (U.S. Govt. Printing Office): 411–416.
- McDuff, R.E., 1985. The chemistry of interstitial waters, Deep Sea Drilling Project Leg 86. *In* Heath, G.R., Burckle, L.H., et al., *Init. Repts. DSDP*, 86: Washington (U.S. Govt. Printing Office), 675–687.
- Meyers, P.A., 1994. Preservation of elemental and isotopic source identification of sedimentary organic matter. *Chem. Geol.*, 144:289–302.
- Morse, J.W., and Mackenzie, F.T., 1990. *Geochemistry of Sedimentary Carbonates*. Dev. in Sedimentology, 48: Amsterdam (Elsevier).
- Müller, P.J., 1977. C/N ratios in Pacific deep sea sediments: effect of inorganic ammonium and organic nitrogen compounds sorbed by clays. *Geochim. Cosmochim. Acta*, 41:765–776.
- Paull, C.K., Matsumoto, R., Wallace, P.J., et al., 1996. *Proc. ODP, Init. Repts.*, 164: College Station, TX (Ocean Drilling Program).
- Piper, D.J.W., 1975. Late Quaternary deep water sedimentation off Nova Scotia and Western Grand Banks. *Can. J. Pet. Geol. Mem.*, 4:195–204.
- Raffi, I., Backman, J., Rio, D., and Shackleton, N.J., 1993. Plio-Pleistocene nannofossil biostratigraphy and calibration to oxygen isotopes stratigraphies from Deep Sea Drilling Project Site 607 and Ocean Drilling Program Site 677. *Paleoceanography*, 8:387–408.
- Raymo, M.E., Ruddiman, W.F., Backman, J., Clement, B.M., and Martinson, D.G., 1989. Late Pliocene variation in Northern Hemisphere ice sheets and North Atlantic deep water circulation. *Paleoceanography*, 4:413–446.
- Reeburgh, W.S., 1976. Methane consumption in Cariaco Trench waters and sediments. *Earth Planet. Sci. Lett.*, 28:337–344.
- Rosenfeld, J.K., 1979. Ammonium absorption in nearshore anoxic sediments. *Limnol. Oceanogr.*, 24:356–364.
- Sayles, F.L., 1970. Preliminary geochemistry. *In* Bader, R.G., Gerald, R.D., et al., *Init. Repts. DSDP*, 4: Washington (U.S. Govt. Printing Office), 645.
- Schaefer, R.G., and Leythaeuser, D., 1984. C_2 – C_8 hydrocarbons in sediments from Deep Sea Drilling Project Leg 75, Holes 530A, Angola Basin, and 532, Walvis Ridge. *In* Hay, W.W., Sibuet, J.-C., et al., *Init. Repts. DSDP*, 75 (Pt. 2): Washington (U.S. Govt. Printing Office), 1055–1067.
- Schmitz, W.J., Jr., and McCartney, M.S., 1993. On the North Atlantic circulation. *Rev. Geophys.*, 31:29–49.
- Schoell, M., 1980. The hydrogen and carbon isotopic composition of methane from natural gases of various origins. *Geochim. Cosmochim. Acta*, 44:649–661.
- Schrag, D.P., and DePaolo, D.J., 1993. Determination of $\delta^{18}\text{O}$ of seawater in the deep ocean during the last glacial maximum. *Paleoceanography*, 8:1–6.
- Shackleton, N.J., Backman, J., Zimmerman, H., Kent, D.V., Hall, M.A., Roberts, D.G., Schnitker, D., Baldauf, J.G., Desprairies, A., Homrighausen, R., Huddleston, P., Keene, J.B., Kaltenback, A.J., Krumsiek, K.A.O., Morton, A.C., Murray, J.W., and Westberg-Smith, J., 1984. Oxygen isotope calibration of the onset of ice-rafting and history of glaciation in the North Atlantic region. *Nature*, 307:620–623.
- Silva, A.J., Hollister, C.D., Laine, E.P., and Beverly, B., 1976. Geotechnical properties of the Northern Bermuda Rise. *Mar. Geotechnol.*, 1:195–232.
- Stow, D.A.V., 1979. Distinguishing between fine-grained turbidites and contourites on the Nova Scotian deep water margin. *Sedimentology*, 26:371–387.
- Suman, D., and Bacon, M.P., 1989. Variations in Holocene sedimentation in the North American Basin determined from ^{230}Th measurements. *Deep-Sea Res.*, 36:869–878.
- Tucholke, B.E., Vogt, P.R., et al., 1979. *Init. Repts. DSDP*, 43: Washington (U.S. Govt. Printing Office).
- Vilks, G., Buckley, D., and Keigwin, L., 1985. Late Quaternary sedimentation on the southwest Sohm abyssal plain. *Sedimentology*, 32:69–82.
- Whelan, J.K., and Sato, S., 1980. C_1 – C_5 hydrocarbons from core gas pockets, Deep Sea Drilling Project Legs 56 and 57, Japan Trench Transect. *In* Langseth, M., Okada, H., et al., *Init. Repts. DSDP*, 56/57 (Pt. 2): Washington (U.S. Govt. Printing Office), 1335–1347.

Ms 1721R-106

NOTE: Core-description forms (“barrel sheets”) and core photographs can be found in Section 4, beginning on page 325. Forms containing smear-slide data can be found on CD-ROM. See Table of Contents for material contained on CD-ROM.

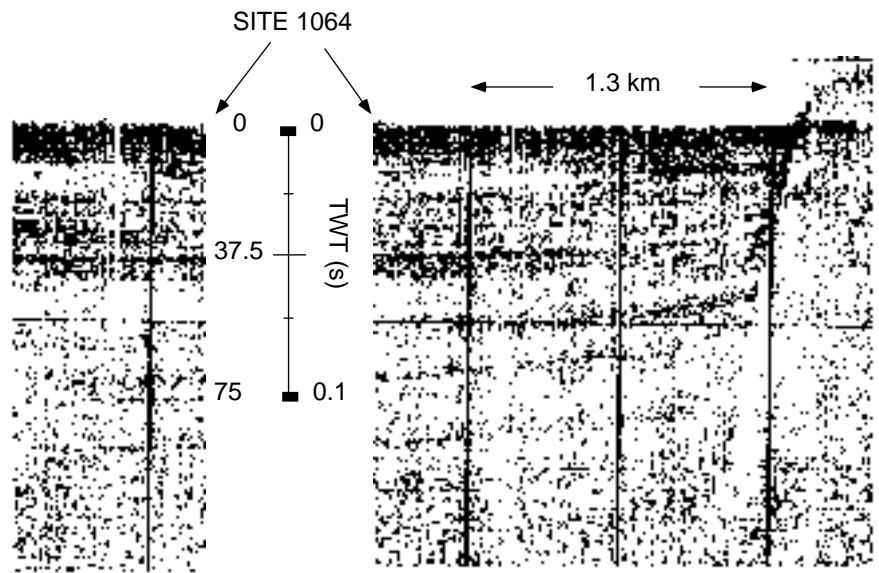


Figure 65. A 3.5-kHz profile at Site 1064. The strong reflector at 37 m corresponds to a sand layer at 27 mbsf at Site 1064. This correlation suggests that 10 m of core was lost due to overpenetration.